Installation and hydrodynamic characterization of a High Rate Algal Pond pilot for the aquaculture wastewater treatment in Vietnam

Auteur : Royaux, Damien
Promoteur(s) : Eppe, Gauthier; Toye, Dominique
Faculté : Faculté des Sciences appliquées
Diplôme : Master en ingénieur civil en chimie et science des matériaux, à finalité spécialisée
Année académique : 2017-2018
URI/URL : http://hdl.handle.net/2268.2/4534

UNIVERSITY OF LIEGE

FACULTY OF APPLIED SCIENCE

Installation and hydrodynamic characterization of a High Rate Algal Pond pilot for the aquaculture wastewater treatment in Vietnam

ROYAUX Damien

Thesis presented for obtaining the Master's degree in

Chemical and Materials engineering

Supervisor : **EPPE Gauthier**

Academic year : 2017 - 2018

Abstract

Vietnam and every country where intensive aquaculture is an important source of income face critical difficulties to treat culture pond wastewater. These waters contain a high amount of nitrogen and phosphorous compounds that are harmful to the environment. In addition, the systematic use of groundwater to partially (or totally) fill the aquaculture ponds is not sustainable for Vietnam. The RENEWABLE project of ARES (Académie de Recherche et d'Enseignement Supérieur) is a collaboration between the University of Liège (Belgium) and the Industrial University of Ho Chi Minh City (Vietnam) and aims at developing a wastewater treatment system using microalgae in a High Rate Algal Pond (HRAP). This technology has been widely studied during the last few decades and may be an economical and sustainable solution for developing countries.

The purpose of the present work is first the hydrodynamic study of a HRAP pilot installed in Vietnam to identify the conditions that offer the best mixing of the microalgae present in the pond and to develop a model to simulate hydrodynamic and biologic phenomena occurring in the HRAP. Second, the gas transfer provided by the airlift aeration system is also evaluated in different conditions. The two parameters that are changed are the water level (0.25m, 0.4m and 0.6m) in the pond and the airlift air flowrate (<5Nm^3/m^2h, 10Nm^3/m^2h, 16.67Nm^3/m^2h and 21.67Nm^3/m^2h). The final goal of this work is to use the data to develop an accurate HRAP model to be able to operate the pond in the optimal conditions.

The work has been realized in two main steps. First, the methodology of the tests has been developed in Arlon (Belgium) and different tracer and gas transfer tests have been realized on a small-scale pilot (5m^2). Then, the same tests, but at a larger scale (130m^2), are conducted in the Ninh Thuan province (Vietnam) on a HRAP pilot implemented there as part of the project. Results show that an air flowrate smaller than 5Nm^3/m^2h is inadequate to provide a sufficient mixing and aeration in the pond. An air flowrate of 10Nm^3/m^2h or higher provides sufficient dispersion (dispersion coefficient greater than 0.268m^2/s) and oxygen transfer (volumetric transfer coefficient of the pond greater than $1.6 * 10^{-3} s^{-1}$) to the wastewater circulating in the HRAP.

Résumé

Le Vietnam ainsi que tous les pays où l'aquaculture intensive est une source importante de revenus font face à des difficultés majeures pour traiter les eaux usées issues des bassins de culture. Ces eaux contiennent de grandes quantités de composés nitrés et phosphorés qui sont nocifs pour l'environnement. De plus, l'utilisation systématique d'eau douce provenant des nappes phréatiques pour alimenter en partie (ou totalement) les bassins d'aquaculture n'est pas une solution tenable à long terme. Cette consommation effrénée des ressources naturelles ne s'inscrit pas dans une démarche responsable et durable de la gestion des ressources hydriques au Vietnam. Le projet RENEWABLE de l'ARES (Académie de Recherche et d'Enseignement Supérieur) résulte de la collaboration entre l'Université de Liège (Belgique) et l'Université Industrielle d'Ho Chi Minh Ville (Vietnam) et a pour but le développement d'un système de traitement des eaux usées à l'aide de microalgues cultivées dans un Chenal Algal à Haut Rendement (CAHR). Cette technique a été largement étudiée au cours des récentes décennies et pourrait s'avérer être une solution économique et durable pour les pays en voie de développement.

Le but de ce travail consiste tout d'abord en l'étude hydrodynamique d'un CAHR pilote installé au Vietnam pour identifier les conditions qui offrent les meilleurs mélanges des microalgues présentes dans le chenal et pour développer un modèle capable de simuler l'hydrodynamique et les phénomènes biologiques ayant lieu dans le CAHR. Ensuite, les transferts gazeux prenant place au système d'aération appelé « airlift » sont aussi évalués. Les deux paramètres qui sont modifiés lors des essais sont le niveau d'eau (0.25m, 0.4m et 0.6m) et le débit d'air ($<5 Nm^3/m^2h$, $10 Nm^3/m^2h$, $16.67 Nm^3/m^2h$ et $21.67 Nm^3/m^2h$). Le but final est d'utiliser les données collectées pour développer un modèle précis du CAHR afin de le faire fonctionner dans les conditions optimales.

Le travail a été réalisé en deux étapes. Premièrement, la méthodologie des essais a été mise en place à Arlon (Belgique) et des tests des traceurs et de transfert gazeux ont été réalisés sur un pilote à petite échelle. Ensuite, les mêmes tests ont été reproduits sur le CAHR installé dans la province de Ninh Thuan (Vietnam) dans le cadre du projet. Les résultats montrent qu'opérer le chenal à un débit d'air inférieur à $5 Nm^3/m^2h$ n'est pas suffisant pour apporter un mélange et un transfert gazeux suffisant. Un débit d'air supérieur ou égal à $10 Nm^3/m^2h$ fournit une dispersion appropriée (coefficient de dispersion supérieur à $0.268 m^2/s$) et un transfert d'oxygène suffisant (coefficient de transfert volumétrique supérieur à $1.6 * 10^{-3} s^{-1}$).

ACKNOWLEDGEMENTS

I would like first to thank my thesis supervisor Prof. Gauthier EPPE who gave me the opportunity to work on this project and who supported and trusted me from the beginning. I especially would like to acknowledge Prof. Jean-Luc VASEL who was of great support at every step of this thesis and made himself available whenever I needed help. Then, I would like to thank the two other members of my jury, Prof. Dominique TOYE and Prof. Andreas PFENNIG for their availability and for finding suitable answers to my questions.

I must express my profound gratitude to all the Vietnamese who helped me during my stay in Vietnam. First, Prof. Le HUNG ANH, who organized my travel and my schedule. Then, Mrs. Thuy CAO and Mr. Dung NGUYEN for their help to realize all the experiments on time in the Ninh Thuan province and, finally, I would like to thank Mrs. Hang NGUYEN and her husband for welcoming and accommodating me in their house.

Then, my sincere thanks also go to all the other people who contributed to the realization of my thesis including the workers of the Marine Breeding Center in the Ninh Thuan province, Mr. Guillaume DELAISSE and Mr. Vincent ROYAUX, my brother, for the technical support, and Mrs. Marie-Claire STAS and Mr. François DEPOUHON for the proofreading of this report and for the accommodation in Arlon. Last but not least, I would like to thank my friends and family for providing me with great support and encouragements during the five years of my studies.

Table of contents

List of figures

List of tables

1. Introduction

Today's world is facing one of the most important climate change ever and for the first time in Earth's history, this temperature increase is predominantly caused by human activities. This problem comes with several challenges such as the development of affordable renewable energies, the improvement of the recycling technologies or the reductions of the harmful pollution due to human activities ranging from using a car to growing shrimps. The majority of the developing countries are dealing with substantial recycling and wastewater treatment problems. Vietnam belongs to these countries. With its 3260 kilometers of coastline, a significant part of the Vietnamese economy is based on intensive aquaculture and most of the wastewaters resulting from this activity are directly poured into the sea without any treatment.

Algae and, more specifically, microalgae are considered as the "green gold" of the 21st Century. They may be used to produce animal feed, medicine, oil, biodiesel, biogas, etc. Microalgae cultures can also be used to treat wastewaters due to their capacity to consume nitrogenous and phosphorous compounds contained in these waters. This biomass has a high potential and many studies are currently conducted to develop efficient and economically advantageous microalgae cultivation and harvesting techniques.

Figure 1 – High Rate Algal Pond pilot installed in Vietnam

This Master thesis is a part of the RENEWABLE project led by the University of Liège (Belgium) and the Industrial University of Ho Chi Minh City (Vietnam). The goal of this collaboration is to develop an innovative and sustainable aquaculture wastewater treatment using microalgae. The microalgae are grown in a High Rate Algal Pond (HRAP), then harvested in order to be valorized afterwards. The microalgae technology may be an economical solution to the wastewater treatment problems faced by local companies. In this project, a HRAP pilot has been installed in Vietnam to assess the feasibility of the treatment using microalgae.

This work is divided into two main parts. The first part deals with a review of microalgal technologies. It introduces the different factors that affect microalgal growth. Then, the two main types of microalgae culture systems are presented, namely the HRAP and the closed photobioreactor (PBR), and, finally, different harvesting and dewatering techniques are reviewed. The second part of this work includes the setting up of a methodology to study the hydrodynamics and the gas transfer behavior of a HRAP pilot equipped with an airlift system. This research has been conducted on a small-scale pilot based in Arlon (Belgium). After that, the HRAP pilot implemented in Vietnam has been characterized using the same methodology. The pilot has been studied with different water levels and different air flowrates in order to obtain a clear idea of the ideal conditions for microalgae growth. In the future, the data collected during these tests will be of great importance to build a model to predict the hydrodynamics, the gas transfers and the biological phenomena occurring in the pond.

2. The RENEWABLE project

The RENEWABLE project is an acronym that stands for **RE**moval of **N**utri**E**nts in **W**astewater treatment via micro**A**lgae and **B**iofue**L**/Biomass production for **E**nvironmental sustainability in Vietnam. It is an ARES (Academy of research and higher education) project for the development cooperation in Vietnam coordinated by both Professor Gauthier EPPE (University of Liège) and Professor Le HUNG ANH (Industrial University of Ho Chi Minh City) and is planned to extend over 4 years between September 2016 and September 2020. The aim of the collaboration is to couple the production of microalgal biomass with the nutrients removal (nitrogen and phosphorous) present in aquaculture wastewater and to convert the biomass into either biofuel or animal feed. The Ninh Thuan province situated at 250kms from Ho Chi Minh City in South-Central Vietnam has been selected to receive a field pilot (see **Figure 2**[1]). This region benefits from an advantageous climate (average temperature around 27°C, driest region of Vietnam and excellent sunlight intensity) that is favorable for microalgae cultivation. Ninh Thuan province is also one of the four biggest fishing grounds of Vietnam with up to 60,000 tons produced every year. The region is well-known to produce and provide most of the seed shrimp for the entire country and there is a marine seed-breeding center equipped with high technology facilities where the pilot of the project will be installed (**Figure 3**). Moreover, the RENEWABLE project receives the help of regional government (DOST, Department of Sciences and Technology) of the province that will participate as a partner.

Figure 2 – Localization of the Ninh Thuan province

[1]Reference: https://www.voyagevietnam.co/cartes-du-vietnam/

Figure 3 – Marine Breeding Center in Ninh Thuan province

One of the primary goals of the RENEWABLE project is to ensure the feasibility of a significant decrease of the pollution load in wastewaters coming from the aquaculture and currently discharged in nature without any treatment. The reduction of the nutrient contents in aquaculture wastewaters will be performed using microalgae that will remove most of the nitrogen and phosphorous compounds and that can be valorized afterwards. This project will be beneficial to farmers, local authorities, shrimp industry and local people who will see their environment quality improved significantly.

The project is led by a consortium of academic professors, scientists, local government and local farmer association, local research center and industrial partners from Belgium and Vietnam who have decided to contribute to the project with their different expertise and skills. An interesting point of the RENEWABLE project is that it is an interdisciplinary project where biologists, geneticists, bio-engineers, chemical engineers, etc. work together in order to develop a viable and sustainable solution for the aquaculture wastewater treatment in Vietnam. This project takes place in a deep desire from the Vietnamese and Belgian authorities to improve the management and the protection of natural resources related to water including both environmental protection and sustainable development aspects.

This project aims at promoting a sustainable development of the aquaculture in Vietnam and, more generally, the technology developed here may be exported to other countries where fish and other crustacean are extensively grown. Emerging countries face considerable difficulties when it comes to wastewater and garbage treatments due to a lack of funds dedicated to these problematics and, also, a default of efficient technologies. A representation of these problems faced by the developing countries is presented in **Figure 4** taken in Phan Rang (Ninh Thuan) at 200 m of the place where the HRAP pilot

is installed. The wastewater coming from the neighboring houses and aquaculture companies is directly discharged in the sea. These waters usually contain high concentrations of nitrogen and phosphorous compounds that are harmful to the environment. The RENEWABLE project is a part of the future evolution of the aquaculture and brings a way to treat the wastewater at minimized costs and, moreover, to produce an exploitable biomass for economic gain. Global improvements are possible in every single part of the world as can be seen in **Figure 5** below taken in Mumbai where the beach has been cleaned from more than 5,000 tons of trash and where wildlife has reasserted itself. Indeed, three years only after this massive cleaning action, sea turtles chose this beach to store their eggs.

Figure 4 – Wastewater discharge in Ninh Thuan province

Figure 5 – Mumbai beach before and after a cleaning action in 2015[2]

[2]Reference: http://www.dailymail.co.uk

3. Theoretical background

3.1. Microalgae

The critical point in the production of final products such as biodiesel, biogas, bioethanol, animal feed or proteins for human usage microalgae as raw material is to obtain a sufficient productivity and, particularly, a suitable composition of the biomass. There are many factors influencing the growth and composition of microalgae, for example, pH, temperature, light, stress, cultivation systems, media composition, mixing frequency, mixing efficiency, etc ([1], [2], [3]). Furthermore, due to the high diversity of the different species and strains of microalgae, some with higher natural lipid content than others exist, which is highly desired for biodiesel production for example. It is thus useful to select carefully the microalgae used depending on the applications that are considered. Finally, genetic studies can be conducted in order to modify existing microalgae to obtain desired characteristics. On the other hand, it is necessary to check if the selected species can grow in the considered field conditions.

Microalgae have many advantages over terrestrial crops:

- They do not compete with food industry and can be grown in non-arable lands;
- Their productivity per unit area of land is higher than the one of terrestrial crops;
- They have a higher photosynthetic efficiency (around 3% but can be potentially above 10% ([4], [5]), compared to $0.2 - 2\%$ for terrestrial culture);
- They grow faster than plants due to their simple structure and can double their biomass within 24h ([6], [7]);
- They do not require large volumes of freshwater [8];

This section will first deal with the growth of microalgae and, second, with the factors influencing both the growth and composition of the biomass.

3.1.1. Growth of microalgae

The growth of microalgae is governed by photosynthesis which is the conversion of carbon dioxide, which is a source of carbon, and water, which is a source of electrons, into oxygen and organic matter using the sun or artificial light as a source of energy for the reaction. The principle of photosynthesis is the conversion of solar energy into chemical energy [9]. In a natural environment, photosynthesis follows a cycle with oxygen production during the day and normal respiration with carbon dioxide production during the night. Thus, the composition of the water in which the microalgae are grown varies with time, with higher dissolved oxygen content during the day and higher CO_2 content during the night.

As a result, the productivity of microalgae also varies during the day and the time of the year which mainly influences the amount of light received by the microalgae.

In a batch cultivation system, the growth of microalgae – considering only one type of substrate – can be summarized in the 6 following steps (**Figure 6**, [10]):

1- Lag phase
2- Exponential phase
3- Linear phase
4- Declining growth phase
5- Stationary phase
6- Death phase

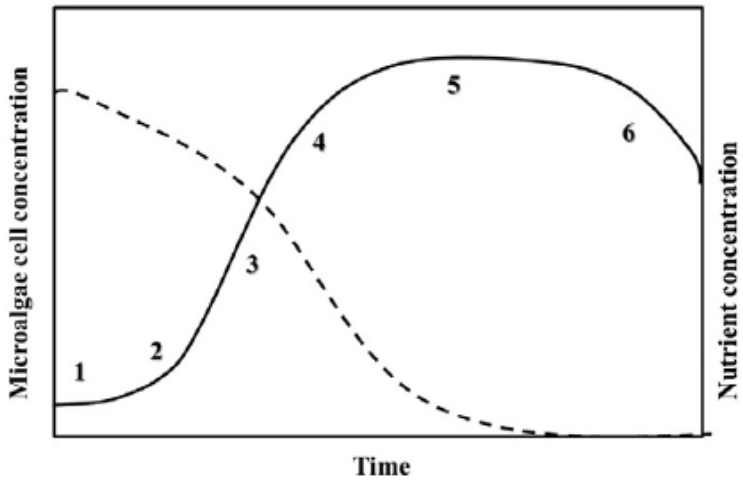

Figure 6 – Growth of microalgae in batch culture (solid line) and nutrient concentration (dashed line)

It has to be said that numerous processes exist and counteract the growth of microalgae. Among these, one can cite microalgae death, respiration, predation, grazing or sedimentation [11].

3.1.2. Factors influencing the growth of microalgae

- **Light**

As it has been presented in **Section 3.1.1**, microalgae production is highly related to photosynthesis efficiency which is itself related to the light climate in the culture media. Light limitation is the main controller of microalgal performance. Light inlet in HRAP can be notably regulated by changes in pond depth or hydraulic retention time (HRT) [12]. These factors have an impact on light absorption by the microalgae. Two different processes lead to a decrease in photosynthetic effect namely photoinhibition and photolimitation. Photoinhibition is the phenomenon by which microalgae receive too

much light so that the photosynthetic capacity of algae is negatively affected. Conversely, photolimitation is due to the deficiency of light in the culture media leading to a decrease in photosynthetic capacity. Even though these two processes are opposite in principle, they may occur simultaneously. Photoinhibition can occur near the surface while photolimitation occurs at the bottom [13]. The solar radiation has been studied many times and verified for dense algal culture. Light absorbance is following the well-known Beer-Lambert's law describing the intensity of the light I at a depth h in an algal medium:

$$I = I_0 \exp(-K_e h)$$

Where:

- I is the irradiance at depth h;
- I_0 is the irradiance at the surface;
- K_e is the overall extinction coefficient;
- h is the depth.

As it has been said, it is proven that the photosynthetic activity increases as the irradiance increases, up to a certain point where the photosynthesis decreases due to photolimitation [14]. The evolution of the photosynthesis activity as a function of the light irradiance is represented in **Figure 7** below. These two effects are taken into account by Steele's equation developed in 1962 [15].

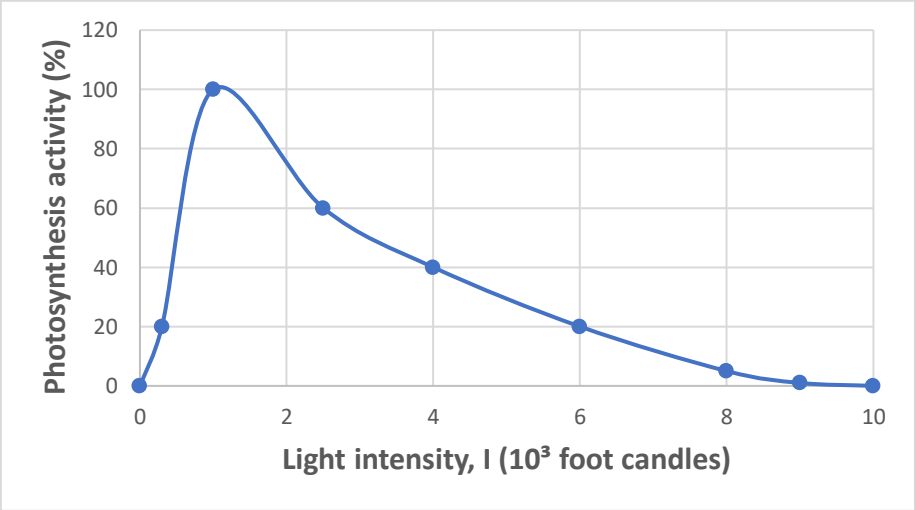

Figure 7 – Evolution of the photosynthesis activity as a function of light intensity in the sea[3]

[3] 1 foot candle (fc) = 10.76 lumen per square meter (lx)

Light absorption is highly related to the HRT: light absorption decreases significantly when the HRT increases due to the fact that self-shading is more likely to occur with higher HRT. It has also been proven that photosynthetic performance of microalgae increases when pond depth increases and the HRT decreases. Indeed, light attenuation is related to biomass concentration. According to Beer-Lambert's law, the higher the concentration, the higher the attenuation. Consequently, increasing the pond depth or decreasing the HRT can lead to a decrease of both biomass concentration and light attenuation. These observations are presented in [12] and, partially, in **Table 1** below. Other work ([16]) also showed that the productivity per unit area can be increased by 134 to 200% by increasing the pond depth from 200mm to 400mm. Increasing the depth which leads most of the time to a decrease in biomass concentration has the main disadvantage of increasing the difficulty of downstream processing of the microalgae, namely, dewatering and harvesting of microalgae [17].

Table 1 – Chl-a areal productivity (mg/m².d) [12]

Pond depth (mm)	HRT 4-days	HRT 6-days	HRT 8-days
200	48	59	78
300	63	82	86
400	79	97	100

It has also been noticed that microalgae are able to counter light attenuation by increasing light conversion efficiency which compensate reduced light availability. This results from a higher production of chlorophyll per cell in light deficient environments. Furthermore, it has been suggested that genetic and metabolic engineering could be used to modify microalgae in order to eliminate photosaturation and photoinhibition [18].

- **Temperature**

Temperature is considered as one of the most limiting factors, after light limitation. On one hand, microalgae are able to cope with temperature up to 15°C lower than their optimal temperature. But, on the other hand, exceeding the optimal temperature by 2 to 4°C may cause total culture loss [19]. Temperature has an effect on the chemical equilibrium of the species present in the water, on the pH and gas solubility. A study revealed the photosynthetic activity decreased as the temperature decreased [20]. The influence of temperature can be taken into account in the modeling of microalgae growth by means of "*thermic photosynthetic factor*". Finally, temperature has an influence on gas transfer due to a decrease in solubility with temperature, and an increase of the transfer coefficient $k_l a$.

- **Stress**

When a stress is applied to microalgae, it can result in the modification of the algal biomass composition and growth. This can be useful especially in the specific case of biofuel production where a high lipid content is required in order to achieve sufficient productivity. Two different types of stress will be discussed. First, nitrogen deprivation and, second, high salinity media.

In case of nitrogen deprivation, a phenomenon occurs inducing the displacement of fixed carbon from protein to either lipid or carbohydrate synthesis. This results in microalgae containing up to 40% of lipid [18]. Nevertheless, carbohydrates can achieve a 70% of dry mass content accumulation in the microalgae without any reduction in productivity, while lipid accumulation is accompanied by a decrease in productivity. This means that an optimum has to be identified as the total lipid production is the productivity of microalgae multiplied by their lipid content.

High NaCl concentrations have been proven to be even more effective than N-starvation for lipids accumulation in microalgae [21]. Indeed, salt stress has the capability to trigger the transition from carbon storage to energy storage leading to a high lipid content. Salt stress also results in cell enlargement and cell membranes damage which facilitates oil extraction. In case of shrimp pond effluents, this second type of stress is probably more attractive than the N-starvation.

- **CO_2 addition**

Carbon dioxide is the main carbon source which takes place in photosynthesis to produce organic matter and oxygen. Many studies ([22], [23], [24]) have suggested that carbon limitation is one of the main limitations in microalgae cultivation. This limitation can be overcome by CO_2 supply into the culture media. The carbon dioxide concentration in water depends on both thermodynamics and mass transfer [6].

The addition of carbon dioxide leads to several effects such as:

- a decrease in self-shading inside the media and, thus, an increase in light absorption efficiency by up to 128%;
- an increase of both electron transport and photosynthesis by up to 256% [22];
- an increase from 61 to 85% of the microalgal biovolume. It has been reported that annual average biomass productivity can be doubled in case of CO_2 addition, up to 16-20 $g/m^2.d$ [24].

- an increase of cell concentration. Indeed, if the system is supplied with 5% of carbon dioxide, the cell concentration reaches 64 million cells/mL whereas the concentration with atmospheric air is 48 million cells/mL in the case of *Nannochloropsis salina* [6].

One way to detect carbon dioxide limitation is to measure the pH which increases during daytime in case of CO_2 limitation. Typical values of the pH in case of daytime carbon limitation are above 10 due to photosynthetic uptake of carbon dioxide and bicarbonate [24].

- **Mixing**

In microalgae culture, a velocity of 10 to 30 cm/s is required to achieve a good mixing and avoid microalgae sedimentation resulting in a productivity decrease [25]. Mixing systems have a critical role in microalgae culture due to the following effects ([9],[25], [26]):

- Avoidance of the sedimentation of microalgae and increased exposition to the sunlight which leads to higher productivity of biomass;
- Avoidance of photoinhibition effect by inducing turbulence and vertical mixing in the waterflow;
- Better contact between microalgae and nutrients;
- Better repartition of the dissolved oxygen in the water;
- Better gas transfer of CO_2 from the atmosphere to the water;
- Maintenance of a uniform pH and temperature;
- Avoidance of dead zone formation that result in anaerobic conditions and the growth of anaerobic bacteria;
- Etc.

There are many different types of agitation systems. The most common one is the paddlewheel but, recently, it has been demonstrated that airlift systems are more efficient. Other aeration systems such as centrifugal surface aerators, vertical pumps, propeller-aspirator-pumps and diffused air systems can also be found ([27], [28]).

A paddlewheel is the most common and simple aeration system (**Figure 8** a and b [29]). This type of system consists in an impeller in which some paddles are fixed at the periphery of the wheels. The aeration efficiency highly depends on the rotation speed [30]. Its efficiency increases when speed is reduced below 100rpm in order to avoid backsplashing. Moreover, rotation speed is directly related to the energy consumption of the paddlewheel resulting in a decrease in energy utilization (half-speed operation demands one-third of the power) while the efficiency increases.

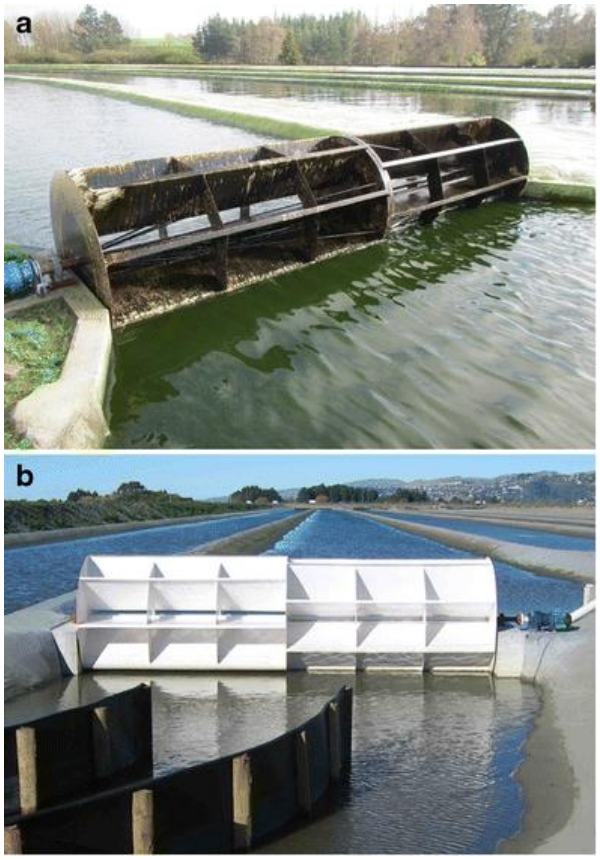

Figure 8 – Paddlewheel aeration systems

Airlift systems consist in insufflating fine air bubbles which creates an efficient oxygen transfer and a high degree of mixing [26]. In these systems, gas is sparged from the base and rises up in the riser and goes down in the downcomer (region with no gas injection) ([31], [32]). Airlift systems can be improved as can be seen in [33] where a vertical triangular airlift loop was designed in order to decrease mixing times and volumetric power consumption. There are many ongoing studies in order to improve mixing efficiency and, more importantly, decrease energy consumption in order to get economically viable cultivation systems. Factors influencing the efficiency of the mass transfer in airlift systems are geometric design, presence of stirrer, sparger type and bubble size [31]. The design of the airlift system used on the HRAP pilot in Vietnam is presented in the following **Figure 9.**

Moreover, it has been studied that mixing frequencies (continuous (M-cont), mixed every 45 min (M-45), mixed every 90 min (M-90) and no mixing (M-0)) can have an impact on microalgal performance depending on the species. For example, after 12 days, the biomass concentration was respectively 35% and 90% lower in M-90 and M-0 than in M-cont for *C. vulgaris*. On the other hand, there were no significant differences between M-cont and M-45 which means that it could be possible to reduce the mixing energy cost by using the paddlewheel every 45 minutes instead of using it continuously. It has also

been noticed that the nutrient removal efficiency decreases when the mixing frequency decreases which is obvious, knowing that microalgae consume these nutrients during their growth [1]. Of course, the risk of sedimentation during the non-mixing period has to be taken into account.

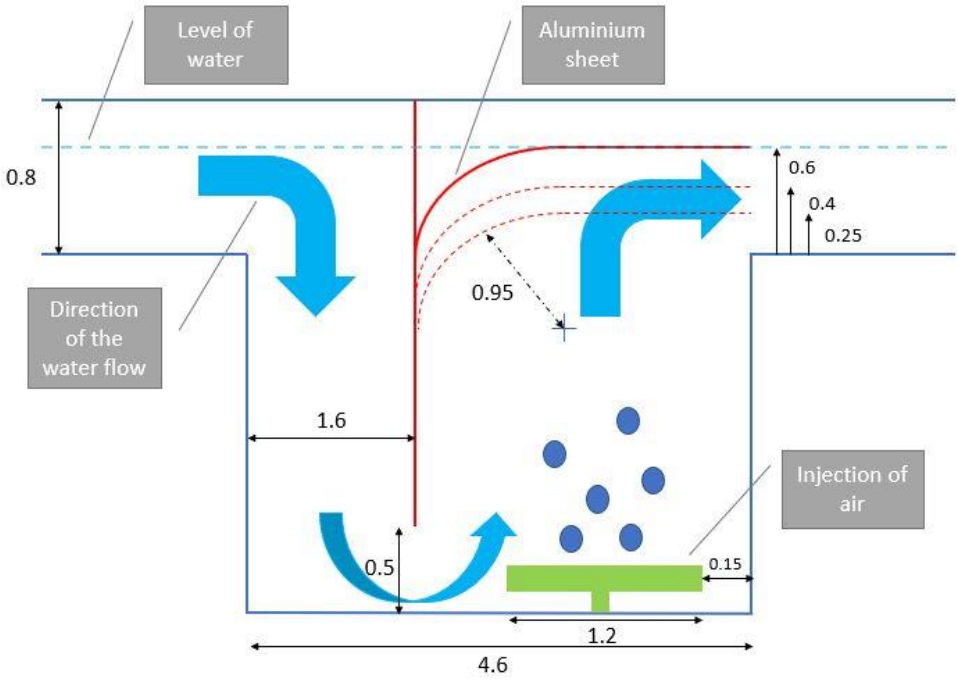

Figure 9 – Design of the airlift system used on the HRAP pilot in Vietnam

Therefore, mixing is an unavoidable point in microalgae cultures but it represents an important investment in terms of both capital and energy. Furthermore, mixing systems lead to the creation of vortexes which are a source of energy dissipation [17] and to the erosion of the installations.

- **Others**

Other factors such as the cultivation systems, seasonal effects or media composition have an influence on microalgae growth. The first one will be discussed in the next section. Seasonal effects can be seen in the pH, the temperature or the amount of light received by the microalgae. Nutrients removal also varies from season to season leading to higher efficiency in Spring than in Winter [16]. Regarding the media composition, this subject will be extensively discussed in a following chapter.

3.2. Reactors

Two main categories of cultivation systems can be distinguished, namely, open and closed systems. Open reactors include open ponds and raceway ponds also known as high rate algal ponds. Closed systems are usually referred to as photobioreactors.

3.2.1. High Rate Algal Pond (HRAP)

HRAPs are an improvement of traditional algal ponds that were first investigated in the 50's [16]. HRAPs are usually designed as open, shallow (from 0.2 to 0.6 m [34]), raceway ponds where the wastewater is introduced in order to be treated. The water is usually set in motion using a paddlewheel or an airlift and the ideal flow velocity is between 10 to 30 cm/s to avoid sedimentation of the microalgae. Many parameters influence the efficiency of a HRAP such as the depth, the nature of the flow (laminar or turbulent), the design, etc. Even though HRAPs are a well-established technology, there are still some possibilities of improvement to enhance the productivity while reducing the cost of production. At a commercial scale, over 95% of the microalgae production worldwide is issued from raceway reactors [35]. A representation of some HRAPs in Israel is presented in **Figure 10**.

Figure 10 – High rate algal ponds generating nutraceuticals in Israel[4]

[4]Reference : https://www.israel21c.org/the-top-12-ways-israel-feeds-the-world/

HRAPs are recognized for their good ability for wastewater treatment and their high microalgal productivity [12]. Compared to other wastewater treatment ponds, HRAPs are effective to remove nutrients and pathogens due to high light availability and microalgal biomass causing a good effluent quality. HRAPs have been widely studied during the last decades because they present the following advantages:

- Lower capital and operational costs due to their simple design and construction compared to photobioreactors;
- High nutrient removal rate;
- Turbulent mixing that leads to high productivity. Indeed, as it has already been discussed in **Section 3.1.2**, a good mixing in HRAPs induces low sedimentation rate, small nutrient and gaseous gradients and good microalgae light exposition;

As it has been said, some features of HRAPs may be optimized in order to obtain a productivity as high as possible. Among these, depth has been identified as being one of the most important characteristics in HRAP as it is the main factor determining the amount of light received by the microalgae and the frequency at which biomass is exposed to the light. Areal productivity of culture systems can be increased between 134 and 200% by doubling the depth from 200 to 400 mm [16]. Improvement of the mixing has also been studied in the late 90's [34] due to the finding that microalgae situated in the deeper layers did not contribute to the treatment process while the microalgae situated in the superficial layer suffered from photoinhibition. Inducing a vertical mixing resulted in a maximal exposure of the microalgae to the light and, consequently, in optimizing the photosynthetic activity of the biomass. Furthermore, higher photosynthetic activity obviously results in higher carbon dioxide utilization by the microalgae, it is thus necessary to manage the CO_2 supply properly.

Other studies have been made on the design of HRAPs and focused on the reduction of energy losses due to water resistance. It appeared that the main energy losses takes place in the curve so that a re-design of the curves may be a solution to reduce the energy requirements for water circulation [36]. Some other re-design criteria have been identified such as reduction of water depth, increase in culture concentration in order to ease downstream processing, substitution of the traditional paddlewheel mixing by a more energy-efficient pumping system (e.g. airlift system) or the reduction of the flow velocity while maintaining a suitable mixing of the microalgae [17].

The main drawbacks of HRAPs are the high risks of contamination (such as bacteria, other competing organisms or predator species) due to the fact that they are highly exposed to their environment, the low biomass concentration (resulting in large surface of land needed) which is an inconvenience for downstream processing such as dewatering,

poor gas-liquid mass transfer (that can be improved by an efficient aeration system) and the lack of temperature control ([35], [17]). Moreover, they have a limited exposure to light, a complex carbon management and a lower long-term productivity as compared to closed photobioreactors [6]. The main operational energy requirements of HRAPs are for the pumping system, mixing and bubbling of CO_2 when necessary [8].

3.2.2. Photobioreactors (PBRs)

PBRs are the most common type of closed cultivation systems. There are several shapes that can be used for the design of the PBRs (tubular, vertical flat-plate, bubble column, split cylinder airlift, plastic bag, etc.). A representation of a serpentine PBR is presented in **Figure 11**[5] below. The light supply usually comes from the sun for outdoor cultivation systems while artificial light (e.g. LED and optical fiber) is commonly used for indoor photobioreactors. Nevertheless, sunlight can be transmitted from outside to illuminate indoor PBRs [37]. In general, PBRs can be classified in two main categories: vertical and horizontal. Vertical PBRs have the advantage of limiting the photosaturation and, as a result, of achieving higher productivity. The photosaturation limitation is possible due to the effect of light dilution resulting from the orientation of the PBRs [9]. The result is that a larger number of microalgae are exposed to a lower light intensity which allows them to optimize their photosynthetic efficiency. Vertical PBRs have several other advantages over horizontal PBRs such as:

- They are more suited for scale-up;
- They use less energy for cooling due to their low S/V ratio;
- They achieve a higher overall productivity;
- They have a high volumetric gas transfer coefficient.

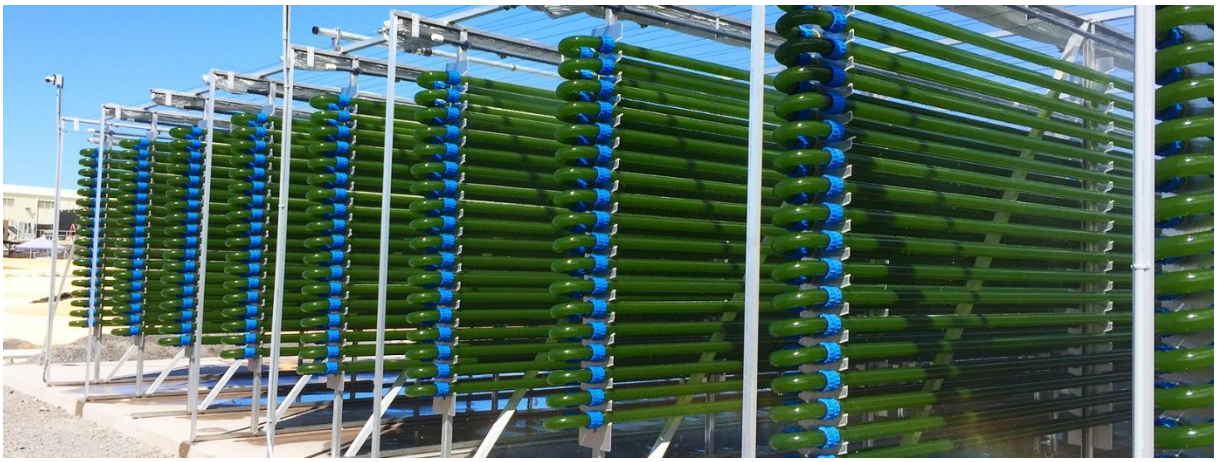

Figure 11 – Vertical serpentine PBR deployed by Varicon Aqua

[5]Reference: www.variconaqua.com

Nowadays, scaling up PBR remains a challenge because it is difficult to keep the different variables (temperature, mixing, light, mass transfer) in the desired range. Most reactors are designed and scaled up thanks to semi-empirical methods [38]. Therefore, some studies are conducted in order to improve current PBRs to achieve larger mass concentration, growth rate and lower energy use and capital costs [39]. By optimizing the operational conditions and the design of PBRs, they could possibly be used at a commercial scale in the future. A recent study has identified the principal features that a PBR should have to be commercially efficient, these characteristics include a highly illuminated surface/volume ratio in order to increase the solar irradiance, easy temperature control, a good mixing and effective mass transfer and, finally, low operating and capital costs [38].

The main limitations of PBRs are the difficulties encountered to control the temperature and the large fraction of dark zones. Compared to open ponds, photobioreactors require a higher initial investment cost, but in some cases, they can produce microalgae at a lower final price. Nevertheless, other work showed that raceway ponds have a lower energy consumption per unit of product than photobioreactors [17]. The question of energy consumption is clearly subject to further debates in order to identify the conditions for which PBRs are favorable over HRAPs. On the other hand, they have a higher productivity, a better contaminant management and an improved utilization of CO_2 and nutrients than open pond systems [6].

Given the fact that PBRs have a higher productivity and are less likely to produce contaminated culture, this type of cultivation system can be combined with HRAPs that have lower operational and capital costs. The first step is the microalgae cultivation within the photobioreactor to produce a sufficient amount of sufficiently pure microalgae that will be injected in the HRAP during the second step. The PBR is thus used for sowing while the HRAP is used for microalgae growing and production.

3.2.3. Comparison of PBRs and HRAPs

The main features of both photobioreactors and high rate algal ponds are summarized in **Table 2** below.

Table 2 – Comparison of PBRs and HRAPs [19]

Culture systems	PBRs	HRAPs
Contamination risk	Low	High
Process control	Easy	Difficult
Mixing	Uniform	Usually poor
Microalgae concentration	High	Low
Operation modes	Batch and semi-continuous	Batch and semi-continuous
Investments	High	Low
Operation costs	High	Low
Light utilization efficiency	High	Poor
Temperature control	More uniform t°	Difficult
Productivity	3-5 times higher	Low
Scale up	Difficult	Difficult

3.3. Harvesting and dewatering techniques for separation

Most of the time, the cultivated biomass is highly diluted and the microalgae are very small which results in huge harvesting and dewatering operational costs and, thus, rendering microalgae products less economically attractive. Microalgae production at commercial scale is highly dependent on the findings of an efficient and cost-effective harvesting and/or dewatering technology in order to be economically viable. Nowadays, numerous studies are conducted ([40], [41], [7], [42], [43]) in order to develop new techniques or to improve existing ones. The reason why this step of the process has received a lot of attention during the last few years is because it is the bottleneck of the microalgae culture. There are many different harvesting and dewatering techniques such as:

- Gravity sedimentation;
- Centrifugation;
- Coagulation-flocculation;
- Filtration and screening;
- Flotation;
- Membrane filtration;
- Magnetic separation;
- Etc.

Nevertheless, only low-cost techniques should be considered in the context of microalgae knowing that lowering the cost is the first priority. For the microalgae production process, the harvesting and dewatering techniques should be chosen considering factors such as downstream processes, end products, energy consumption and costs. It has been shown that for biodiesel production, most of the current technologies for biofuel production result in a negative net energy balance which means that the process consumes more energy than that produced while burning biofuel [41]. The dewatering process represents 20 to 40% of the global energy demand of the process [41]. Furthermore, depending on the final product considered, the solid percentage to be reached may vary. For lipid extraction leading to biodiesel production, the algal biomass needs to contain 90% of solids in order to be allowed to utilize the same technology as for soybean lipid extraction. For biomass co-fired with coal, biomass should have between 50 and 90% of solid content [8]. The dewatering techniques presented below allow to reach a solid content around maximum 30%. Consequently, another technique has to be considered to reach higher solid percentages namely the evaporation.

A general representation of microalgae culture and processing is represented in **Figure 12** below. The algae effluent containing between 0.02 and 0.06 % TSS is harvested and concentrated in one or two step(s) in order to reach sufficiently high concentrations (from 15 to 25% or above) which are suitable for further processing such as biodiesel production [7]. In the case of biodiesel production, microalgae should be concentrated as much as possible in order to ease the lipid extraction step. High microalgae concentration decreases the extraction and purification costs.

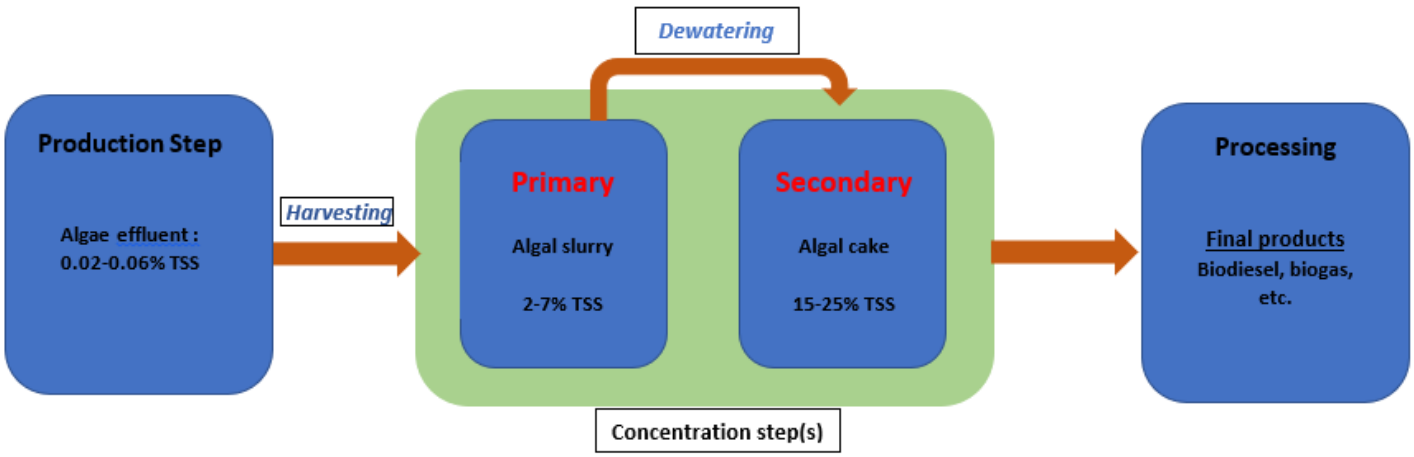

Figure 12 – Schematic representation of microalgae culture and processing

Existing harvesting and dewatering techniques can be compared based on the rate of water removal (productivity), the solid content that can be achieved and the efficiency/yield of the technique (number of recovered microalgae as a fraction of total processed algae effluent).

3.3.1. Gravity sedimentation

This is the simplest technique for microalgae harvesting. It separates the algal effluent into a concentrated slurry and clear liquid. It usually requires a lamella separator and sedimentation tanks. A general representation of the gravity sedimentation process using lamella is presented in **Figure 13** below. The microalgal suspension is continuously inserted with the use of pumps while the slurry is collected discontinuously. The main energy consumption comes from the pumps used to convey the algal slurry. As it will be discussed later in **Section 3.3.3,** flocculants can be added to increase the sedimentation rate. Sedimentation is not widely used in the industry but is a reliable process allowing to reach up to 1.5% TSS in the slurry. The performances of this technique highly depend on the density of the biomass. Indeed, it has been demonstrated that microalgae with low density do not settle sufficiently and are poorly removed from the suspension [7].

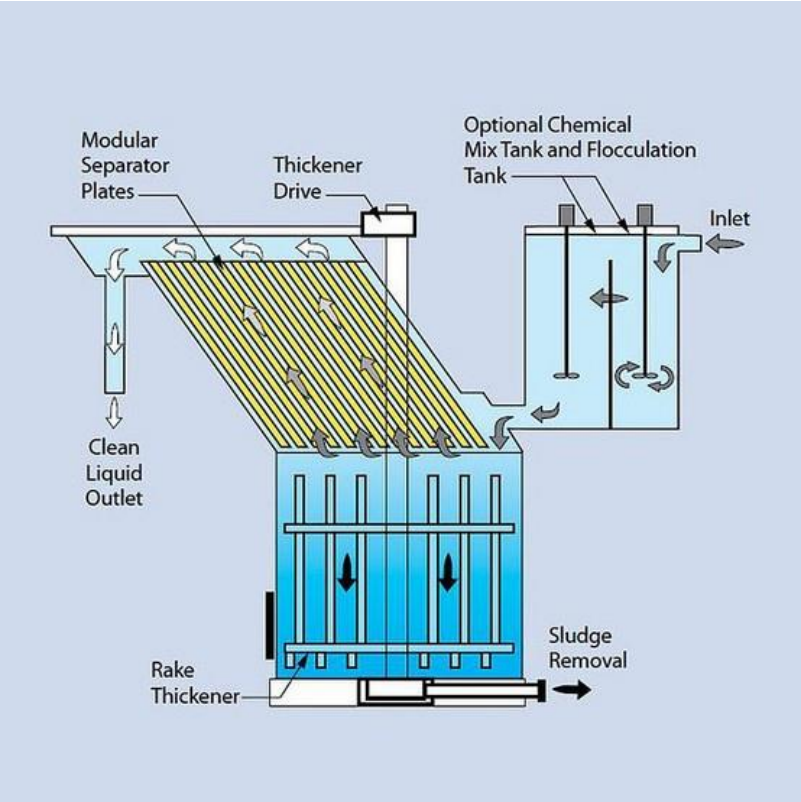

Figure 13 – Lamella clarifier[6]

[6]Reference: https://www.savonaequipment.com/en/lamella-gravity-settler-p130957

3.3.2. Centrifugation

Centrifugation processes use centrifugal forces to separate liquids and solids using particle size and density differences of the medium components. It has been demonstrated that centrifugation is efficient for microalgae recovery. Furthermore, lab-scale experiments showed that 80-90% of microalgae could be clarified and recovered within 2 to 5 minutes at 500g-1000g [7].

An example of the microalgae separation process using centrifugation is presented in **Figure 14** below. It can be seen that, as it is often the case, a pre-concentration step is used in order to reach a sufficient concentration factor. It has been demonstrated that this machine is able to reach 22 to 25% TSS by using a centrifugal force up to 10,000g.

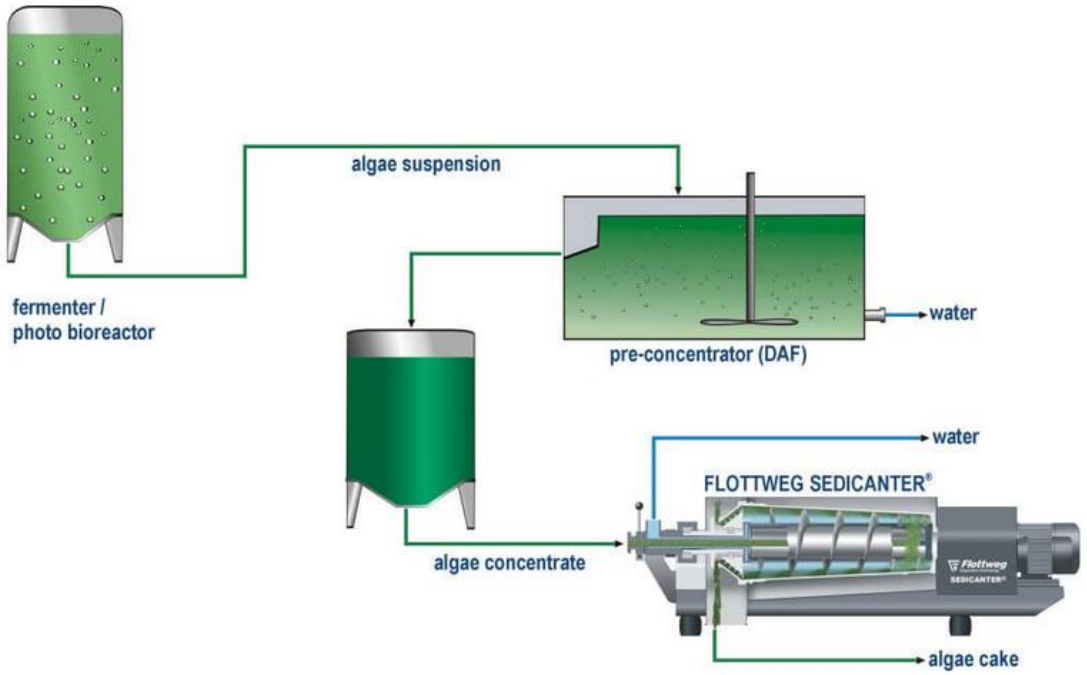

Figure 14 – Separation of algae suspension using centrifugation and a pre-concentration step[7]

Energetic consumption of this process varies from 0.5 to 8 kWh/m^3. The main advantages are that it is commercially established for microalgae products (nutraceuticals, nutrient supplements). Among the drawbacks one can highlight that it is cost and energy intensive and it often requires to be combined with other pre-concentration techniques. In addition, the exposure of microalgae to high centrifugal and shear forces can damage cells. Last, the processing of large volumes of algae effluents can be too long and costly [41].

[7]Reference: https://www.flottweg.com/fr/applications/graisse-et-huile-biocarburants/algues/

3.3.3. Coagulation-Flocculation

Coagulation-flocculation followed by solid/liquid separation is one of the low-cost (pre-concentration) technique which is capable of managing large amounts of water and biomass. This technique results in a solid (pre-)concentration in microalgae from 1 to 5% w/w. Coagulation generally consists in the neutralization of the negative charges carried by microalgae resulting from the ionization of certain functional groups [7] while flocculation is the aggregation of these neutral microalgae that will later form some flocs. The superiority of this harvesting technique over traditional harvesting techniques such as centrifugation or flotation comes from the fact that it is able to treat large volumes of algae effluents and it is applicable to a high diversity of algae species. Coagulation requires the use of a coagulant that should be chosen taking into account downstream processing. For example, salts of aluminum or iron were commonly used as a coagulant but they can contaminate the end products. The use of natural organic coagulants (tannin, modified starch) may be a solution to overcome this drawback. These coagulants (or flocculants) are becoming more and more popular notably due to health concerns about polyacrylamide based flocculants [40]. Generally, organic polymers used as a flocculant result in more than 90% of biomass recovery for coagulation-flocculation and sedimentation or flotation processes.

Figure 15 shows the principle of coagulation-flocculation. Flocculant is added (**Step 2**) inducing the neutralization of the microalgae negative charges that are now able to agglomerate (**Step 3**) and to form flocs that are more suited for sedimentation (**Step 4**).

Flocculation itself has been proven to be efficient for microalgae concentration but it may be insufficient in specific conditions [7]. It means that sedimentation of microalgal flocs cannot occur and that flocculation should be combined with some other technique such as flocculation-flotation or flocculation-centrifugation to be more effective. The flocculation process is then used as a pre-concentration step. Moreover, to each flocculant corresponds an adequate dose and pH range for which the flocculation effect is optimal.

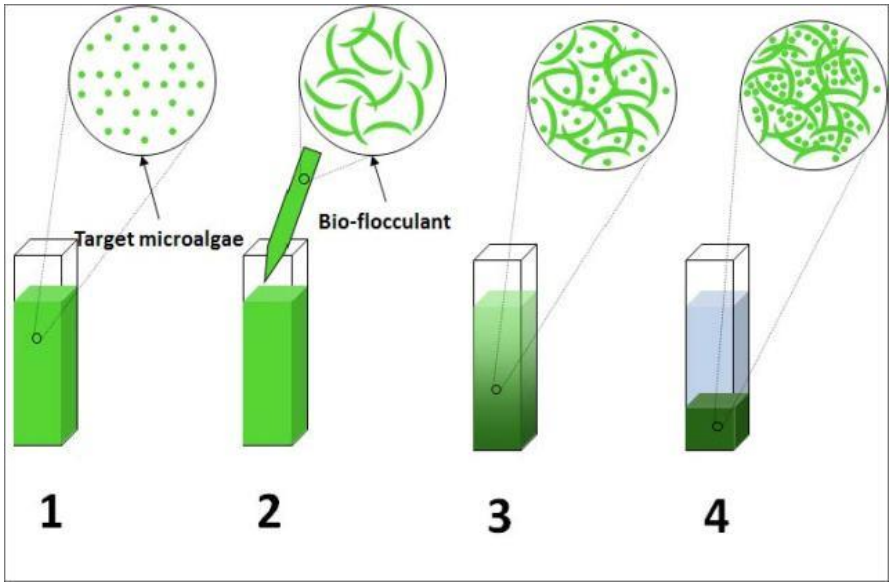

Figure 15 – Principle of coagulation-flocculation[8]

There are different types of flocculation process and the principles of flocculation vary slightly from one type to another. The first type is the polyelectrolyte flocculant whose flocculation principle is based on charge neutralization and particle bridging. This involves bonds between the polymer molecule and the microalgal surface. Bonds can be of electrostatic or chemical nature. These bonds lead to a 3-dimensional matrix constituting the flocs. The second type is inorganic flocculants that rely on the neutralization of the negative charge carried by microalgae by providing a sufficient amount of positive charge as previously explained. Once the microalgae are neutralized, they start to form flocs that can either sediment or float. The next type is called combined flocculation which is a flocculation process that uses more than one type of flocculant. It has been demonstrated that this multistep flocculation is able to reach a higher microalgae recovery and to reduce the degree of inorganic flocculant needed.

Then, autoflocculation has been widely studied during the past few years. It corresponds to the spontaneous floc formation and sedimentation of microalgae. It has been shown that this type of flocculation is associated with a rise in pH due to carbon dioxide consumption, resulting from synthetic activity of the algae, and the precipitation of inorganic precipitates. Another mechanism, namely the aggregation between microalgae and bacteria has also been cited. Changes of alkaline conditions to reach the suitable values for autoflocculation have also been proven to be effective to induce the floc formation [7]. A study has demonstrated the efficiency of bio-flocculation which is the addition of autoflocculating microalgae to the algal effluent. The recovery efficiencies for a bio-flocculation process are in the same range as for chemically induced flocculation

[8]Reference: https://www.wur.nl/en.htm

when autoflocculating microalgae are added at a ratio of 0.25 [44]. The recovery increased from 25% to 41% in the better case while the energy demand for centrifugation proceed after bio-flocculation was reduced.

It has to be mentioned that for marine microalgal flocculation, the water salinity has a great influence on the efficiency of the flocculant. For example, it has been demonstrated that high salinity induces the inhibition of the flocculation with polyelectrolytes. Consequently, other types of flocculant such as inorganic flocculant should be considered in the case of marine environment [7].

Energetic consumption of this process varies from 0.1 to 14.8 kWh/m^3, taking only into account the electricity used during dewatering operations [41]. The main advantages are that it is energy efficient and that the technology is established in water and wastewater. Among the drawbacks one can highlight the life cycle impact of the flocculant, the limited conditions (pH, ionic strength) under which this technique can be applied for certain species and the potential contamination of the biomass for non-natural organic flocculants [41].

3.3.4. Filtration and screening

This method uses a permeable medium that allows liquid to pass through while solids are retained. This technology has been proven to be suitable for large microalgae but it becomes inefficient for the smaller ones [45]. Screening consists in passing a solution through a screen with a specific pore size allowing the particles with a smaller diameter than the pore size to pass through and stopping the others. The two main types of screens that are utilized for microalgae harvesting are microstrainers and vibrating screen filters. Microstrainers consist in rotating filters (rotating drum) equipped with fine mesh screens and continuous backwashing. A representation of a microstrainer is shown in **Figure 16**. The main factor that determines the cost is the flow-through rate of the filter which is determined by the size of the screen openings. Two problems can be encountered depending on the microalgae concentrations. High concentrations can result in blocking of the screen and low concentrations can induce inefficient microalgae capture.

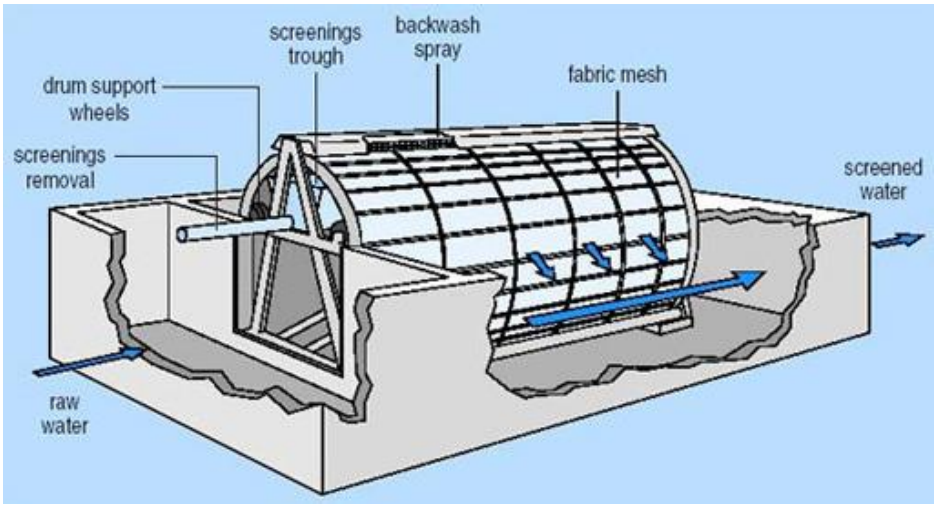

Figure 16 – Typical microstrainer[9]

Filtration requires a pressure drop across the filter in order to be efficient and to force the fluid through the filter. The driving force used (gravity, vacuum, pressure, or centrifugal) depends on the level of pressure to be applied. Two main types of filtration exist:

- Surface filters: a thin film or cake formed by the solids that are deposited on the filter medium;
- Depth filters/Deep bed filters: the solids are deposited within the filter medium.

The major constraint in the case of microalgae filtration is that media that are sufficiently fine to retain microalgae tend to bind so that backwashing is required leading to lower microalgae concentrations.

One potential filtration device that could be used for large volume of algal effluent is the tangential flow filtration also called cross flow filtration. In this technique, the medium flows tangentially across a membrane and the retentate is recirculated across the membrane which allows to keep the cells in suspension and to partially avoid fouling. This technology achieves higher filtration rates compared to tradition filtration, or other techniques such as centrifugation, flocculation or sedimentation. Biomass recovery between 70 and 90% can be reached. This system has the advantages to preserve the structure of the microalgae (motility, negative surface charge), to be suitable for shear sensitive biomass and to be cheap [7].

[9]Reference: http://www.open.edu/openlearn/ocw/mod/oucontent/view.php?id=3317&printable=1

Press or belt-filtration can be used for microalgae harvesting. A filter press uses pressure filtration to separate the microalgae from the water. The filter is usually made up of a cloth and most of the filtration is done by the filter cake that is building on the cloth during the filtration [46]. A belt filter, for its part, uses a moving cloth and the filtration is often induced by vacuum under the filter cloth [47].

Energetic consumption of this process varies from 0.5 to 5.9 kWh/m^3 [41]. The main advantage is that no chemical is used so that biomass contamination cannot occur. Among the drawbacks the incapability to filter small microalgae cells, that filters have to be cleaned and replaced regularly and that the biomass recovery is lower than for the other harvesting techniques [41].

3.3.5. Flotation

The flotation technique for microalgae harvesting can be considered as more effective than sedimentation. It is a physico-chemical type of gravity separation where air or gas is bubbled through the algal suspension and the gaseous particles bond to the solid particles contained in the solid-liquid mixture. These particles go upwards to the surface where they accumulate and form a float that can be removed. The size of the particles present in the suspension is an important factor in a flotation process; the smaller the particles, the more likely the particles can be carried to the surface. Another important factor is the probability of bonding between bubbles and particles which is also influenced by the size of both the particles and the bubbles. Three main flotation techniques can be highlighted: dissolved air flotation, dispersed air flotation and electrolytic flotation. These techniques will be briefly presented in the following [7].

Energetic consumption of this process varies from 1.5-20 kWh/m^3. The main advantage is its increased effectiveness compared to natural sedimentation. Among the drawbacks, one can highlight the fact that small bubbles are more efficient but more energy intensive and that pre-flocculation is often required [41].

- **Dissolved air flotation**

This is the most widely used flotation technique applied in industrial effluents and it can be used for microalgae harvesting as well. The first step consists in the pre-saturation of the water stream in air and its reduction in pressure. This liquid containing the dissolved air is injected in a flotation tank using nozzles or needle valves. This process will generate bubbles that move upwards through the microalgal suspension carrying the solid particles with them. Then, the floats can be collected at the surface.

The bubbles have a size ranging from 10 to 100 µm and the size is controlled by the saturator and the injection flow rate. Small bubbles can be obtained by applying a saturator pressure above atmospheric pressure. On the other hand, the injection flow rate should be high enough to provide a sufficient pressure drop and to prevent backflow and bubble growth at the pipes. The concentration of the slurry skimmed at the surface of the flotation tank depends on both the velocity of the skimmer and its height above the surface of the water.

The dissolved air flotation technique is represented in **Figure 17** below. In this case, as it has already been mentioned, the flotation is preceded by a pre-flocculation to increase the efficiency. The algal effluent flows continuously into the unit. Flocculant is added and mixing is applied to accelerate the flocculation. Then, the flocculated microalgae reach the flotation cell where small air bubbles are rising.

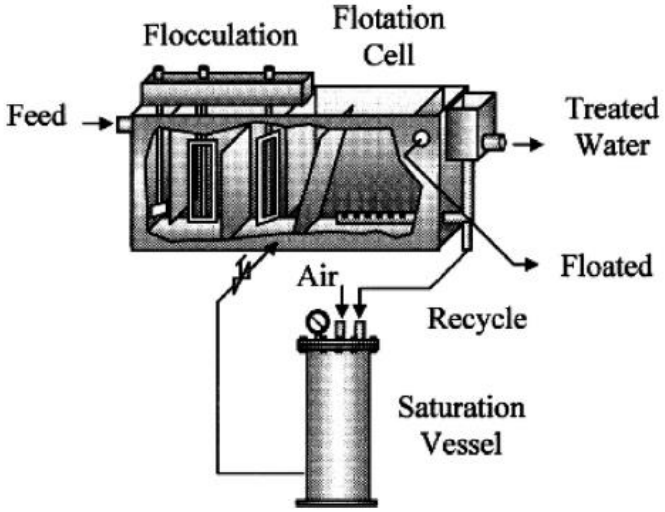

Figure 17 – Dissolved air flotation for microalgae harvesting [7]

- **Dispersed air flotation**

In this case, the bubbles are induced by a high-speed agitator and an air injection system. The gas is introduced at the top and mixed with the liquid. Then, it is allowed to pass through a disperser that will form bubbles that can range from 700 to 1500µm in diameter. In this case, a surfactant is used to prepare the microalgae surface for flotation or to improve the agglomeration. Surfactants modify the hydrophobicity of microalgae surface to increase the probability of microalgae-bubble bonding.

- **Electrolytic flotation**

The principal advantage of electrolytic flotation compared to both dissolved or dispersed air flotation is that this technique does not use any chemical compound. These chemical additions result in the increase of total dissolved solid and the higher risk of contamination of the medium. Electrolytic flotation uses the fact that microalgae can behave like colloid particles meaning that they can be separated from a water-based medium solution using an electric field to set them in motion. The main advantages are:

- Environmental compatibility;
- Versatility;
- Energy efficiency;
- Safety;
- Selectivity;
- Cost effectiveness.

Among the electrolytic flotation processes, one can cite electrolytic coagulation, electrolytic flotation, and electrolytic flocculation. Electrolytic coagulation uses metallic electrodes that will release the positive ions that induce the coagulation of the microalgae cells that are negatively charged. Electrolytic flotation uses an inert electrode coupled with a reactive metal cathode that will introduce hydrogen bubbles coming from the hydrolysis of water. On one hand, the positively charged ions such as Al^{3+} will attract the negatively charged microalgae to form the flocs and, on the other hand, the hydrogen bubbles will carry the flocs towards the surface of the water. Finally, electrolytic flocculation utilizes two inert metal electrodes to which an electric charge is applied. The microalgae will be attracted by the positively charged anode where they will lose their negative charge. From that time, the molecular attractive charges will become predominant and the microalgae can flocculate [48].

3.3.6. Membrane filtration

Compared to other commercial dewatering techniques such as centrifugation, flocculation or belt and chamber press filtration, membrane filtration does not require any chemical addition and usually consumes a lower amount of energy than the previously listed techniques. A membrane serves as a selective barrier that allows passage of water but not microalgae. Two types of membranes are commonly studied: microfiltration (MF – 0.1-10 µm pores) and ultrafiltration (UF – 1-100 nm pores). Membrane filtration also permits to reuse the permeate that has been cleared from microorganisms bigger than the pore size leading to a disinfected growth medium.

Membrane filtration systems can be divided into four main configurations: cross-flow, submerged, dynamic or shear-enhanced and forward osmosis. UF and MF are most of the time used in cross-flow mode with a flow directed tangentially to the membrane surface (**Figure 18**). UF and MF operated in submerged mode consists in the direct placement of the membrane bags into the water containing the microalgae. Then, a pressure gradient is applied by means of vacuum pump (**Figure 19**). Dynamic or shear-enhanced membrane filtration integrates rotating disks or rotating or vibrating membranes. Finally, UF and MF can also be operated in forward osmosis that requires an osmotic pressure gradient between the algae medium and the outer water source (**Figure 20**).

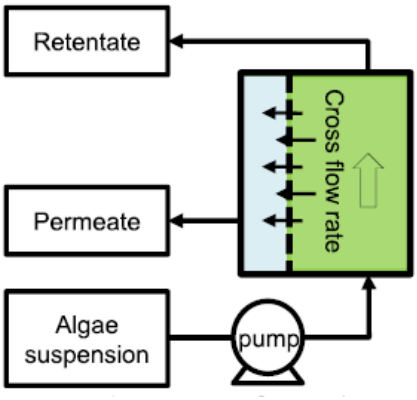

Figure 18 – Membrane filtration operated in cross-flow mode [41]

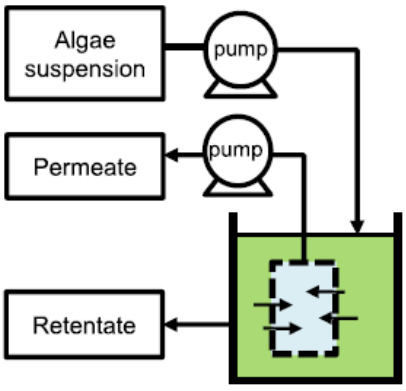

Figure 19 – Membrane filtration operated in submerged mode [41]

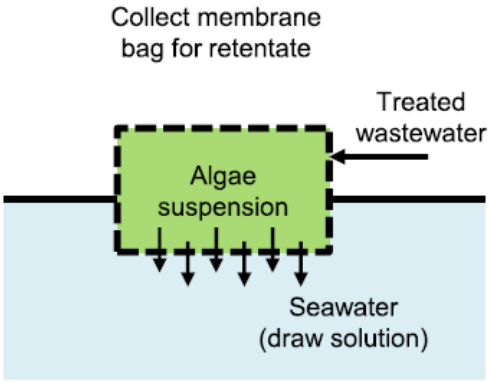

Figure 20 – Membrane filtration operated in forward osmosis mode [41]

The main advantages and drawbacks of the four different configurations have been summarized in **Table 3** below.

Table 3 – Advantages and drawbacks of different membrane configurations [41]

Membrane configuration	Advantages	Drawbacks
Cross-flow	• Potential for high productivity due to high cross-flow velocity + shear rates at the membrane surface	• Fouling • High energy consumption (applied pressure + liquid crossflow) • Hydrodynamic may cause cell breakage + extracellular polymers release that promote fouling
Submerged	• Reduced energy and cost requirements (no liquid pumping) • Lower shear (lower cell rupture risks → lower fouling and higher biomass recovery)	• Only lab and pilot scale • Lower productivity • May not be compatible with continuous processes and open cultivation systems
Dynamic or shear enhanced	• Enhanced shear → increased flux and reduced fouling • Higher productivity than submerged systems • Higher biomass recovery than cross-flow systems	• Only lab scale • Complex and high equipment costs • Consumes more energy (to provide vibration and for pumping)
Forward osmosis	• Potential for high energy and cost efficiency • Being tested by NASA at pilot scale	• Biofouling on the seawater exposed side • Final concentration relatively low • Only for coastal cities

Membranes can be organic or inorganic and their performances (permeate flux and fouling resistance) are highly dependent on the composition. Organic membranes (mostly polymers) predominate due to their availability. Inorganic membranes are mostly used for applications requiring high temperature and/or high chemical stability. Once fouling happens, both organic and inorganic membranes can be washed by backflushing in order to remove the foulant. Conversely to organic membranes, inorganic membranes can withstand chemical cleaning and the back-pressure applied for the backpulsing. The most performant organic membrane that has been tested for dewatering is the polyacrylonitrile (PAN).

The energetic consumption of this process varies from 0.17 to 2 kWh/m^3. The main advantages are:

- Potentially better harvesting performances, energy requirements and costs;
- Allows for reuse of permeates;
- No chemical input or biomass contamination. This lead to simplified downstream processing (extraction, conversion, refining) for biofuel production.

Among the drawbacks one can highlight the research needed to improve existing technologies and the membrane fouling and pressure losses when high biomass concentrations are encountered [41].

3.3.7. Magnetic separation

Harvesting of microalgae using magnetic nanoparticles have been reported more than forty years ago and studies are motivated by the necessity of finding a cheap and efficient separation technique for microalgae processing. Magnetic separation is a quick and simple method permitting the capture of the algal biomass from the algal effluent using functional magnetic particles that are driven by an external magnetic field. It has been demonstrated that magnetic separation is efficient for in situ removal of extracellular proteins and for immobilization of enzymes and whole cells ([49], [50]). Nevertheless, some requirements need to be fulfilled by magnetic particles to maintain a high recovery efficiency. Among these, one can cite the reusability, the chemical stability, the adsorptive capacity and their ability of being produced at low-cost [43]. The main advantages of this method are its simplicity and reliability, its low running costs and low energy requirements. The principle of magnetic separation is presented in **Figure 21** below. A microalgae cell (in green) which carries an overall negative charge while the magnetic nanoparticles (in this case Fe_3O_4, in pink) are positively charged. The nanoparticle will be adsorbed on the microalgae cell and then, the flocs formed will be separated in a magnetic field.

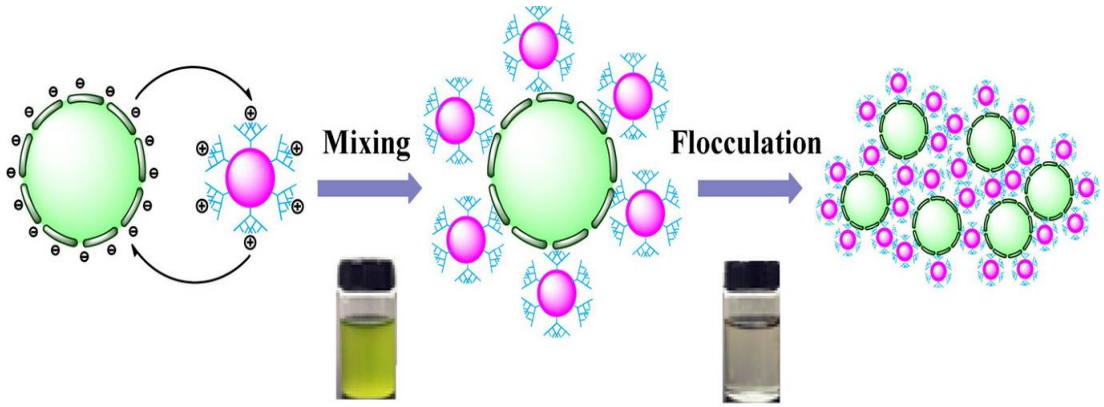

Figure 21 – Adsorption of the magnetic nanoparticles on a microalgae cell [51]

A first study uses naked Fe_3O_4 nanoparticles that are inserted in the microalgae culture. Then, the mixture is agitated by stirring during 1 minute to allow the microalgae to be adsorbed and, finally, a permanent magnet is used for the decantation of the solution. Different parameters were identified to play an important role in the recovery efficiency of this method. Among these, the stirring speed, the pH and the nanoparticle dose. Increasing the stirring speed from 40 rpm to 120 rpm had a positive effect on microalgae recovery but no significant improvement was noticed above 120 rpm. The optimal pH is different for each microalgae strain. Finally, the increase of the number of nanoparticles added in the solution obviously favored the recovery. It has to be mentioned that the nanoparticles can be regenerated and reused in the process. For instance, regeneration of the magnetic nanoparticles can be done by dissolving them into a HCl solution and using micro-filtration to recover the microalgae. The technique, developed at lab-scale, has reached a recovery efficiency above 98% within 1 minute for both *B. braunii* and *C. ellipsoidea* that were tested [42].

The second study tested magnetic separation on both fresh water and marine microalgae and, in each case, the recovery efficiency was above 95% using iron oxide (Fe_3O_4) and silica-coated magnetic particles. Silica-coated magnetic particles appear to be a good low-cost alternative to iron oxide. The impact of different parameters such as the particle concentration, the pH and the medium composition on the efficiency of the technique has also been evaluated. A high pH increased the process efficiency in presence of di- and trivalent ions notably by enhancing the flocculation. The medium composition (fresh water or marine water) did not inhibit the magnetic separation [43].

3.3.8. Recapitulative table of the harvesting and dewatering techniques

Table 4 summarizes the information presented in the previous subchapters.

Table 4 – Recapitulative table of the harvesting and dewatering techniques ([7], [41], [45])

Techniques	Energy consumption & Highest concentration factor (CF)	Advantages	Drawbacks
Gravity sedimentation	0.5 – 8 kWh/m^3; Low lamella separator: 0.1 kWh/m^3; CF: 16	➢ Reliable	➢ Efficiency depends on the density of the biomass ➢ Slow
Centrifugation	0.1 – 14.8 kWh/m^3; CF: 120 (self-cleaning disk stack centrifuge)	➢ Commercially established for microalgae	➢ Preconcentration step often required ➢ High energy input ➢ High gravitational and shear forces that can damage the cells
Coagulation-Flocculation	1.5 – 20 kWh/m^3 CF: N/A	➢ Possible to treat large volumes of algae effluent	➢ The use of coagulant can be fastidious (contamination) ➢ Flocculant can be expensive
Filtration and screening	Press or belt-filtration: 0.5 – 5.9kWh/m^3 Low vibrating screen filter: 0.4 kWh/m^3; Chamber filter press: 0.88 kWh/m^3 CF: 15-60 (natural filtration) & 50-245 (pressure filtration)	➢ Suitable for large microalgae ➢ Preserve the microalgae structure & Suitable for sensitive microalgae ➢ Cheap	➢ Inefficient for small microalgae ➢ Efficiency depends on the biomass concentration
Flotation	1.5 – 20 kWh/m^3 CF: N/A	➢ More efficient than natural sedimentation	➢ Pre-flocculation is often required ➢ Small size of bubbles more efficient but more energy intensive
Membrane filtration	0.17 – 2 kWh/m^3 CF: N/A	➢ No chemical addition ➢ Low energy consumption ➢ Reuse of the permeate possible	➢ Membrane fouling and pressure losses ➢ Further developments and research required
Magnetic separation	0.331 – 1.5 kWh/m^3 CF: N/A	➢ Simple ➢ Reliable ➢ Low running cost • Low energy requirements	➢ Further developments needed (reusability, chemical stability, etc.)

3.4. Coupling with wastewater treatments

The growth of microalgae is based on photosynthesis that converts carbon and energy of the sun into oxygen and chemical energy in the form of organic matter. In biodiesel production, the carbon source represents up to 60% of the costs with nutrients [4]. As it has already been mentioned, a critical point in microalgae cultivation is to reduce the cost, whatever the final product, in order to be economically attractive. Biofuels production leads to particular constraints to the microalgae cultivation systems: biofuels must be produced in a sustainable way at large scale and the specific cost should be as low as possible. Consequently, necessary conditions include the reduction of investment and operational costs, minimal production costs and maximal GHG savings [17]. Microalgae have the capacity to fix nitrogen and phosphorus contained in water very rapidly which opens a good opportunity for wastewater treatment [26]. The cost of microalgae production may be dramatically reduced if wastewater is used instead of artificial amendments. In recent years, the use of HRAPs for wastewater treatment has received more and more attention due to increased pressure to reduce nutrient content in wastewater [16] and because HRAPs are advantageous over traditional wastewater treatment processes. Some of the advantages are:

- Lower capital and operational costs;
- High nutrient removal rate;
- Ability to recover resources (algal biomass) that can be valorized [1];
- High removal efficiencies due to long hydraulic retention times [52];
- Production of oxygen during photosynthesis leading to reduced requirement for intensive aeration [11].

HRAP takes a part of its success over other wastewater treatment processes in its simple open pond raceway design agitated by either a paddlewheel or an airlift system. Shallow channel and high nutrient concentrations lead to biomass proliferation up to 3000 mg/m^3 for the *chlorophyll-a* [1]. While the production of biofuel is not yet economically viable, coupling of wastewater treatment using microalgae and biofuel production is considered to be financially feasible. The results of a study conducted in 2013 in Iran are presented in **Figure 22** & **Figure 23** below. The researchers have tested 5 different microalgae strains and they notably measured the ability of the biomass to remove nitrogen-nitrate and orthophosphate in batch culture using urban wastewater. The results show that the maximal percentage of N-removal is 84.11% while the maximal percentage for P-removal is 100%. It can also be noticed that the majority of the nutrient consumption takes place during the first 4 days which is in agreement with another work that showed that most of the nitrogen (>80%) was removed during the first 5 days and phosphorous during the first 1 or 2 days [3]. Also, it should be mentioned that the removal rates of N for the *Chlorella Sp. (1)* is 11.46 $\mathbf{mg_N.L^{-1}.d^{-1}}$ while the removal rate of P for *Chlamydomonas Sp. (1)* is 1.95 $\mathbf{mg_P.L^{-1}.d^{-1}}$. The wastewater composition has a N/P ratio of 9.98, meaning that initial concentration of nitrogen was almost 10 times higher than for phosphorous, that can explain the fact that final percentages of phosphorous are lower than the ones of nitrogen. In addition, there is also a natural decomposition of the phosphorous as can be seen in the blank (**Figure 22**) [53], this decomposition is not observed for the nitrogen.

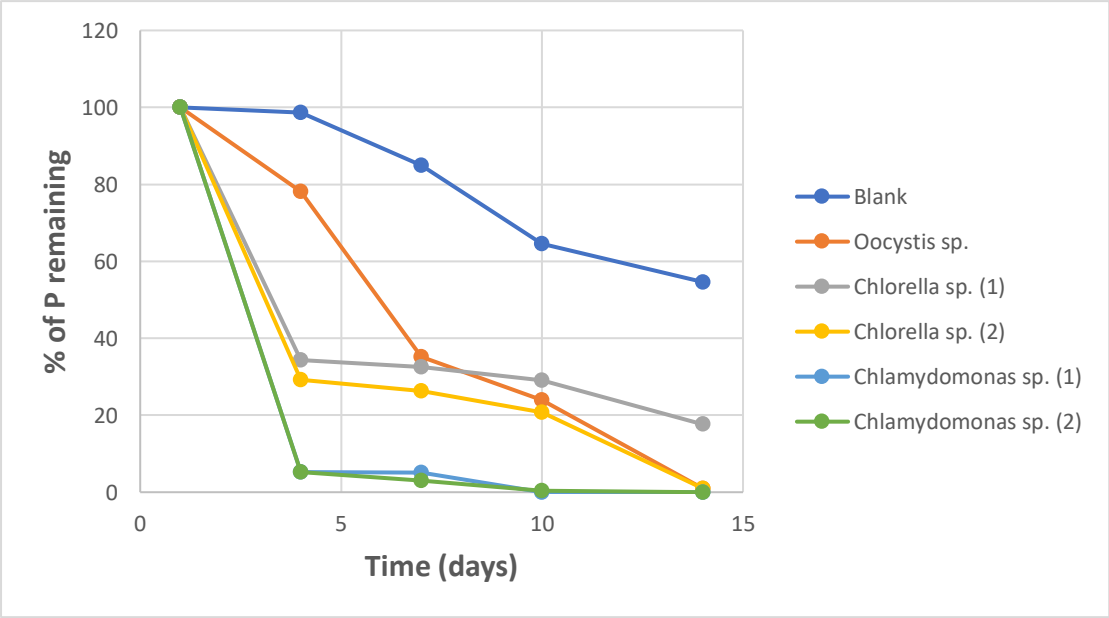

Figure 22 – Remaining phosphorous percentages in wastewater

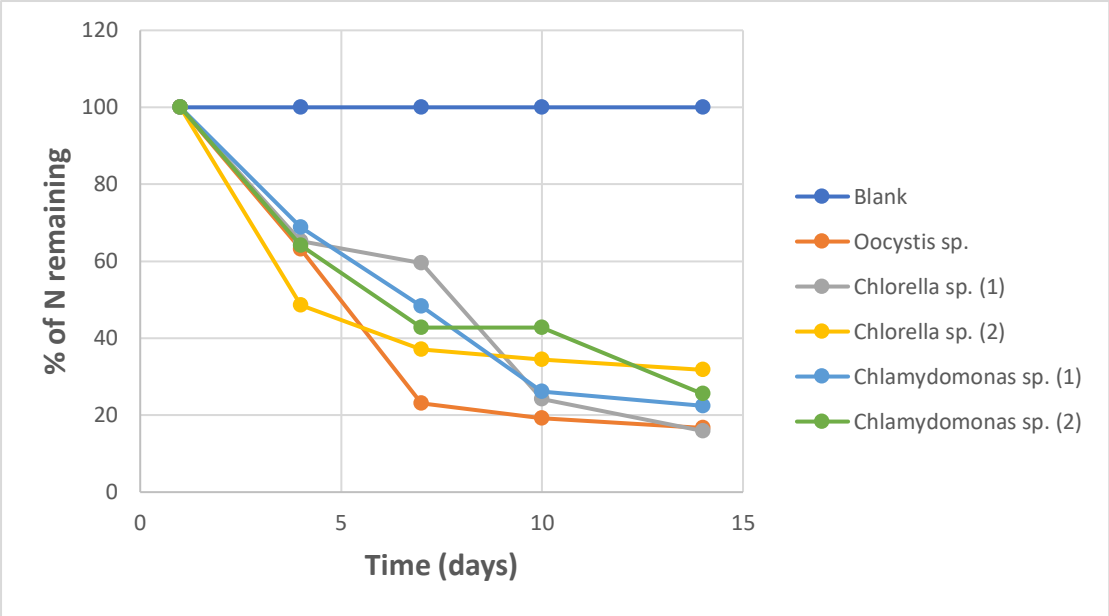

Figure 23 – Remaining nitrogen percentages in wastewater

A research [23] has studied the effect of different wastewater compositions used for the growth of *Chlorella vulgaris*. This study was conducted because one needs to take into account the high variability of wastewater composition and the potential toxicity effects that can be induced at different stages of the wastewater treatment process. The nutrient uptake was evaluated for the different stream compositions. At the end of each trial, a reduction in both N and P was observed. The optimum conditions led to a nitrogen uptake of 9.7 and 9.8 $\mathrm{mg_N.L^{-1}.d^{-1}}$ for N/P ratio of 0.7 and 2 respectively which is in agreement with another study that noticed that the ideal N/P ratio was lower than 4 [54]. In all experiments, the removal of P was higher than 92% and the rate of removal was between 0.5 and 3 $\mathrm{mg_P.L^{-1}.d^{-1}}$. In most of the cases, microalgal wastewater treatments were able to reach the European Directive 98/15/EC allowing 10 mg/L of nitrogen and 1 mg/L of phosphorus in the effluent for disposal. These removal rates are similar to the ones presented above. The study also showed that depending on the wastewater composition, the biomass composition in C, N and P varied significantly. Carbon percentages in the final biomass ranged between 43 and 56%, nitrogen percentages between 1 and 10% and phosphorus around 1%.

Microalgae are not only used for the wastewater treatments but also for the removal of emerging contaminants (EC) such as antibiotics. Algae can biodegrade the contaminants directly by heterotrophic metabolism or using extracellular enzymes. It may also happen that microalgae enhance the biodegradation of the EC via a symbiotic relationship with some bacteria present in the medium [52]. It has notably been reported that *Chlorella pyrenoidosa* cultures were able to remove 90-99.9% of four cephalosporins while the removal efficiency in an abiotic system was comprised between 8.5-27.3%. Thus

researchers concluded that the presence of microalgae caused 62 to 85% of the antibiotic removal [55].

As previously mentioned, microalgae may be used for biofuel production such as biodiesel. Coupling microalgae cultivation with wastewater treatment would lead to energetically favorable biofuel production and would offset most of the environmental burdens faced by aquaculture companies in emerging countries [8]. The energy revenue of such process depends on the harvesting and dewatering methods used. Some of them have been evaluated and in every configuration but one (the one using evaporation as a dewatering system), the energy losses are less than the potential gain. The greatest energy surplus was obtained for the chemical flocculation process followed by gravity sedimentation and a belt filter press. The study [8] also revealed that the relatively high energy content of algal biomass could lead to the fact that direct combustion of algae is more viable than the production of biofuel, especially for microalgae that contain low percentages of lipid (around 10%). Recently, a research was conducted on the possibilities of improvement by adding wastewater to the seawater in which the microalgae are grown. This will enhance the growth by supplying sufficient amounts of nitrogen and phosphorous to microalgae because the concentration of these nutrients is usually too low in seawater. A suitable seawater to wastewater ratio has to be identified in order to get the best lipid productivity for biodiesel production [21].

4. Experiments

4.1. Introduction

The experimental part of this work is divided into two parts which are themselves split into two different types of experiments. The tests are first conducted in Arlon (Belgium) on a small-scale pilot installed in a farm (Frères Kessler SCRL) that collaborates on different projects including one concerning the treatment of biomethanation digestate from agricultural wastes using microalgae. In this project, they have at their disposal 3 small-scale HRAP pilots in order to evaluate the feasibility of the digestate treatment using microalgae. After that, the second and main part of the work is conducted in the Marine Breeding Centre located in Ninh Thuan province (Vietnam). It has to be stressed that the main purpose of the first tests performed in Arlon is to develop a methodology that is suitable for the study of the HRAP and, also, to get the expertise to be able to conduct them once in Vietnam.

First of all, tracer tests are conducted on the HRAP pilots. These tests will be presented in more detail later but, basically, it consists in a salt injection and a continuous measure of the conductivity in the channel. The recorded data obtained from these experiments can be simulated by a model based on Voncken's equation that represents the impulse response of a dispersed plug flow reactor with recirculation. From these experiments, several data can be calculated such as:

- Péclet number (Pe);
- Dispersion coefficient (E_z);
- Circulation time (t_c) and water velocity (u);
- Volume of water (V).

In a second phase, the gas transfer capacity of the airlift system is evaluated in both Arlon and Vietnam. The experiments consist in an injection of Na_2SO_3 – in the presence of a Cobalt catalyst – that will consume all the dissolved oxygen present in the water and then, one measures the increase of dissolved oxygen resulting from the gas transfer in the airlift system and the gas transfer between the atmosphere and the channel. From these tests, it is possible to characterize the oxygen transfer of the HRAP and, notably, these three different volumetric transfer coefficients:

- $(k_l a)_R$: volumetric transfer coefficient of the entire HRAP;
- $(k_l a)_{Channel}$: volumetric transfer coefficient of the channel;
- $(k_l a)_A$: volumetric transfer coefficient of the airlift.

It has been decided to change the conditions of each test by modifying both the water level and the air flowrate of the blower (related to the power of the blower) of the airlift systems. The different tests are summarized in **Table 5** below. Ideally, all assays should be performed 3 times but it is not possible within the allocated time.

Table 5 – Conditions and number of tests for both tracer (**black**) and gas transfer tests (orange)

Depth / Power – air flowrate	0.25 m	0.4 m	0.6 m
0.6kW – <5 Nm^3/m^2h	1/1	1/1	1/1
1.2kW – 10 Nm^3/m^2h	2/2	2/4	2/2
1.8kW – 16.67 Nm^3/m^2h	2/2	1/2	2/2
2.4kW – 21.67 Nm^3/m^2h	1/1	1/1	1/1

The purpose of these experiments is to get the knowledge of the hydrodynamics and the gas transfer within the HRAP at different depth and air flowrate conditions in order to develop a good management strategy of the wastewater treatment pond. The data collected from the tracer tests and, notably, the Péclet number are injected in a model built to simulate the flow and the biological phenomena that occur within the pond. This model has been developed by the Sustainwater company belonging to Prof. Jean-Luc VASEL. Another use of the calculated parameters would be to simulate the hydrodynamic and biologic phenomena occurring in the HRAP by using a different representation of the reactor. From the dispersed plug-flow and the Péclet number derived from this representation, it is possible to model the reactor by a series of perfectly mixed tanks. There is a formula, that will be presented later on, linking Pe to the number of tanks to be put in series to model the reactor. In a second time, the information collected during the gas transfer test will give a general idea of the aeration performances of the airlift system and the entire reactor in general.

By varying the conditions of depth and air flowrate and by developing an accurate model of the HRAP pilot in Vietnam, it will be possible to identify the ideal conditions to run the system. As it has been discussed in the previous chapter, it is decisive to get a sufficient mixing of the microalgae present in the HRAP so that they are sufficiently exposed to the light and, also, to avoid different types of stratification (in pH, in temperature, etc.). On the other hand, it is necessary to have a good description of the gas transfer in the HRAP in order to manage the oxygen and carbon dioxide supplies that lead to highest performances. Indeed, during the day, microalgae will consume carbon dioxide that is sometimes the limiting factor for the growth and during the night, oxygen may be consumed (depending on the type of microalgae).

There is a compromise that needs to be looked for in terms of both performances and energy consumption which is one of the main perspectives of this work. The model developed will be useful to simulate the aeration and mixing performances of the airlift system used in the pilot. Furthermore, this model can also be used to predict the growth and productivity of the microalgae used for the wastewater treatment. Once the microalgae strains will be selected, it will be possible to identify the ideal conditions to operate the HRAP in order to get a sufficient water quality at the outlet, a high microalgae productivity, which is directly linked to the wastewater treatment quality, and an energy consumption as low as possible.

4.2. Experiments conducted in Arlon (Belgium)

4.2.1. Tracer tests

This chapter deals with three tracer tests performed on one of the three pilot scale raceway ponds present in Arlon. The principle of these tests is to determine the Péclet dimensionless number in order to find both the dispersion coefficient (E_z) and the number of tanks (j) to be put in series in order to model correctly a plug-flow reactor with recirculation. The first goal was to gather the knowledge about tracer tests conducted in HRAP in order to be able to reproduce them on larger scale on the pilot installed in the Ninh Thuan province once in Vietnam. The HRAP pilot in Arlon is presented in **Figure 24** below.

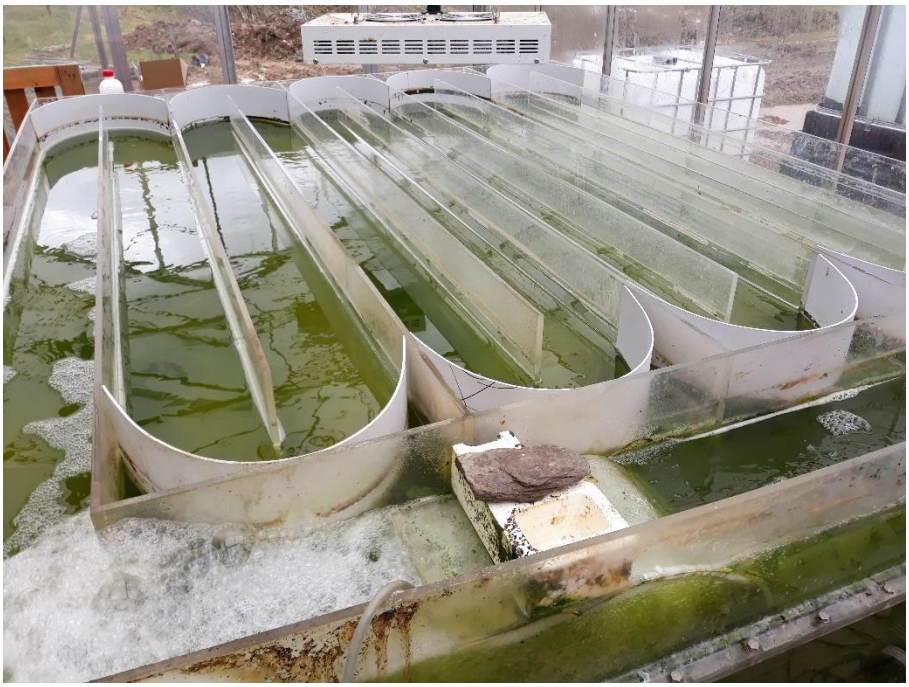

Figure 24 – HRAP pilot in Arlon

i. Methodology

The tracer tests consist in a Dirac injection of a given mass of NaCl dissolved in water performed in clear water on the biggest pilot reactor present in Arlon. The concentration of salt in the pond will be evaluated using a conductivity meter recording the water conductivity at a frequency of 0.2 Hz. From the conductivity data it is possible to obtain the actual salt concentrations using a calibration curve as presented below.

The principle of a pulse input experiment is to inject a given quantity of tracer N_0 into the feedstream of the reactor in a time as short as possible. Then, the outlet concentration is measured as a function of time. In our case, given the configuration of the HRAP, there is no inlet and no outlet so that the concentration will be measured at the exit of the airlift as a function of time. The concentration-time curve is often called the C curve

when residence time distribution analysis is performed. The shape of the C curve depends on the type of flow considered. As it will be discussed later, if no dispersion is observed, then the output is the same as the input curve. It is the case when an ideal plug-flow reactor is considered. In this case, one can define the C curve considering a time increment Δt sufficiently small, $C(t)$ the concentration of tracer exiting between t and $t + \Delta t$. It comes out that the amount of tracer ΔN leaving the reactor between t and Δt is given by:

$$\Delta N = C(t) v \Delta t$$

Where v is the volumetric flowrate at the exit. Considering N_0, the total amount of tracer injected in the reactor, it comes:

$$\frac{\Delta N}{N_0} = \frac{vC(t)}{N_0} \Delta t$$

Which represents the quantity of tracer with a residence time comprised between t and $t + \Delta t$. For a pulse injection, one defines the residence-time distribution function as follow:

$$E(t) = \frac{vC(t)}{N_0}$$

$E(t)$ can be interpreted as a quantitative manner to describe how much time the fluid elements spent in the reactor. Moreover, the quantity $E(t)dt$ is the fraction that exits the reactor that has spent a time between t and $t + dt$ in the reactor. Finally, knowing the definition of ΔN, one can easily imagine that N_0 is given by:

$$N_0 = \int_0^\infty vC(t)dt$$

And considering the fact that v can be considered constant most of the time, it comes:

$$E(t) = \frac{C(t)}{\int_0^\infty C(t)dt}$$

Where $\int_0^\infty C(t)dt$ is the area under the C curve. This part summarizes the theory of the pulse input experiments in the case of an ideal plug flow reactor [56]. In the case of the HRAP, two main features have to be taken into account. First, the response to the Dirac injection will be affected by the dispersion resulting from the mixing at the airlift and the non-ideal flow. Second, there is no inlet and no outlet in the case of the pilot pond but total recirculation needs to be taken into account.

Once the pulse response given by the conductivity is obtained and converted into concentration, it is possible to represent the distribution of dimensionless residence time $E(\theta) = \frac{C}{C_0}$, where $\theta = \frac{t}{t_c}$ is the dimensionless time, t_c the circulation time, C the tracer concentration at time t and C_0 the homogenized tracer concentration in the entire reactor. Depending on the type of flow, different responses can be observed. **Figure 25** shows the ideal plug flow response corresponding to a Dirac injection. In this case, no dispersion occurs meaning that the signal is not modified between the inlet and the outlet and all the tracer comes out at the same time τ which corresponds to the residence time. In general, the plug flow is not ideal meaning that a certain degree of mixing occurs inside the reactor and the response will be affected as shown in **Figure 26**. In addition, it can also be noticed that the injection has not been performed in an infinitely small time but in a time reasonably small enough (<1% of the circulation time) to be accurate. The tracer tests conducted here take into account this restriction in order to be as accurate as possible.

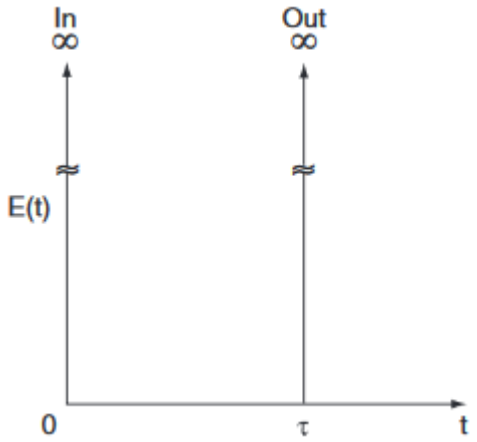

Figure 25 – Ideal plug flow response to a Dirac injection[10]

[10]Reference: http://www.umich.edu/~essen/html/byconcept/chapter13.pdf

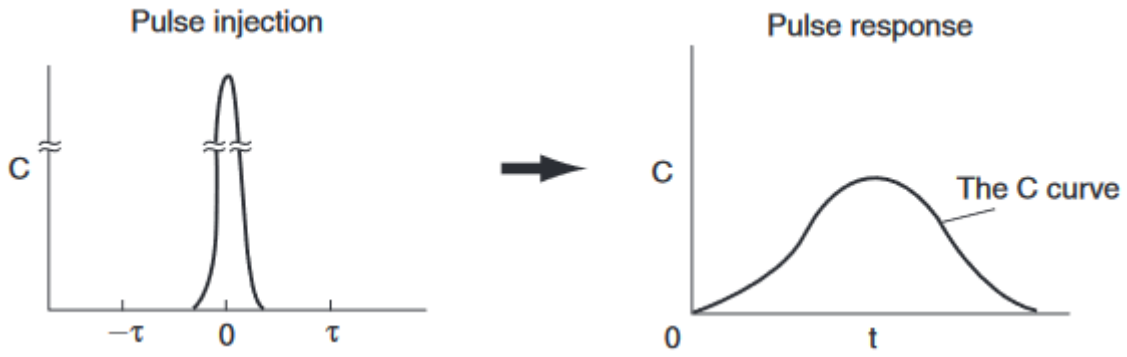

Figure 26 – Pulse injection and response in a plug flow reactor[11]

The model that would be able to represent the HRAP is a plug flow reactor with total recirculation, no inlet/outlet and with dispersion. The response expected to a pulse injection is represented in **Figure 27** below. Each peak represents the time when the tracer appears in front of the conductivity meter. The time between each peak is the circulation time, t_c. Due to the dispersion, the maximal concentration of tracer at each peak will decrease with time and the peak will be lowered until the tracer is perfectly mixed in the entire reactor. The concentration C(t) tends towards C_0 when $t \to \infty$.

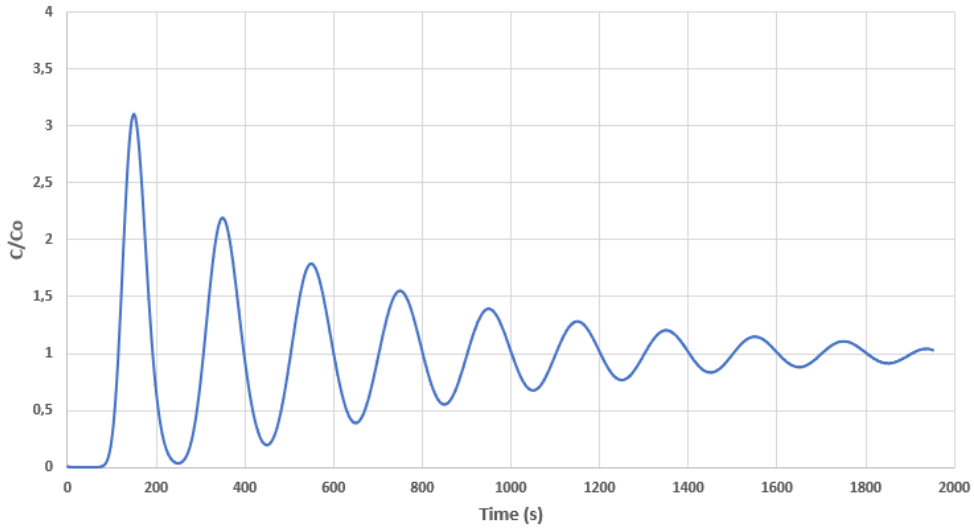

Figure 27 – Pulse response in a plug flow reactor with no inlet/outlet and with dispersion.

[11]Reference: http://www.umich.edu/~essen/html/byconcept/chapter13.pdf

It could also be interesting to evaluate the effect of the dispersion on a pulse response. The following **Figure 28** shows two different pulse responses for Péclet number equal to 30 and 120. Knowing the definition of the Péclet number:

$$Pe = \frac{u * l}{E_z}$$

Where:

- u is the flow velocity,
- l is the length of the plug flow reactor and,
- E_Z is the dispersion coefficient.

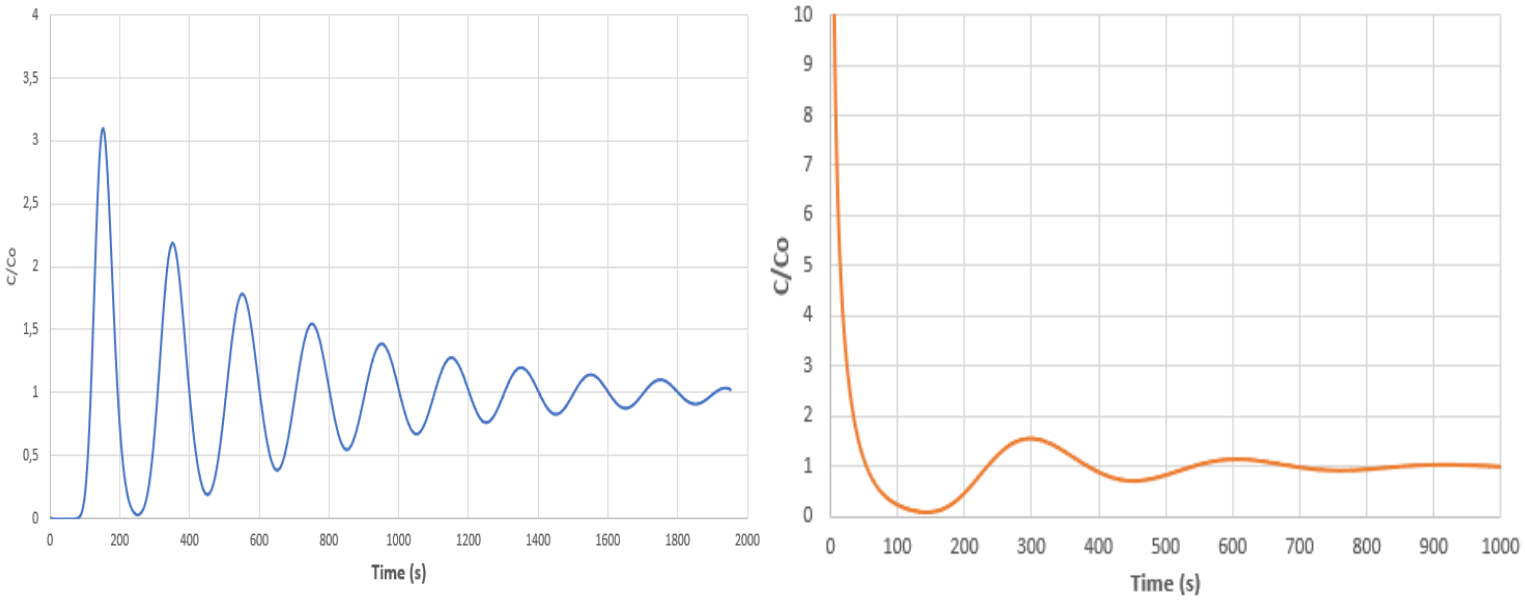

Figure 28 – Comparison of the impulse responses for Pe = 120 (left) and Pe = 30 (right)

Decreasing the Péclet number at constant flow speed means that the dispersion coefficient is higher which results in a higher mixing intensity. Given the fact that the flow velocity is constant, the circulation time is the same in each case. Nevertheless, one can see that in the second case (**Figure 28**, right), it takes around 900 seconds until perfect mixing is obtained while in the first case, perfect mixing is not achieved after 2000 seconds.

Some articles ([57],[58]) dealt with hydrodynamics characterization in the past and both of them used what is called the Voncken's equation **(Equation 1)** which represents the impulse response of a dispersed plug flow reactor with recirculation. It has to be taken into account that in the case of the pilot reactor of Arlon, no inlet and outlet should be considered (see **Figure 29**) meaning that the salt concentration C(t) tends towards C_0 when $t \to \infty$. This is not the case in [58] but it is in [57].

$$\frac{C}{C_0} = E(\theta) = \sqrt{\frac{Pe}{4\pi\theta}} * \sum_{j=0}^{p} \exp\left[-\frac{Pe}{4\theta} * (j-\theta)^2\right] \qquad \textbf{(Equation 1)}$$

Where:

- $C = C(t)$: concentration at time t;
- C_0 : concentration of tracer homogenized in the entire reactor;
- $E(\theta)$: distribution of adimensional residence time;
- Pe : Péclet number (dimensionless);
- $\theta = \frac{t}{t_c}$: adimensional time;
- t_c : circulation time, namely, length of time taken by the tracer to make a complete loop of the photobioreactor;
- p = number of peaks considered in the model.

Figure 29 – Plug flow reactor with total recirculation

After that, two variables were adjusted using MATLAB in order to match the theoretical response to the experimental result namely, the circulation time, t_c, and the Péclet number, Pe. In each test, the Péclet number corresponding to the minimum of squared errors has been determined. Then, the circulation time was adjusted simultaneously to find the t_c that leads to the best theoretical response. This parameter influences the position of each peak in the theoretical impulse response. Nevertheless, the circulation time could have been calculated by taking the average time between each peak of the experimental response. Also, in order to calculate the Péclet number, the flow velocity has to be evaluated knowing the circulation time and the length of the circulation loop, it comes:

$$u = \frac{L}{t_c}$$

Where L has been estimated using the dimensions of the pilot given in the following **Figure 30** and where t_c is given by the adjustment of Voncken's equation. In the case of the small-scale pilot reactor in Arlon, the length is approximately 24m.

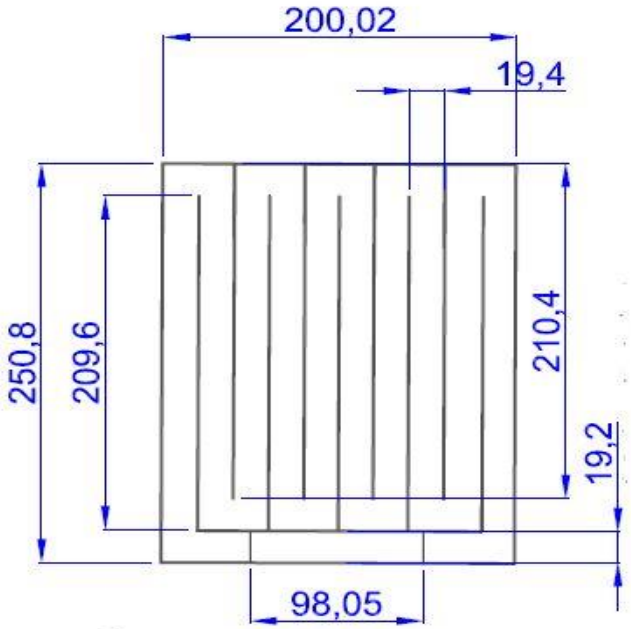

Figure 30 – Dimensions of the small-scale pilot HRAP in Arlon (measures in centimeter)

From the Pe, Octave Levenspiel [59] has demonstrated that it is possible to derive the number of tanks j to be put in series in order to model the plug flow. The following equation **(Equation 2)** gives the link between the Péclet number and the number of tanks j:

$$\sigma^2 = \frac{1}{j} = \frac{2}{Pe} - \frac{2}{Pe^2}(1 - \exp(-Pe)) \qquad \textbf{(Equation 2)}$$

a. Calibration curve

In order to translate the conductivity data into tracer concentrations, it is required to derive the calibration curve in the water used for the experiments. The concentration range should be as close as possible to the concentrations encountered during the tracer tests. In this case, the calibration curve is derived for salt concentrations between 0 and 3 g/L. To improve the quality of the curve, constant concentration increments should be used for each point. This will be done for the next calibration curves.

Table 6 – Data used for the calibration curve

Concentration (g/l)	Conductivity (µS/cm)
0	809
0.17	1176
0.26	1392
0,45	1817
1	2700
3	6230

The resulting calibration curve is presented in **Figure 31** below. The linear interpolation with $R^2 = 0.9989$ gives the following equation **(Equation 3)**.

$$Conductivity\left(\frac{\mu S}{cm}\right) = 1782.3 * [NaCl]\left(\frac{g}{L}\right) + 904.28 \qquad \textbf{(Equation 3)}$$

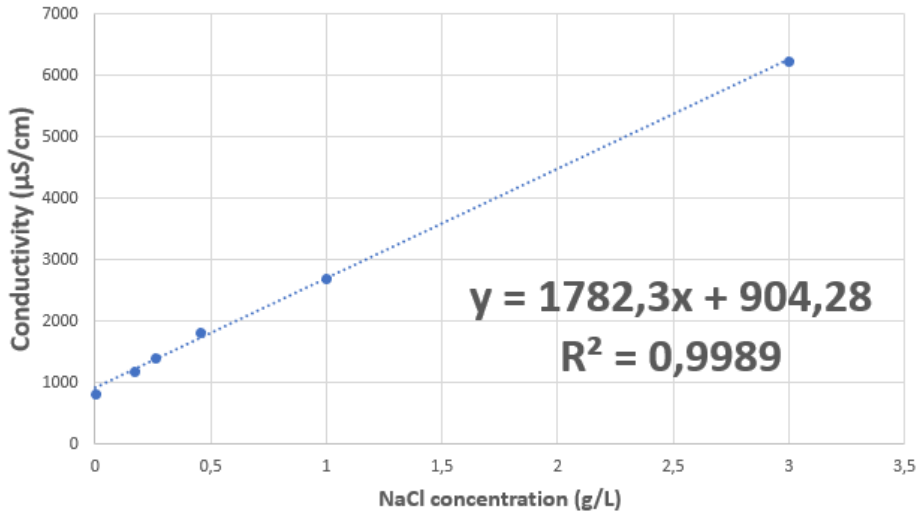

Figure 31 – Calibration curve for the conductivity as a function of the concentration

ii. Tracer tests

For each test, the airflow rate of the pump has been kept constant but the configuration of the HRAP has been modified in order to compare the dispersion coefficient and flow velocity of the different configurations.

- **Test 1**

For this first test, the shape of the curve of the HRAP has been modified according to [36] in order to minimize the head losses. The exterior of each curve has been shifted from two 90° angles to a semi-circular shape using flexible wood sheets while the interior has been complemented by cut plastic bottles in order to mimic the drop-shape structure presented in **Figure 32** coming from [36]. This design has been proven to reduce the energy consumption of the mixing device by facilitating the flow. Furthermore, the

stagnation regions (dead zones) within the flow are removed or reduced. The assembly realized is shown in **Figure 33** below.

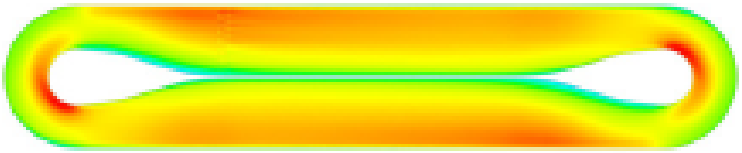

Figure 32 – Optimized shape of the curves in a HRAP

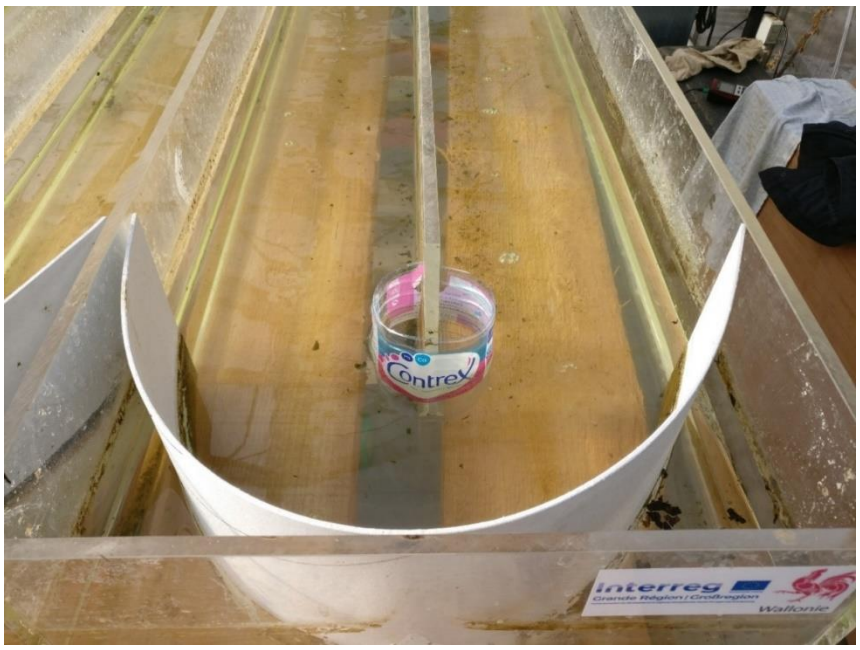

Figure 33 – Design of the curve for test 1

The resulting curve of the Voncken's equation has been adjusted in order to fit the experimental data as accurately as possible. To do so, considering that the tracer has been injected just after the conductivity meter, so a time shift of a bit less than t_c needed to be considered when the model is adjusted. This time shift can be seen in **Figure 27** where the response is equal to 0 until $t \approx 100s$. In this way, the data recorded before the first peak have been deleted and the time 0 of the experimental data corresponds to the time when the first maximum is reached. By doing the adjustment in this way, one takes into account the fact that the Voncken's equation considers that the response to the Dirac injection is recorded as if the tracer was added directly on the probe. The response of the impulse is shown in **Figure 34** as well as the theoretical approximation of Voncken's equation. The Péclet number minimizing the error is 81.05 and the flow velocity in this case is 9.45 cm/s. According to **(Equation 2)**, this Péclet number corresponds to 41 tanks required for the modeling of the dispersed plug flow.

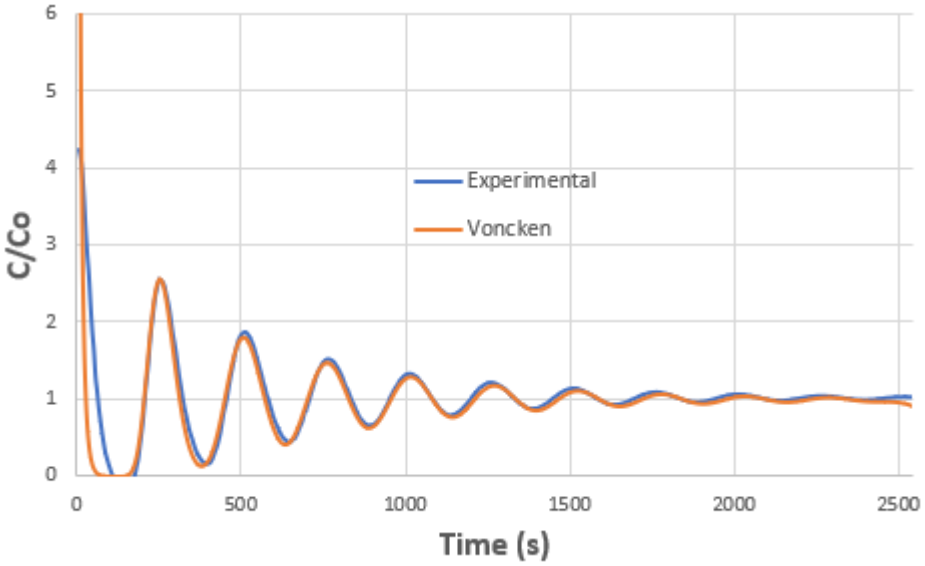

Figure 34 – Distribution of adimensional residence time for test 1

- **Test 2**

In this case, only the wood sheets at the exterior of the curves have been kept. The bottles were removed and a sufficient time has been considered in order to let the hydrodynamic regime stabilize. Again, the response of the impulse is shown in **Figure 35** as well as the theoretical approximation of Voncken's equation. The Péclet number minimizing the error is 55.33 and the flow velocity in this case is 8.75 cm/s. According to **(Equation 2)**, this Péclet number corresponds to 28 tanks required for the modeling of the dispersed plug flow.

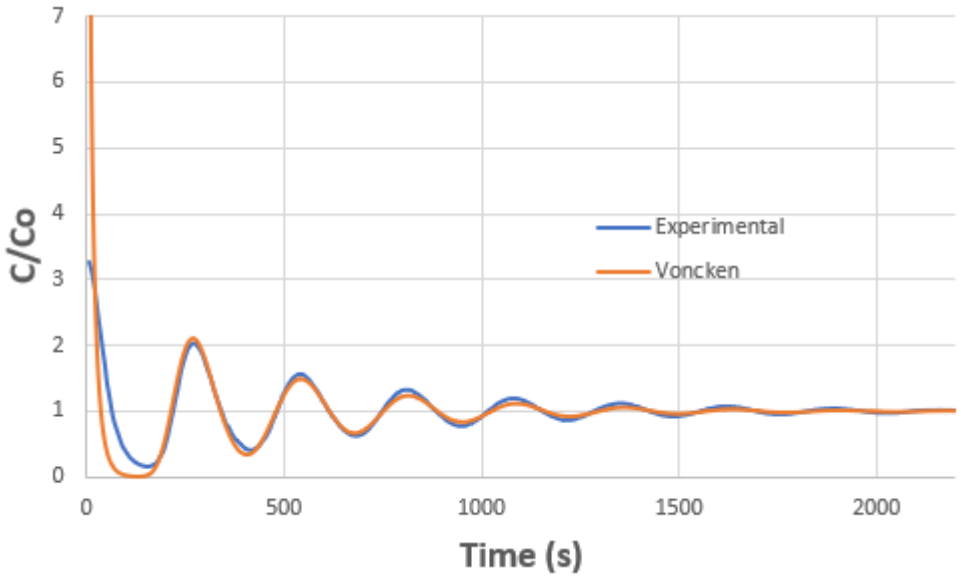

Figure 35 – Distribution of adimensional residence time for test 2

- **Test 3**

The final test has been conducted in the HRAP without any modification (no wood sheet and no plastic bottles). The test is shown in **Figure 36** as well as the theoretical approximation of Voncken's equation. The Péclet number minimizing the error is 73.98 and the flow velocity in this case is 9.18 cm/s. According to **(Equation 2),** this Péclet number corresponds to 37 tanks required for the modeling of the dispersed plug flow.

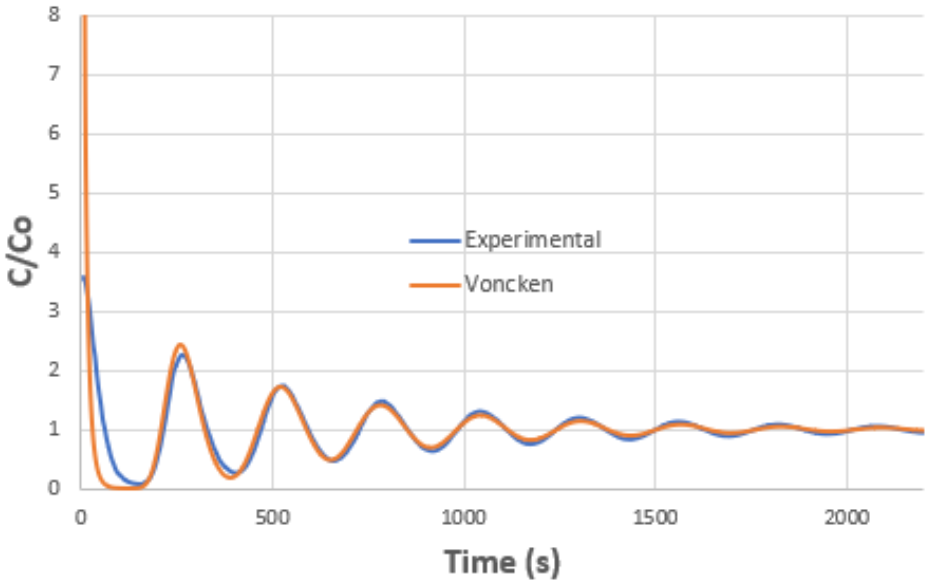

Figure 36 – Distribution of adimensional residence time for test 3

iii. Results

The results are presented in the following **Table 7.** The evolution of the configurations of the curves was done in order to increase the dispersion inside the pond from test number 1 to test number 3. Nevertheless, it can be seen that only a slight increase of the dispersion coefficient E_Z occurred for tests 2 and 3 compared to test 1. Furthermore, from test 2 to 3 the flow velocity increases and the dispersion coefficient decreases which is counter-intuitive because the third configuration is the less adapted for a smooth flow. Test 1 shows a shorter circulation time t_c compared to test 2 and 3 which is explained by a better hydrodynamic configuration of the pond resulting in lower head losses and higher velocity. Last, volumes have been compared for the three tests and were supposed to rise slightly from test to test because the active volume increases when the components used to improve the hydrodynamics are removed. Volume calculation for test 1 can be wrong due to some mistakes that were done during the weighing of the salt or some salt losses during the preparation of the injection mixture. Finally, from test 2 to test 3, the 3L increase due to the curve removal is relatively close to reality.

Table 7 – Results of the 3 tracer tests

Test	Péclet number [-]	Circulation time $t_{c,exp}$ (expérimental) [s]	Circulation time $t_{c,adj}$ (adjusted) [s]	Flow velocity u [m/s]	Dispersion coefficient E_z [m²/s]	Volume [L]
1	81.05±1.46	254.17	253.9	0.0945	0.028	564.826
2	55.33±1.44	273	274.05	0.0875	0.038	416.42
3	73.98±0.99	261.67	261.3	0.0918	0.030	419.37

Despite numerous inconsistencies in the results shown above, the main goal of these small-scale tests is to get an overview of the tracer tests and to verify if they are suited to the hydrodynamic study of HRAPs in order to be able to conduct them once in Vietnam. That is the reason why they are not performed a second time.

4.2.2. Oxygen transfer tests

This chapter deals with the oxygenation capacity of the small-scale HRAP situated in Arlon. The results of these tests will allow the determination of the volumetric mass transfer coefficient $k_l a$ for the entire pond, the channel and the airlift system. The goal is to find an appropriate methodology to evaluate the oxygen transfer taking into account the particular configuration of the algal pond equipped with an airlift and, also, to be able to realize the tests once in Vietnam.

i. Methodology

These tests have been realized in February 2018 in Arlon on the small scale HRAP in the same configuration as for the tracer tests in **Test 2** (only semi-circular wood sheets were placed in the curve). Three oxygen probes have been placed in the HRAP at three strategic positions. Two of them were situated at the entrance and exit of the airlift system and are supposed to allow the determination of the volumetric mass transfer coefficient for the airlift, $(k_l a)_{airlift}$. The last probe has been placed in the middle of the channel and will be used to determine the $k_l a$ for the entire reactor and for the channel. The different positions of the probes have been represented in **Figure 37** below. Due to some interferences caused by the bubbles rising in the airlift system, the results recorded by probe A are not usable as can be seen in **Figure 38**.

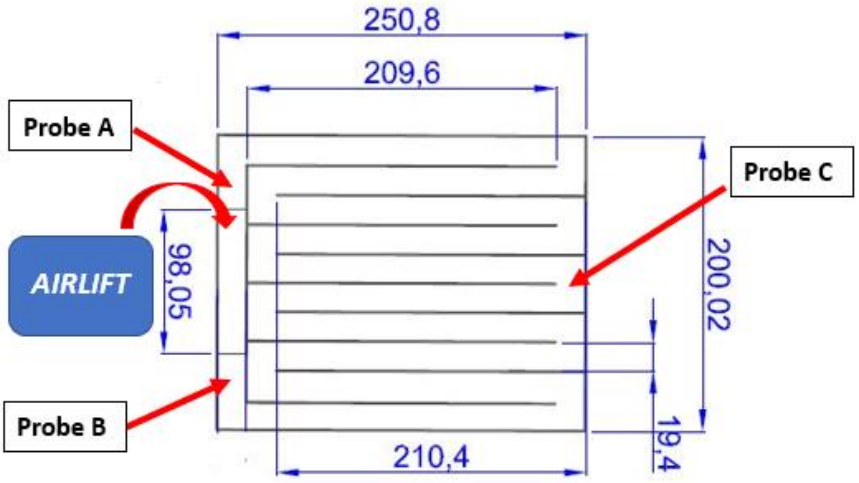

Figure 37 – Configuration of the HRAP for oxygen transfer tests

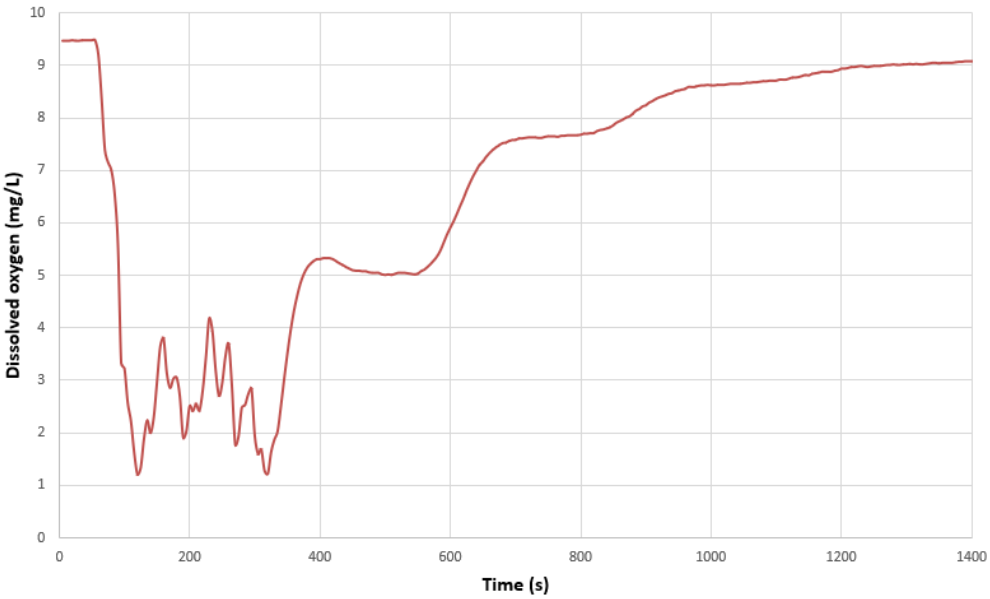

Figure 38 – Example of experimental data recorded by probe A

The principle of the oxygen transfer tests is first to remove all the dissolved oxygen (DO) present in the water and then to observe how the DO evolves with time. It is expected that each time the water passes through the airlift, the DO increases proportionally to the concentration difference between the atmosphere and the water. Other transfer may happen between the atmosphere and the water along the channel but it is several orders of magnitude smaller than the transfer occurring at the airlift.

One way to remove the oxygen from the water is to make it react with sulfite SO_3^{2-}. This reaction requires the presence of a cobalt catalyst, $CoCl_2.6H_2O$. Usually, sulfite is inserted into the water using a solution where anhydrous sodium sulfite Na_2SO_3 is dissolved. The overall reaction sequence is presented below.

$$Na_2SO_3 \rightarrow 2Na^+ + SO_3^{2-} \quad (1)$$

$$2SO_3^{2-} + O_2 \xrightarrow{Cobalt} 2SO_4^{2-} \quad (2)$$

The catalyst is inserted first and one waits around five times the circulation time in order to let the pond homogenize. Around 1 mg/L of Cobalt is required to get an effective catalytic action. Then, a sulfite solution has been prepared considering that 7.9 mg of Na_2SO_3 are required to react with 1 mg of O_2. The DO should be measured first in order to add the exact amount of sulfite which is necessary to remove the oxygen completely. In our case, the DO was estimated around 9 mg/L. In clear water, at 23°C, the saturation value of DO is 8.6 mg/L [60]. Nevertheless, in the case of the pilot in Arlon, some microalgae were present in the reactor and the DO was higher than the saturation value (around 10 mg/L) due to photosynthetic activity of the biomass that produced oxygen during daytime.

Once the catalyst is well homogenized in the pond, the sulfite solution can be added. One way to be sure that sulfite will be present in the entire reactor is to inject the solution in a time corresponding to the circulation time t_c. From the tracer tests realized previously, Test 2 corresponding to the present configuration gave a mean circulation time of 273 seconds. Then, in order to be sure to avoid any overlapping that would lead to a waste of sulfite, it has been decided to inject the sulfite solution in around 250 seconds. To do so, ten solutions of 100 mL containing 10% of the sulfite are prepared and every injection lasts 25 seconds for a total of 250 seconds. The injections have been carried out at the exit of the airlift where the bubbles rise up to the surface and offer a good mixing.

These tests were conducted in order to get a better knowledge of the volumetric transfer coefficient $k_l a$ of each part of the reactor (airlift and channel). The $k_l a$ describes the efficiency of the oxygen transfer in the HRAP for a given set of conditions. These tests are very important when dealing with bioprocesses requiring different substrates such as oxygen or carbon dioxide. A lack of these elements can result in a dramatic decrease in productivity. Consequently, it is necessary to know the characteristics of the transfer behavior of the algal pond in different conditions. These experiments are very important to determine the processing conditions that provide an adequate amount of oxygen to the biomass. The tests realized in Arlon were a prelude to the tests that have been done in Vietnam. Indeed, only a single set of conditions is tested in order to be familiar with the methodology. The goal is not to observe the impact of modified operating conditions but to verify if the methodology is suitable and to practice for the experiments conducted in Vietnam.

Table 8 – Recapitulative data of the oxygen transfer tests

Volume of water	527 L
Mass of Na_2SO_3	37.47 g
Mass of $CoCl_2.6H_2O$	2.126 g
Injection time	250 s

- **Volumetric transfer coefficient of the channel $(k_l a)_{channel}$**

The calculation of the volumetric transfer coefficient of the channel have been realized thanks to the data collected by probes B and C that are separated by a section of the channel excluding the airlift in the calculations. It is based on the oxygen balance assuming:

- a plug flow between probes B and C;
- no oxygen consumption and production;
- only gas transfer between atmosphere and water.

The oxygen balance is:

$$V_{section}\frac{dC}{dt} = (k_l a)_{channel} V_{section}\left(C_s - C(t)\right)$$

$$-\frac{dD}{dt} = (k_l a)_{channel} D \qquad \text{where } D = C_s - C(t)$$

$$D(t) = D_0 \exp(-(k_l a)_{channel} t)$$

From this, one obtains the volumetric transfer coefficient of the channel:

$$(k_l a)_{channel} = \frac{-\ln\left(\frac{D}{D_0}\right)}{t} \qquad \textbf{(Equation 4)}$$

Considering:

- C_s : Concentration of dissolved oxygen at saturation;
- $D(t) = C_s - C(t)$: where $C(t)$ is the oxygen concentration at probe B;
- $D_0 = C_s - C_0$: where C_0 is the oxygen concentration at probe C;
- $t = t_{c,section}$: Time taken by the water between probe B and C;
- $V_{section}$: Volume of water between probe B and C.

(Equation 4) above is valid from the moment where the oxygen consumption stops until the time at which oxygen saturation is reached. These two moments can be found directly in the graphs of the dissolved oxygen. The mean value of the $k_l a$ is taken over the entire range where the equation is valid.

- **Volumetric transfer coefficient of the entire HRAP $(k_l a)_R$**

<u>1st Method</u>

This method assumed that the response to the oxygen transfer can be approximated by a perfectly mixed tank. To perform the calculation, it only requires the data of one probe. It has been decided to repeat the derivation on both probes B and C to compare the results.

The response is:

$$D = D_0 \exp(-(k_l a)_R t)$$

$$\ln\left(\frac{D}{D_0}\right) = -(k_l a)_R t \qquad \text{(Equation 5)}$$

By plotting the $\ln\left(\frac{D}{D_0}\right)$ as a function of time, one can approximate the slope of the curve by linear interpolation. An example is given in **Figure 39** below. The data are taken between 400 and 1100 seconds approximately which is the interval where **(Equation 5)** is valid.

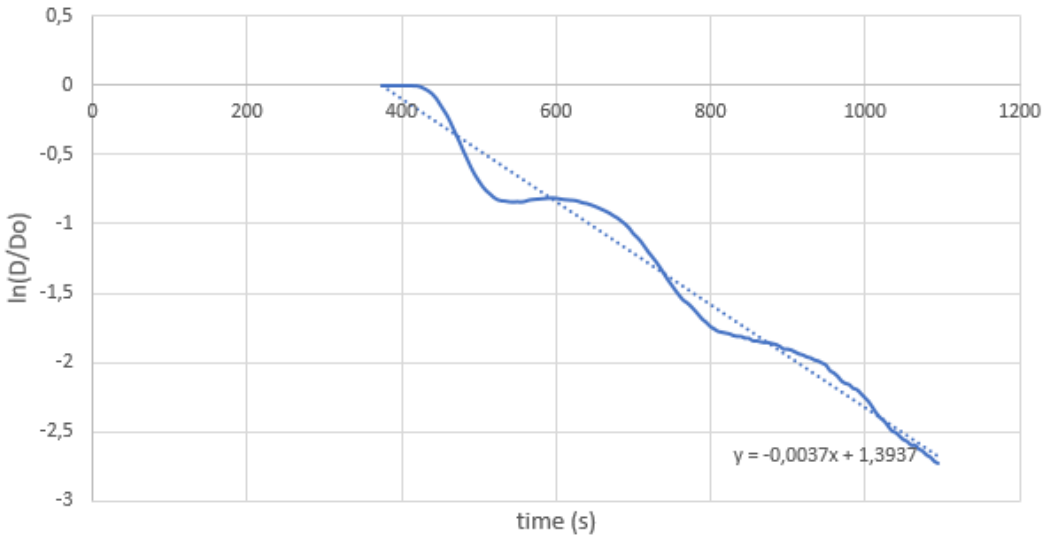

Figure 39 – Example of linear interpolation for the determination of the volumetric transfer coefficient of the HRAP

2nd Method

This method is a graphical method that will use the difference of concentration at each loop of the reactor to derive the $k_l a$ according to:

$$D_{i+1} = D_i \exp(-(k_l a)_R t_c) \qquad \text{(Equation 6)}$$

Where:

- $D_i = C_s - C_i(t)$ at loop i;
- $(k_l a)_R$ volumetric transfer coefficient of the reactor;
- $t_c = 273s$ circulation time;

The graph below shows the results given by a probe situated at the entrance of the airlift. The data taken to apply **(Equation 6)** have been highlighted in **Figure 40**. For each test, only three steps were usable with sufficient accuracy. Then, the mean value of the three $(k_l a)_R$ was calculated in each case to obtain the final answer.

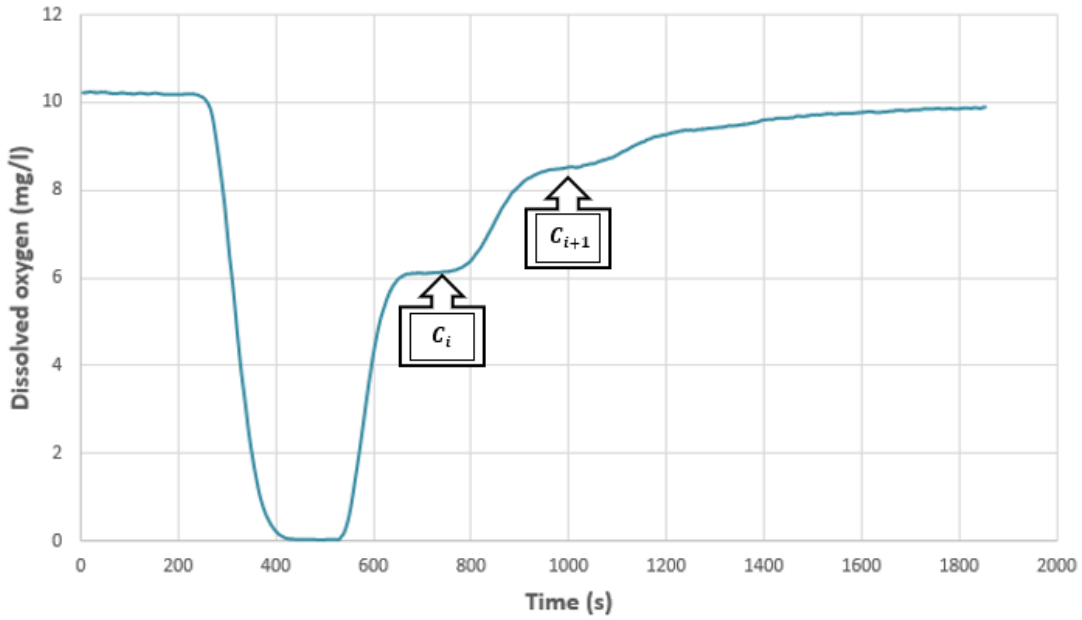

Figure 40 – Application of the second method for the calculation of $(k_l a)_R$

- **Volumetric transfer coefficient of the airlift $(k_l a)_A$**

The calculation of $(k_l a)_A$ is based on the oxygen balance assuming that the transfer between the atmosphere and the water is negligible in the channel and that all the oxygen transfer occurs at the airlift. This approximation is only valid because the transfer in the channel is low, in Vietnam this transfer is not negligible because the HRAP is installed outside and exposed to wind. In the present case, the oxygen balance can thus be written as the equality between the overall oxygen transfer in the entire reactor and the oxygen transfer at the airlift:

$$(k_l a)_R (C_S - C_0) V_R = (k_l a)_A (C_S - C_0) V_A$$

Where:

- C_S: Concentration of dissolved oxygen at saturation;
- C_0: Initial concentration of dissolved oxygen, $C_0 \cong 0\, mg/l$;
- V_R: Volume of the entire reactor;
- V_A: Volume of the active part of the airlift (where the bubbles rise up).

From this balance, one can find the volumetric transfer coefficient of the airlift which is given by the following (**Equation 7**):

$$(k_l a)_A = (k_l a)_R * \frac{V_R}{V_A} \qquad \textbf{(Equation 7)}$$

ii. Results and discussions

The same experiment is conducted three times on February 22nd on the pilot scale reactor in Arlon. The tests are supposed to be conducted with clear water but, due to the sunny conditions, some remaining microalgae proliferated so that the HRAP was full of microalgae. The presence of algae is a source of error in the results of these tests in the sense that the dissolved oxygen was over its saturation value due to oxygen production resulting from photosynthetic activity of the biomass. A simple evidence is that, given the temperature of the water $20.5°C$ at the beginning of the tests, the DO values should be around 9 mg/L. But in practice, it was not the case. Probe C indicated a value of 10.2 mg/L in the middle of the HRAP while probe B, at the entrance of the airlift, showed a value of 10.31 mg/L for the DO. Nevertheless, it has been decided to neglect this oxygen input for the interpretation of the results given the fact that the primary goal of these experiments is to get the overview of how they should be performed in order to be able to reproduce them once in Vietnam.

For each experiment, it was decided to model the response registered by probe B based on the experimental data of probe C. To do so, only the $(k_l a)_{channel}$ was required due to the fact that the two probes were only separated by the channel. Then, the model can be implemented by the following equation:

$$\mathrm{D(t) = D_0 \exp(-(k_l a)_{channel} t)}$$

Where:

- $D(t) = C_s - C(t)$: where $C(t)$ is the oxygen concentration at probe B;
- $D_0 = C_s - C_0(t)$: where $C_0(t)$ is the oxygen concentration at probe C;
- $t = t_{c,section}$: time between probes B and C.

It has to be mentioned that there are 3 parameters in this equation namely C_s, $(k_l a)_{channel}$ and t. The first one has been adjusted in order to minimize the error between experimental values and the model. The second one is the one that is being looked for. And the third one can be deduced from the graphs of the experimental data or calculated directly using the corrected flow velocity which is the velocity in the channel ignoring the airlift system.

- **1st test**

The first test conducted on the pilot in Arlon was realized at 20.5°C at the start. Given the fact that thermal equilibrium was not reached at the beginning of the experiment, the final temperature was 21.5°C at the end due to sunny conditions. This has an influence on the value of the DO given that the concentration of oxygen dissolved in water decreases when the temperature increases. This was not taken into account in the calculations but it highlights the fact that temperature should be as constant as possible before starting any gas transfer experiment.

For this first test, the volumetric transfer coefficient that has been found for the channel $(k_l a)_{channel}$ is $6 * 10^{-4}\ s^{-1}$, the one of the entire reactor $(k_l a)_R$ is $30{,}91 * 10^{-4}\ s^{-1}$ from the 2nd method and the one of the airlift system $(k_l a)_A$ is $0.1724\ s^{-1}$. The model for the oxygen concentration at the entrance is presented in **Figure 41** below. The dissolved oxygen at saturation minimizing the error is: $C_s = 10.275\ mg/L$. This value is above the theoretical values in the range of temperature encountered here which can be explained by the presence of microalgae in the HRAP. Another clue of the supersaturation is that the concentration at the exit of the airlift was lower than the one at the entrance which means that the aeration system was actually stripping the oxygen out of the pond.

Each step of the curve in the figure below corresponds to the water passing through the airlift system where the majority of the oxygen transfer happens. Then, between each step one can see a plateau that corresponds to the flow within the channel with negligible gas transfer. It can be seen that the oxygen saturation is reached after the fourth passing through the aeration system which proves that this system is very efficient for oxygen transfer to the water of the HRAP.

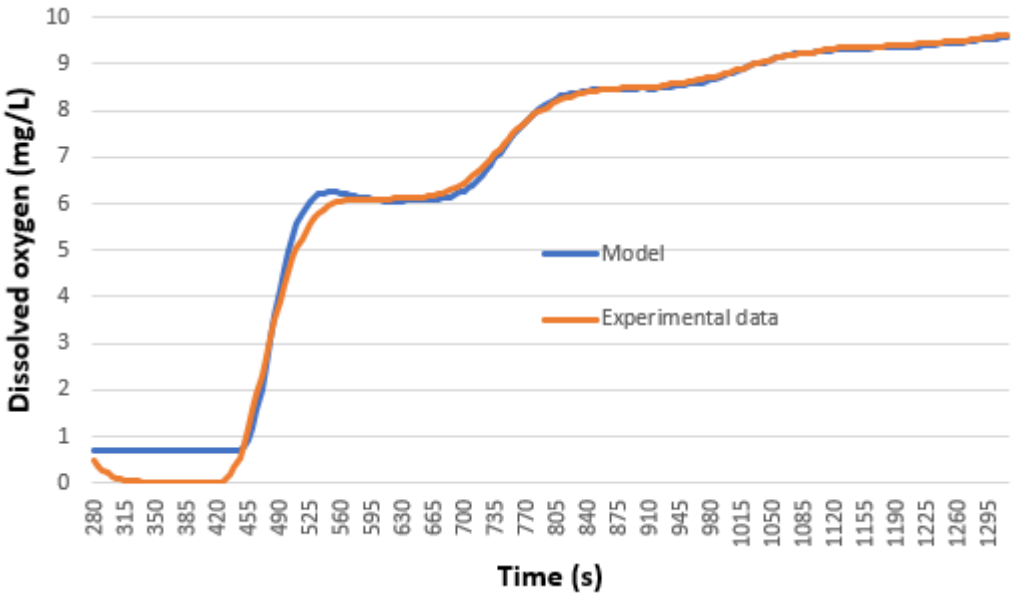

Figure 41 – Comparison between model and experimental data at the entrance of the airlift for test 1

Between 280 and 430 seconds, it can be observed that the model exceeds the value of the experimental data. This comes from the fact that the model does not take into account the presence of sulfite but only the supply of oxygen coming from the atmosphere while the oxygen is still consumed in the pond. The actual oxygen concentration is close to 0 mg/L. As it has already been said, the model is valid when the oxygen reaction with sulfite has ended. This moment is around 430 seconds, where the oxygen concentration starts to rise.

- **2nd test**

For this second test, the initial temperature is 21.5°C and the final temperature 22.2°C. The volumetric transfer coefficient that has been calculated for the channel $(k_l a)_{channel}$ is $8.2 * 10^{-4}\, s^{-1}$, the one of the entire reactor $(k_l a)_R$ is $31.3 * 10^{-4}\, s^{-1}$ from the 2nd method and the one of the airlift system $(k_l a)_A$ is $0.1748\, s^{-1}$. The model for the oxygen concentration at the entrance is presented in **Figure 42** below. The dissolved oxygen at saturation minimizing the error is: $C_s = 10.275\, mg/L$ which is the same value as for the first test.

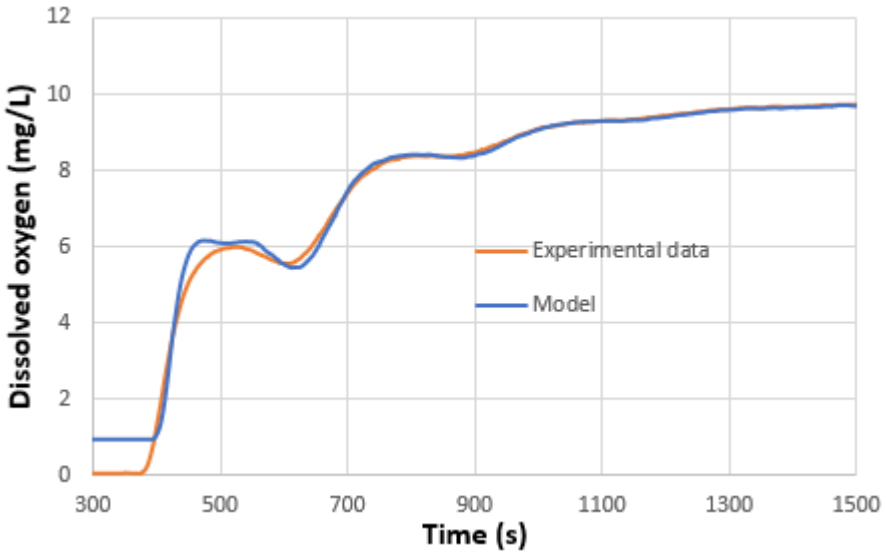

Figure 42 – Comparison between model and experimental data at the entrance of the airlift for test 2

The fluctuations occurring around 500 seconds are the reflection of the fluctuations recorded by probe C. Indeed, the model is based on the experimental data of probe C situated in the middle of the pond. Because of this, any irregularity that is happening at probe C is translated in the model. These variations may be caused by some errors during the recording of the data that could be due to the presence of air bubble on the sensor.

- **3rd test**

For this third test, the initial temperature was 22.2°C and the final temperature 23.2°C. The volumetric transfer coefficient that has been calculated for the channel $(k_l a)_{channel}$ is $2.03 * 10^{-4}\ s^{-1}$, the one of the entire reactor $(k_l a)_R$ is $32.22 * 10^{-4}\ s^{-1}$ from the 2nd method and the one of the airlift system $(k_l a)_A$ is $0.1792\ s^{-1}$. The model for the oxygen concentration at the entrance is presented in **Figure 43** below. The dissolved oxygen at saturation considered here was $C_s = 9.8\ mg/L$ based on the value reached at the end of test 2.

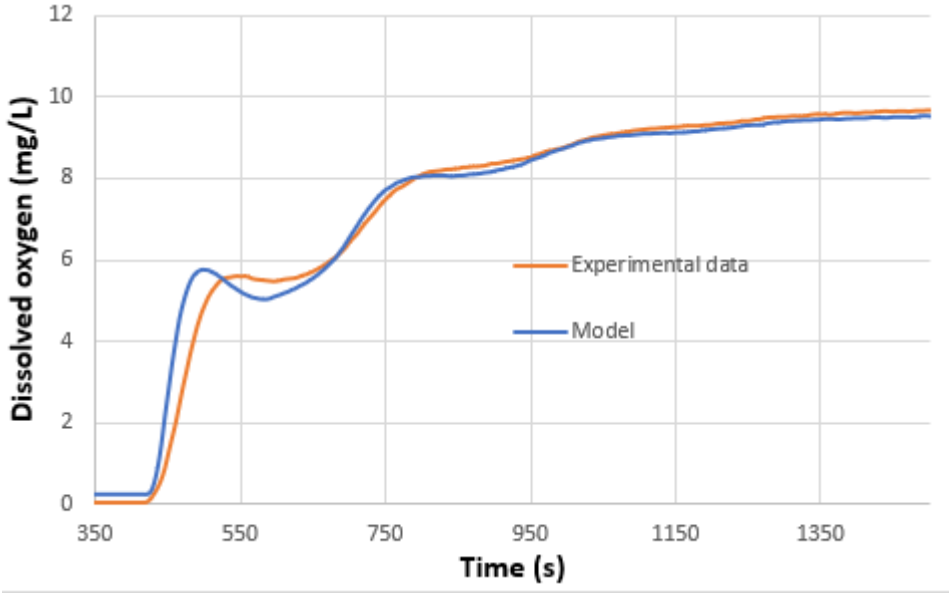

Figure 43 – Comparison between model and experimental data at the entrance of the airlift for test 3

➢ **Comparison**

Based on the results of the three tests, the volumetric transfer coefficients of the different sections of the reactor (entire reactor, airlift and channel) have been calculated and are summarized in **Table 9** below. Except for the volumetric transfer coefficient of the channel, the results are consistent between each test. One can see that the $(k_l a)_R$ is around six times greater than the $(k_l a)_{channel}$ because the majority of the gas transfer occurs at the airlift. Consequently, it is normal and expected that the $(k_l a)_A$ is two orders of magnitude greater than the two others. Finally, it is interesting to compare the difference between the two methods used to obtain the $(k_l a)_R$. The results are pretty much the same for the two methods which tends to comfort the credit of these methods and results.

Table 9 – Results of the oxygen transfer tests in s^{-1}

Essai	$(k_l a)_{channel}$	$(k_l a)_R$ (Method 1)	$(k_l a)_R$ (Method 2)	$(k_l a)_A$
1	6.10^{-4}	Sonde B : 31.10^{-4} Sonde C : 31.10^{-4}	$30{,}91.10^{-4}$	0.1724
2	$8.2.10^{-4}$	Sonde B : 30.10^{-4} Sonde C : 28.10^{-4}	$31{,}3.10^{-4}$	0.1748
3	$2{,}03.10^{-4}$	Sonde B : 37.10^{-4} Sonde C : 34.10^{-4}	$32.22.10^{-4}$	0.1792
Mean values	$5.41 * 10^{-4}$	$31.83 * 10^{-4}$	$31.48 * 10^{-4}$	0.1755

4.3. Experiments conducted in the Ninh Thuan province (Vietnam)

The second and main part of this work is conducted at the Marine Breeding Center located in the Ninh Thuan province (Vietnam). It consists in the setup of a HRAP pilot which will be intensively studied during the next 3 years to evaluate the feasibility of treatment of shrimp pond effluents by a raceway pond (RENEWABLE project). The first part of the work made is the supervision of the construction of the pilot. This involves different working fields such as masonry, electricity, plumbing and welding. After that, the different experiments (tracer and gas transfer tests) are conducted on the operational HRAP. The Vietnamese pond is presented in the following **Figure 44** as well as the design of the airlift system (**Figure 45**). It has been decided to improve the shape of the curves in order to reduce head losses (**Figure 46**) according to the plan presented in **Figure 47**. As introduced previously, all experiments are conducted at three different depths (0.25m, 0.4m and 0.6m) and four different air flowrates (<5Nm^3/m^2h, 10Nm^3/m^2h, 16.67Nm^3/m^2h and 21.67Nm^3/m^2h) corresponding to four different powers (0.6kW, 1.2kW, 1.8kW and 2.4kW) of the air blower. The air flowrates are expressed by unit area of the column where the bubbles rise within the airlift so that future comparisons can be realized afterwards. The final goal is to develop a model which is able to simulate the hydrodynamics, the gas transfers and the biological phenomena occurring within the HRAP. This model may be used to find the optimal conditions in which the pond should be operated depending on the selected microalgae strain. These results will be of high value for the next steps of the project that deal with the wastewater treatment capacity of the microalgae and the economic feasibility of this technology.

The technical characteristics and the instructions for the operations of the HRAP pilot are summarized in the "**Appendix A** – Technical characteristics and instructions for the Vietnamese HRAP pilot".

Figure 44 – HRAP pilot installed in the Ninh Thuan province

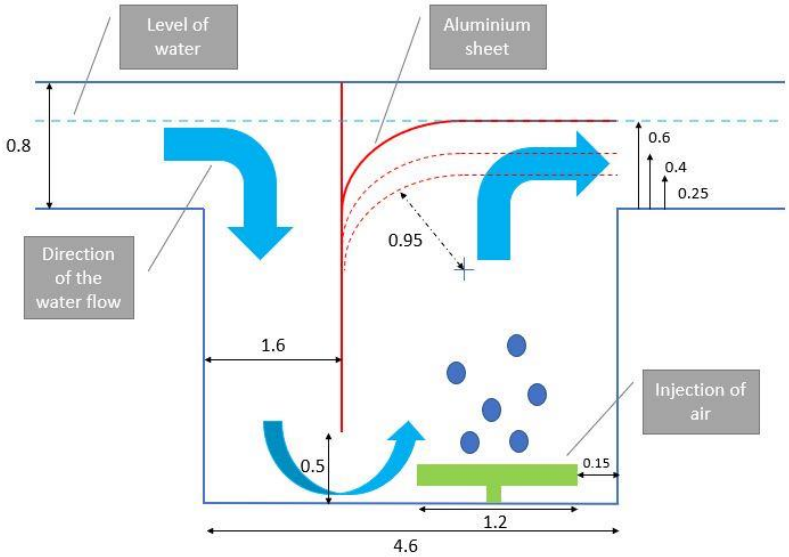

Figure 45 – Drawing of the airlift system (measures in meter)

Figure 46 – Shape of the curves

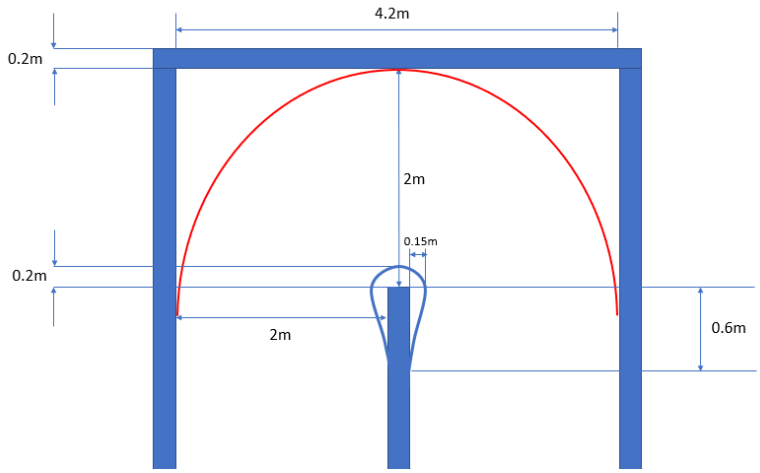

Figure 47 – Drawing of the improved shape of the curves

4.3.1. Tracers tests

i. Methodology

The principles of the tracer tests have been introduced previously in the **Section 4.2.1**. The methodology is the same in this case except that the quantities of salt have been adjusted to the configuration and the size of the HRAP pilot; these quantities are summarized in **Table 10** below. The data are recorded with two different conductivity meters (HandyLab 680 and YSI Multiprobe). The Multiprobe can measure conductivity values down to 0.1 µS/cm while the HandyLab 680 sensor has a sensitivity down to 0.1 mS/cm in the range of conductivity encountered in the wastewater. The calculations are based on the results recorded by the Multiprobe and the HandyLab 680 is used to double-check the results.

Table 10 – Quantities of salt for the tracer tests in Vietnam

Depth	Mass of salt based on the results in Arlon (kg)	Adapted mass of salt (kg)
0.25	5	8.8
0.4	7.2	11
0.6	9.6	13.4

First of all, the salt used is selected based on different criteria such as the crystals size, the purity, the water content and the cost. The results of the different calibration curves are presented in the "**Appendix B** – Calibration curves of three different potential salts" that can be found at the end of the document. Also, it was necessary to verify the linear response of the conductivity as a function of the added salt. Indeed, this response is linear up to a certain concentration and then, the slope decreases and the linear relationship is not respected anymore. As a matter of security, it was decided to change the water contained in the pond every 6 tests so that the salt concentration stays sufficiently low and in the range of the linear response. Thereafter, a new calibration curves will be required every time the water is freshened so that the equation linking the concentration of added salt to the measured conductivity is as accurate as possible. These linear interpolations are presented in the "**Appendix C** – Calibration curves for the tracer tests" as well as the equations that give the conductivity as a function of the added salt concentration.

It has to be mentioned that the conductivity is a function of the temperature. The HandyLab 680 conductivity meter and the Multiprobe are presumed to take into account the influence of the temperature on the conductivity. Nevertheless, it may be interesting to construct the calibration curves in a temperature range close to the one of the wastewater circulating in the pond which is between 29 to 35°C. In this way, even if the correction of the probe is not perfect, the influence on the data recorded and their conversion in concentrations is small and the accuracy is increased.

The preparation of the tracer tests conducted in Vietnam includes a prediction of the hypothetic response based on a comparative study made between the results of tracer tests done on a HRAP (using an airlift aeration system) implemented in Morocco [61] and the one studied in the Ninh Thuan province. The theoretical water velocity (13cm/s) and the length of the channel (57.6m) being known, one only requires the dispersion coefficient E_z, obtained from the research made in Marocco, to obtain the Péclet number and simulate Voncken's equation. It appears that the predicted curve matches quite well with the tracer tests carried out in Vietnam (**Figure 48**).

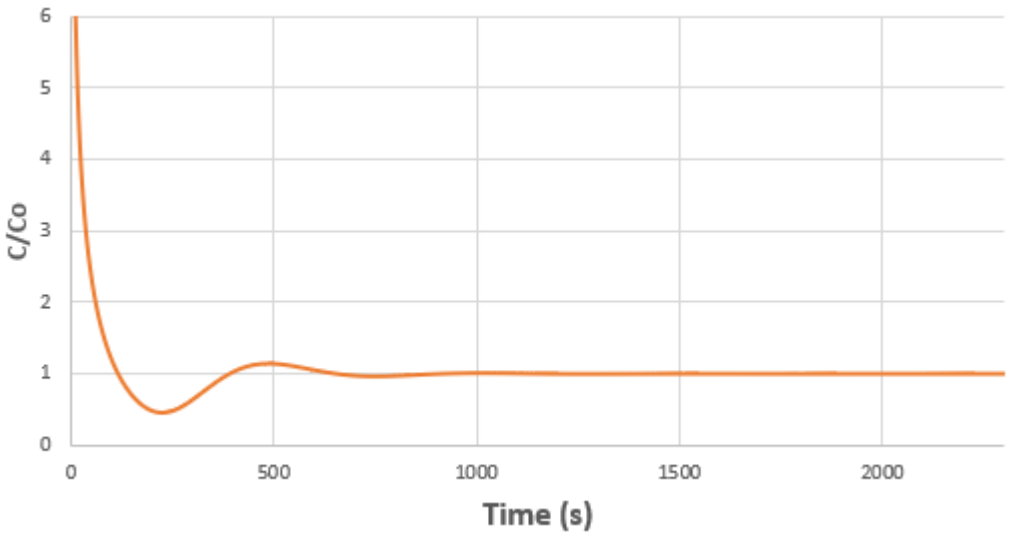

Figure 48 – Prediction of the tracer tests

The first trials failed due to several possible reasons such as:

- **Low salt concentration**: even though these concentrations are calculated based on the water flow and the quantities used in Arlon, it appears that the response is too low and the interpretation is difficult. The quantities are adapted in order to obtain a satisfying response (**Table 10**).
- **Position of the conductivity meters**: both the Multiprobe and HandyLab680 were first placed just behind the injection point meaning that the salt has to do one loop before it is first detected by the probes. It is decided to inject the salt at

the output of the airlift system and to measure the conductivity before the first turn. By doing this, only 10 meters separate the injection point to the measurement point. One disadvantage of such configuration is that the injection of salt is not ideally mixed when it is first measured and it can explain the multiple conductivity peaks at the beginning of each test.

- **Injection of salt:** the injection needs to be done carefully and smoothly to obtain a rather homogeneous injection. This prevents the occurrence of high fluctuations around the first peak.

The planning of the tracer tests is presented in the following **Table 11**. The code TXXYZ corresponds to a tracer test done with XX cm of water, at a speed of the blower of Y (in this report, the speed of the blower relates to the position of the button that controls the air flowrate; this button can be adjusted from 0 to 10) and Z stands for the number of the test. The speed and direction of the wind may have an influence on the results in case of strong winds. The meteorological data corresponding to the day of every experiments are also present in **Table 11** below.

Table 11 – Planning of the experiments conducted in Vietnam

Date	Tracer tests	Wind (direction – maximal speed [m/s])
12-05-2018	First trials and adjustment of the methodology	E – 8
13-05-2018	T4041 – T4061 – T4062 – T4063 – T4081 – T40101	ESE – 8
15-05-2018	T2541 – T2561 – T2562 – T2581 – T2582 – T25101	ESE – 8
16-05-2018	T6041 – T6061 – T6061 – T6081 – T6082 – T60101	ESE – 10

ii. Results and discussion

The results of the different tracer tests are presented in the form of three tables corresponding to the three different depths. Each of the three tables summarizes the information of interest, namely:

- Frequency of the blower [Hz];
- Power of the blower [kW] and air flowrate [Nm^3/m^2h];
- Circulation time [s];
- Péclet number [-];
- The number of perfectly mixed tanks corresponding to the configuration [-];
- Velocity [cm/s];
- Dispersion coefficient [m^2/s];
- Volume of the HRAP [m^3].

The power of the blower has been estimated based on the electrical consumption indicated by a dedicated electrical meter due to the unavailability of a proper way to measure the power. Consequently, it is only an approximation of the real power developed by the blower. Concerning the air flowrates, a flow meter (rotameter) is used to measure them. All the tests are realized without the rotameter installed on the pilot and the presence of the flow meter induces head losses so that the measured air flowrates are slightly lower than the real values. The Péclet number and the circulation time have both been adjusted by using MATLAB to minimize the mean squared error between the experimental data and the theoretical curve represented by Voncken's equation **(Equation 1)**. Based on the Péclet number, it is possible to get the number of perfectly mixed tanks j to be put in series to model the HRAP pilot **(Equation 2)**.

After that, based on the length of the raceway pond ($L = 57.6m$, calculated using the plan of the pilot), the water velocity (u) and the definition of the Péclet number, it is possible to get the dispersion coefficient E_z for each test:

$$Pe = \frac{u * L}{E_z}$$

Finally, knowing the exact mass of salt injected for every experiments and, also, the relationship between the conductivity and the added salt concentration, the volume of the pond can be deduced from the following formula:

$$V(L) = \frac{m_s\,(g)}{C_0\left(\frac{g}{L}\right) - C_i\left(\frac{g}{L}\right)} \qquad \textbf{(Equation 8)}$$

Where :

- V is the volume of the HRAP [L];
- m_s is the mass of added salt for one test [g];
- C_o is the homogenized added salt concentration at the end of the test [g/L];
- C_i is the initial added salt concentration [g/L].

The graphs of all the experiments are presented in the "**Appendix D** – Graphs of the tracer tests".

a. Results

Table 12 – Results of the tracer tests at a depth of 40 cm

Test	Frequency [Hz] – *Power (kW)*	Air flowrate [Nm³/m²h]	Circul-ation time, t_c [s]	Péclet number [-]	Number of tanks, j [-]	Velocity, u [cm/s]	Dispersion coefficient, E_z [m²/s]	Volume [m³]
T4041	17.8 - *0.6*	<5	648	25.252±0.511	14	8.89	0.2028	56.701
T4061	30.65 - *1.2*	10	375	20.249±0.382	11	15.36	0.4369	48.889
T4062	30.65 - *1.2*	10	*320*	*20.347±0.457*	*11*	*18*	*0.5096*	*47.888*
T4063	30.65 - *1.2*	10	385	21.866±0.410	12	14.96	0.3941	50.482
T4081	47.85 - *1.8*	16.67	304	23.894±0.503	13	18.95	0.4568	51.080
T40101	49.7 - *2.4*	21.67	289	22.423±0.605	12	19.93	0.5120	49.554
							Average volume	**50.766**

With the exception of T4062, the results of each test are consistent at a depth of 40cm (**Table 12**). The results of T4062 are incoherent and no plausible explanation has been found to explain these variations, this test will be ignored in the analysis. The velocity increases with the power of the blower starting at 8.89 cm/s at the lowest and rising up to 19.93 cm/s when the air flowrate is maximal. As it has been said previously, a water velocity between 10 and 30 cm/s is required in order to obtain a sufficient mixing and to avoid microalgae sedimentation. This means that a power of 0.6 kW would be too low to assure a good efficiency and productivity of the HRAP. Increasing the power from 0.6 to 1.2kW leads to an increase of 70.5% of the water velocity resulting in a satisfying value of 15.16 cm/s. The rise in water flowrate is lower when the power is increased from 1.2 to 1.8kW (25%) and even lower in the last case (5.17%). This means that the benefit of increasing the power of the blower decreases for high developed powers. This has to be taken into account when the conditions of growth will be chosen in the following of the project. The same conclusions can be made for the dispersion coefficient E_z. Increasing the power from 0.6 to 1.2kW, from 1.2 to 1.8kW and from 1.8 to 2.4kW induces rises of 94.3%, 15.9% and 12.1% respectively (considering T4041, T4063, T4081, T40101). The amplitude of the increases of the dispersion coefficient decreases when the power increases as it was the case for the velocity. The advantage of increasing the air flowrate being significant at low powers compared to high powers. The dispersion coefficients E_z in the case of the HRAP pilot implemented in Vietnam are one order of magnitude higher than the E_z obtained in Arlon. This could possibly mean that the dispersion significantly increases with the size of the pond. But it is explained notably by the power of the blower

which is proportionally higher in Vietnam and, also, by the presence of a lot of turbulences and recirculation zones in the Vietnamese pond.

The volume has been calculated based on **(Equation 8)** and the results show a mean value of 50.766m^3 which is similar to the value obtained using the data recorded by HandyLab 680 (54.43m^3). These results should be compared to the theoretical value based on the drawing of the HRAP pilot which is 61.83m^3. The values are similar and the difference may come from the real dimensions of the pilot that differ from the drawing and, also, from the lack of accuracy of the results recorded. This lack of precision could come from the fact that some salt may sediment in the pond instead of completely solubilize so that the final concentration measured is lower than the effective salt concentration.

The Péclet numbers are similar and range from 20.249 to 25.252 for this configuration. Consequently, the numbers of perfectly mixed tanks required for the modelling of the HRAP are also close and stand between 11 and 14 tanks. It is interesting to compare the modelled curves given by Voncken's equation where the circulation times and the Péclet numbers have been implemented to simulate each test (**Figure 49**). The Péclet numbers being similar, the height of the peak recorded after one loop is also in the same range. It is possible to observe that it is slightly higher for T4041 which has the highest Péclet number than for T4061 which has the lowest Péclet number. The moment when the first peak appears after one turn corresponds to the circulation time. This time decreases with increasing blower speeds and this is observed in the graph below where the first peak corresponds to T40101 in blue whereas the last one represents T4041 in green.

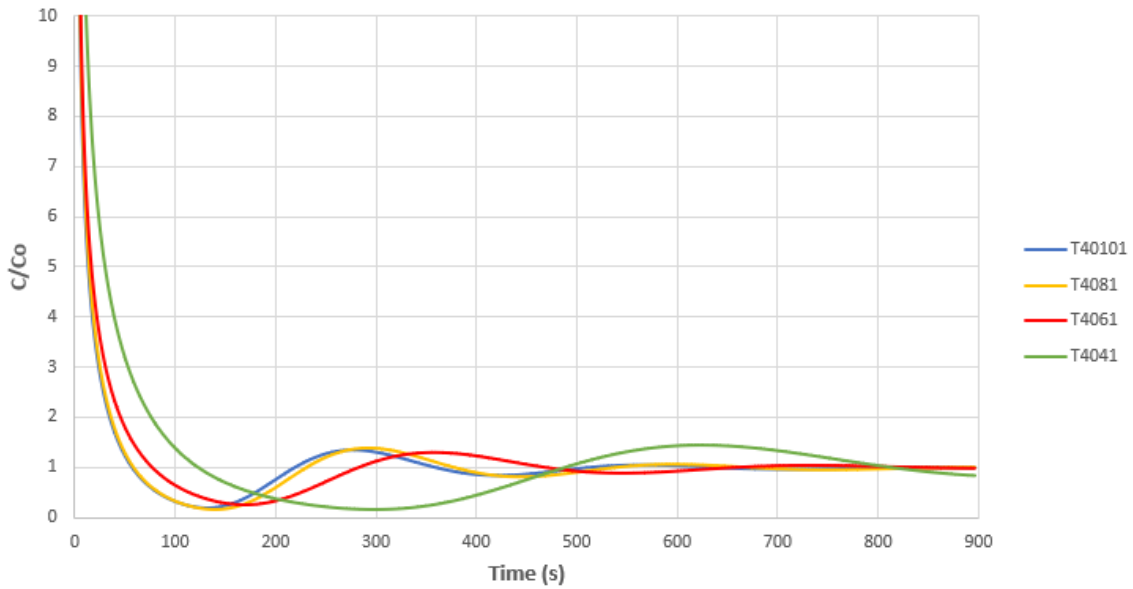

Figure 49 – Comparison of the powers of the blower using Voncken's equation (40cm)

Table 13 – Results of the tracer tests at a depth of 25 cm

Test	Frequency [Hz] – *Power [kW]*	Air flowrate [Nm³/m²h]	Circulation time, t_c [s]	Péclet number [-]	Number of tanks j [-]	Velocity, u [cm/s]	Dispersion coefficient E_z [m²/s]	Volume [m³]
T2541	17.8 - *0.6*	<5	665	22.389±0.542	11	8.66	0.2228	44.172
T2561	30.65 - *1.2*	10	384	17.164±0.535	8	15	0.5034	39.873
T2562	30.65 - *1.2*	10	384	18.792±0.609	9	15	0.4597	39.532
T2581	47.85 - *1.8*	16.67	318	19.513±0.776	9	18.11	0.5346	38.562
T2582	47.85 - *1.8*	16.67	312	17.729±0.568	8	18.46	0.5997	39.076
T25101	49.7 - *2.4*	21.67	297	19.708±0.736	9	19.39	0.5694	39.250
							Average volume	40.077

For the next two water levels, it is decided to perform the tracer tests two times for a power of 1.2kW (instead of three times) and two times for a power of 1.8kW (instead of one time). The two other powers are studied only one time. The confidence in the results for the powers studied twice will thus be increased.

At a depth of 25cm (**Table 13**), the general trend of the results is the same than for 40cm. The velocity and the dispersion coefficient into the pond increase with the power of the blower but these rises become lower at high levels of power. Moreover, the dispersion coefficient calculated at 2.4kW (0.5694m²/s) is almost equal to the average dispersion at power 1.8kW (0.5672m²/s) meaning that the increase of power does not lead to a significantly higher dispersion but only to a slightly higher velocity (19.39cm/s compared to 18.46cm/s). Obviously, these conclusions have to be treated carefully due to the low number of experiments.

The average volume calculated in this configuration, based on the final concentrations of added salt, is 40.077m³ compared to a theoretical value of 45.197m³. The Péclet numbers range from 17.164 to 22.389 leading to similar numbers of perfectly mixed tanks (between 8 and 11 for this configuration).

Table 14 – Results of the tracer tests at a depth of 60 cm

Test	Frequency [Hz] – *Power [kW]*	Air flowrate [Nm³/m²h]	Circulation time, t_c [s]	Péclet number [-]	Number of tanks j [-]	Velocity, u [cm/s]	Dispersion coefficient E_z [m²/s]	Volume [m³]
T6041	17.8 - *0.6*	<5	687	39.473±0.893	19	8.38	0.1223	76.571
T6061	30.65 - *1.2*	10	379	31.195±0.666	15	15.2	0.2807	87.581
T6062	30.65 - *1.2*	10	388	31.806±0.394	15	14.84	0.2687	78.363
T6081	47.85 - *1.8*	16.67	309	32.453±0.4367	16	18.64	0.3308	74.033
T6082	47.85 - *1.8*	16.67	308	32.88±0.426	16	18.70	0.3276	72.315
T60101	49.7 - *2.4*	21.67	283	33.447±0.487	16	20.35	0.3505	71.696
							Average volume	76.760

The last case at a depth of 60cm shows also consistent results with a similar evolution than the two first water levels (**Table 14**). The increases of power from 0.6 to 1.2kW, from 1.2 to 1.8kW and from 1.8 to 2.4kW lead to rises of 79.24%, 24.30% and 9% respectively for the velocity and 124.6%, 19.84% and 6.99% respectively for the dispersion coefficient. The same conclusion than for the two previous cases can be made which is that the benefits of an increase of the air flowrate decrease at high developed powers.

The average volume calculated from the homogenized salt concentration is 76.76m³ compared to a theoretical volume of 84m³. From test T6061 to test T60101, the volumes are decreasing which is the sign that the final concentration after each test increases even though the mass of added salt is the same. One possible explanation is that the salt of the previous tests, which may have sedimented, is remixed when the power is increased leading to higher final concentrations.

Finally, the Péclet numbers range from 31.195 to 39.473 leading to numbers of perfectly mixed tanks between 15 and 19.

b. Comparison

The experiments conducted in Vietnam are performed at three different depths and four different air flowrates corresponding to four different powers. The influence of these two parameters on the velocity, the dispersion coefficient, the Péclet number and the number of perfectly mixed tanks necessary for the modelling is discussed in the following.

- **Water velocity**

The comparison of the water velocity for each experiment is represented in **Figure 50** below. It comes directly that the trends of the evolution of the velocity with the power of the blower are similar at each water level and this has already been discussed in the previous section. A depth of 25cm leads to the lowest velocities which can be confusing. Indeed, the energy input being the same as for the two other water levels, one might expect that it results to a higher velocity when there is less water in the HRAP pilot. A possible explanation is that the configuration of the airlift aeration system is not suitable for low water levels. Indeed, for a small depth, the exit of the airlift is narrow (**Figure 45**) and constitutes a *"bottleneck"* for the water flow. The amount of water that could flow through the exit of the airlift being limited, this might slow down the water. Then, at 60cm, the velocity is also lower than at 40cm (with the exception of T60101). In this case, the difference comes from the amount of water to be put in motion. The volume being higher at 60cm, the velocity is lower compared to the one recorded at 40cm if we consider a same developed power. The fact that the calculated velocity for T60101 is higher than for T40101 is partially explained by the meteorological conditions. During the recording of T60101 the wind was stronger than for the other tests and could have slightly influenced the waterflow.

Figure 51 shows a different visual of the different velocities by comparing the circulation times of all tests. Low power (0.6kW) leads to a circulation time which is at least 70% higher than the time recorded at a power of 1.2kW. Then the decrease of the t_c follows the same pattern than discussed previously meaning that the reduction decreases at high powers which corresponds to a smaller negative slope.

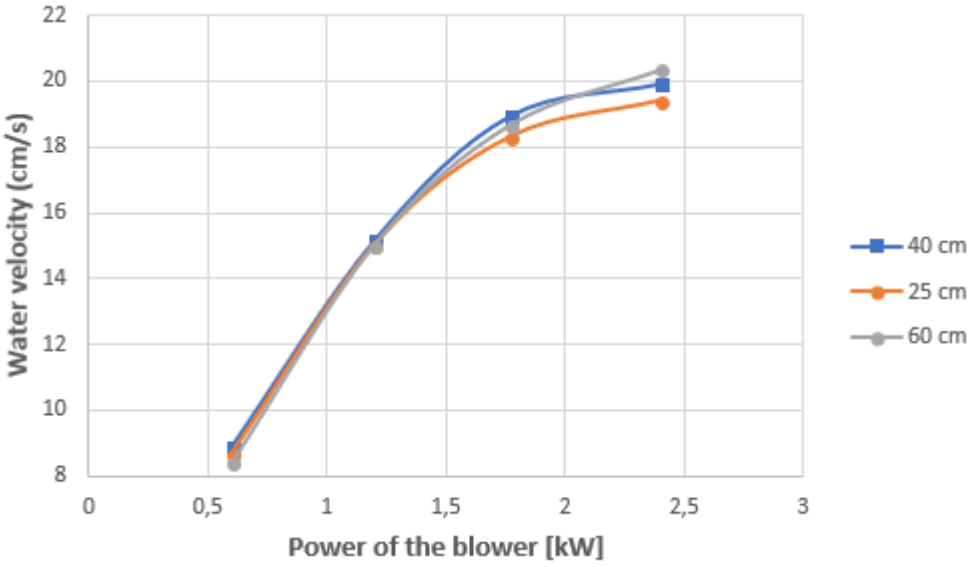

Figure 50 – Comparison of the water velocities for all tracer tests

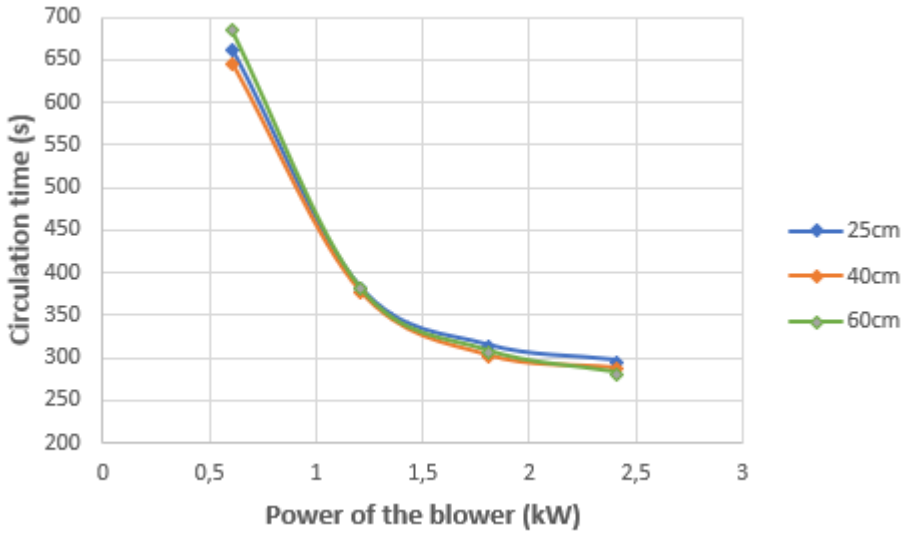

Figure 51 – Comparison of the circulation times for all tracer tests

➢ **Dispersion coefficient**

One of the primary goals of these series of tracer tests is to evaluate the mixing capacity of the airlift aeration system. This is assessed by means of the dispersion coefficient E_z. The evolution of the E_z with both the power and the depth is represented in **Figure 52**. As previously, the general trends are the same for each depth. It appears that, even though the velocity is not maximal at a 25cm depth, the recorded dispersion is the highest in this case. It comes from the fact that one uses the same power as in the two other cases to mix a reduced amount of water. Consequently, the degree of mixing brought by the airlift is higher than in the two other cases. The opposite reasoning is valid for a depth of 60cm. In this case, the amount of water to be stirred is higher than in the two

other cases, as a result, the dispersion coefficient is significantly lower in this case. For example, at a power of 1.2kW, the dispersion coefficient is 13.7% smaller at 40cm than at 25cm and 42.96% smaller at 60cm than at 25cm.

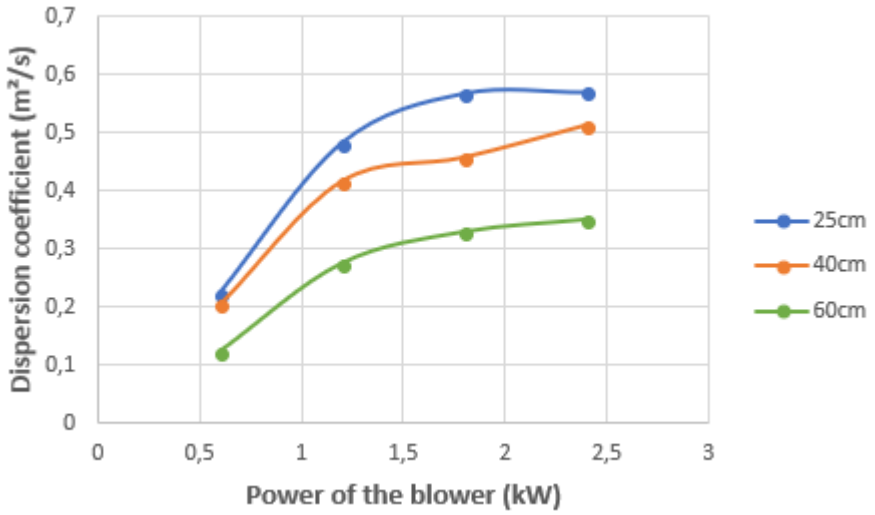

Figure 52 – Comparison of the dispersion coefficients for all tracer tests

Another way to compare these results is to represent the dispersion coefficient as a function of the water depth (**Figure 53**). This graph clearly shows the positive influence on the mixing of a shallow pond compared to a deep pond. Nevertheless, it also has to be mentioned that the water level has an influence on the bulk concentration which itself affects the absorption in the bulk of the liquid. If the light absorption is too high, it induces photolimitation which leads to a reduced microalgae productivity of the HRAP. The following steps of the RENEWABLE project will have to consider the hydrodynamic conditions but also the other factors influencing the microalgal growth.

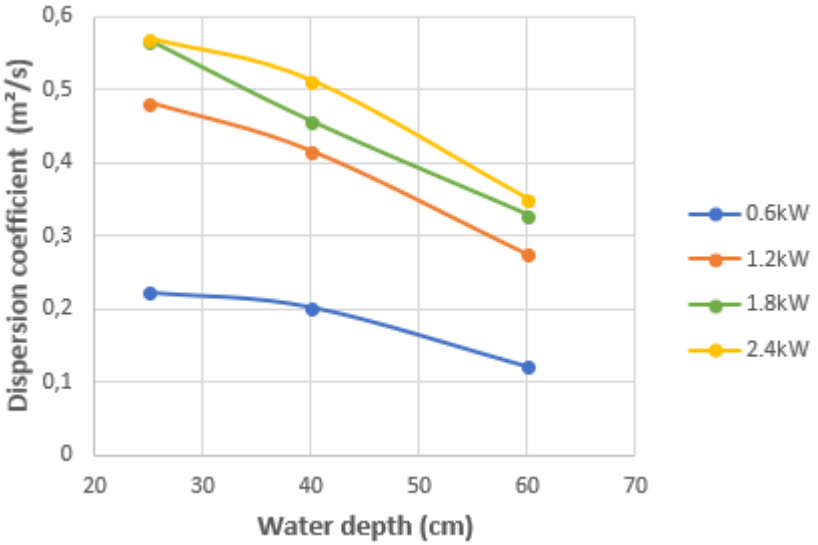

Figure 53 – Evolution of the dispersion coefficient with the water depth

➢ **Péclet number and number of perfectly mixed tanks**

These two different numbers are directly related by the **(Equation 2)** and this is the reason why the discussion is made at the same time. The Péclet number gives the relative importance of advection compared to diffusion. High Péclet numbers correspond to an advectively dominated flow while low Péclet numbers reveal a flow where diffusion is predominant. The evolution of the Péclet number for each tracer test is represented in **Figure 54** below. The first element that is noteworthy is that for every depth, the Péclet number is maximal at the lowest power. This comes from the fact that the mixing is decreased when the developed power is equal to 0.6kW. In this case, the advection in the pond is more significant compared to dispersion which leads to higher Péclet numbers. This has been noticed previously when the dispersion coefficients were compared. Then, the minimal Péclet number occurs for a power of 1.2kW. This means that for every depth, the diffusion is more important for this air flowrate compared to the advection, even though the dispersion coefficient is not the highest in this case. Finally, no general significant trend can be drawn for the evolution between 1.2 and 2.4kW. The Péclet numbers are similar in these cases. The same general evolution can be observed for the number of perfectly mixed tanks to be put in series for the modelling of a given configuration.

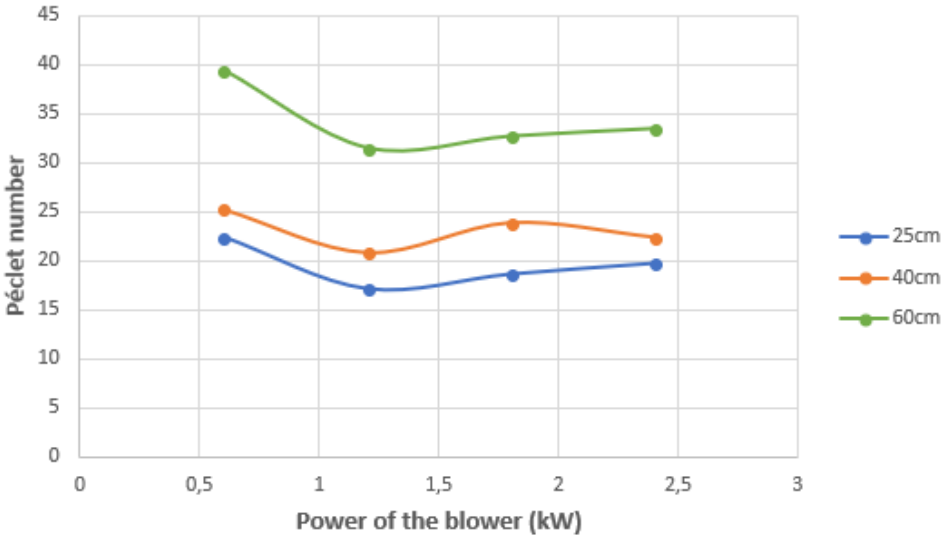

Figure 54 – Comparison of Péclet numbers for all tracer tests

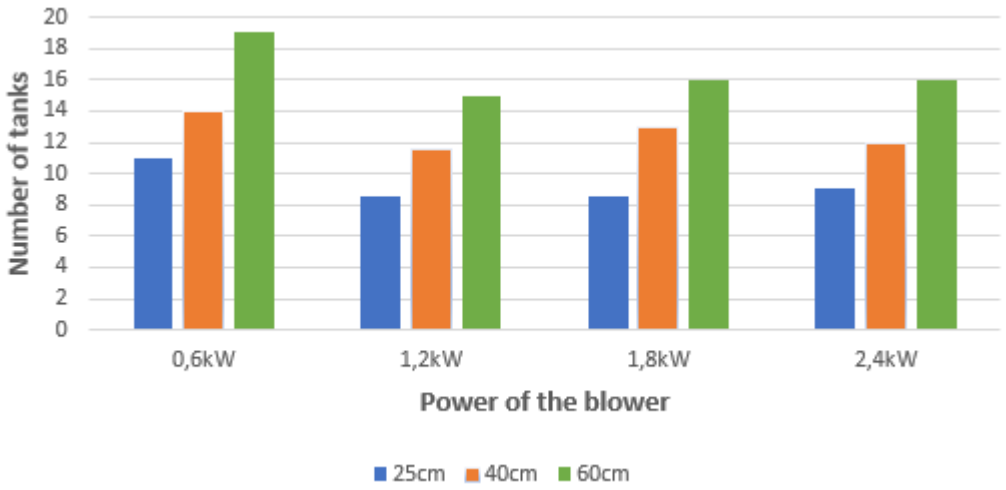

Figure 55 – Comparison of the numbers of perfectly mixed tanks for all tracer tests

The following **Figure 56** compares three tracer tests realized at a power of 1.2kW. It can be seen that the higher the water level, the longer it takes to homogenize the salt. The time of homogenization is directly related to the Péclet number. The higher the Péclet number, the lower the dispersion and the longer it takes to mix the salt.

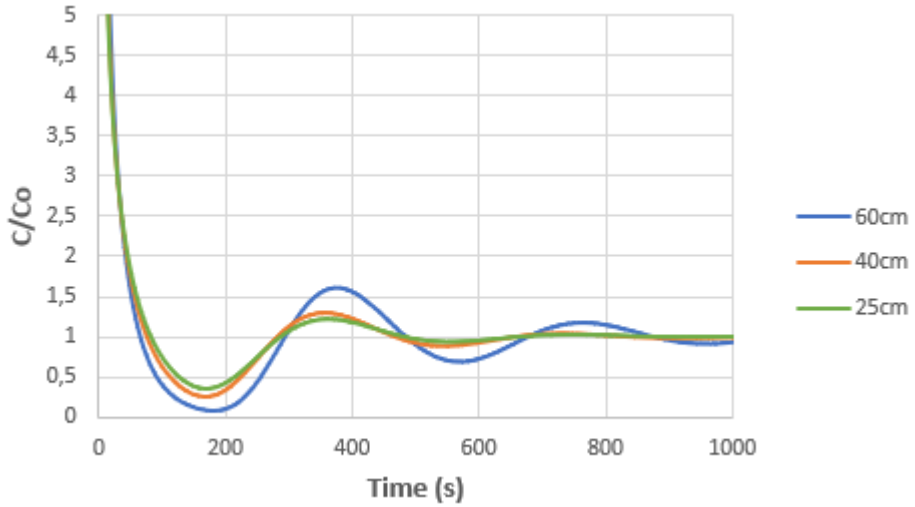

Figure 56 – Comparison of the evolution of the salt concentration for three different depths at a power of 1.2kW

c. Discussion

The results of the tracer tests show the significant effects resulting from changes of operational conditions (depth and power of the blower i.e. air flowrate). The limitations of the airlift system have been highlighted notably by the fact that the water velocity is lower at a depth of 25cm compared to the one at 40cm for a same developed power. It is also an evidence that the design of the airlift can still be improved. The dispersion within the pond is higher at low water levels leading to the best mixing conditions.

Nevertheless, as it has been mentioned, the concentrations of substrate and other compounds depend on the water depth meaning that a shallow medium could lead to a lower productivity even though the mixing is better than for a deeper configuration.

The ideal water velocity for microalgae growth stands between 10 and 30cm/s meaning that a power of 0.6kW is insufficient for each depth. A power higher than 0.6kW should then be chosen to grow the biomass. The velocity gain induced by an increase of power decreases at high developed powers. Thus, for example, if a water flow of 18.5cm/s yields almost the same productivity than at 19.5cm/s, one should choose to grow the microalgae at 18.5cm/s. In this way, the energy consumption is reduced by 25% (from 2.4kW to 1.8kW). The purpose of this project being to develop an economical and sustainable technique to treat the wastewaters, reducing the electrical consumption is a lead to achieve this goal.

Then, the dispersion is satisfying for developed powers higher than or equal to 1.2kW. The necessary times for the complete mixing of the salt are similar for depths of 25 and 40cm. This time is almost doubled at 60cm. For a power of 0.6kW, the dispersion coefficient is significantly lower than in the other cases and the mixing is then also lower. Due to the reduced number of experiments, the previous discussion has to be treated carefully. Furthermore, several causes of mistakes can be identified. Among them, the turbulences and recirculation zones present in the pond, the influence of the wind, the difference of water content of the salt or even the systematic error of the measuring material.

Finally, a comparison with the theoretical data provided by ROBUSCHI® and a model developed by Sustainwater – Prof. Vasel's company – is realized in the "**Appendix E** – Comparison between the theoretical data and the results of the tracer tests".

4.3.2. Oxygen transfer tests

i. Methodology

As it was the case for the previous tracer tests, the methodology for the oxygen transfer tests conducted on the HRAP pilot in the Ninh Thuan province is the same as the experiments carried out in Arlon, except for the quantities of products that should be adapted considering the volume of water in the pond and the DO (**Table 15**). It has to be noted that the DO is expected to be lower than the value observed in Arlon due to the fact that it is temperature dependent and that the water temperature is higher. This is measured in practice: the initial DO being ≈7.8±0.3g/L at 32±2°C in this case compared to ≈10±0.2g/L at 21.5±1.5°C (in presence of microalgae) in Arlon. Consequently, the quantities of Na_2SO_3 are adapted in order to avoid an excess or default of sulfite which would make the calculations difficult.

Table 15 – Quantities of products for the oxygen transfer tests in Vietnam

Depth [m]	Mass of Na_2SO_3 [kg]	Mass of $CoCl_2.6H_2O$ [g]
0.25	**3**	115
0.4	4	155
0.6	5	200

All the mathematic developments to get the different volumetric transfer coefficients, $(k_l a)_i$, are based on the same principles as in Arlon. These calculations require only the use of two oxygen probes. The location of the two probes (YSI Multiprobe (Probe A) and HandyLab 680 (Probe B)) is shown in **Figure 57** below.

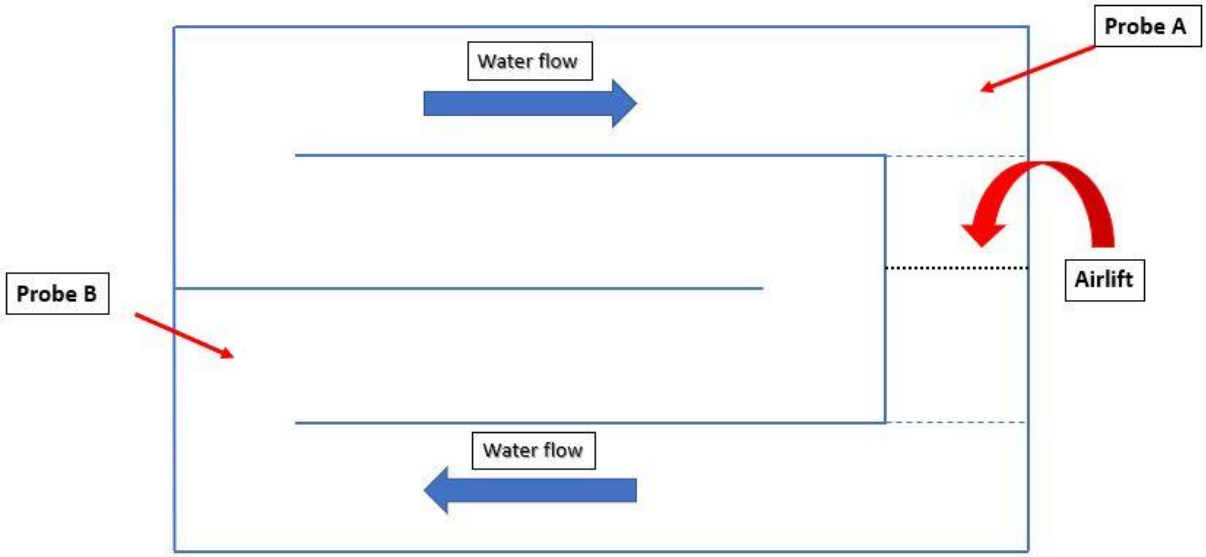

Figure 57 – Location of the two dissolved oxygen probes

Given the fact that, most of the time, only one stage is observable in the recorded graphs – the stage corresponding to the first loop – only the second method presented to measure the volumetric coefficient of transfer of the entire HRAP, $(k_l a)_R$, can be used. The average of the data recorded by the two probes is calculated. It comes out that the accuracy of these calculations is lower than the results obtained in Arlon. Nevertheless, it still gives an idea of the oxygen transfer characteristics in the pond. Moreover, as it has been introduced in the previous **Section 4.2.2**, the oxygen transfer tests should be conducted at a temperature as constant as possible. It is not possible in practice and for some tests a temperature increase or decrease of 1.5°C is observed between the beginning and the end of the experiments. This has an impact on the DO that one must keep in mind.

For the calculation of the $(k_l a)_A$, it was decided previously to neglect the transfer between the atmosphere and the channel. The error being low in the case of the small-scale HRAP pilot in Arlon because it was installed inside so that no wind was affecting the water surface. It is not the case for the Vietnamese pilot which is positioned outside

and exposed to strong winds. The following equations give the definition of the volumetric transfer coefficient of the airlift system when the $(k_l a)_{channel}$ is not negligible.

$$(k_l a)_R (C_S - C_0) V_R = (k_l a)_A (C_S - C_0) V_A + (k_l a)_{Channel} (C_s - C_0) V_{Channel}$$

$$(k_l a)_A = \frac{(k_l a)_R V_R - (k_l a)_{Channel} V_{Channel}}{V_A}$$

With:

- C_S: Concentration of dissolved oxygen at saturation;
- C_0: Initial concentration of dissolved oxygen, $C_0 \cong 0\, mg/l$;
- V_R: Volume of the entire reactor;
- V_A: Volume of the active part of the airlift (where the bubbles rise up);
- $V_{Channel} = V_R - V_A$: Volume of the channel.

The graphs of each test are presented in "**Appendix F** – Graphs of the oxygen transfer tests (Vietnam)". The planning of the experiments as well as the meteorological data are summarized in the following **Table 16**.

Table 16 – Planning of the experiments conducted in Vietnam

Date	Tracer tests	Wind (direction – maximal speed [m/s])
19-05-2018	O4061 – O4062	ESE – 7
20-05-2018	O4081 – O4082 – O40101 – O4041	ESE – 7
21-05-2018	O2561 – O2562	ESE – 8
24-05-2018	O2581 – O2582 – O25101 – O2541	ESE – 7
25-05-2018	O6061 – O6062 – O6081 – O6082	E – 7
26-05-2018	O60101 – O6041 – O4061b – O4062b	E - 6

ii. Results and discussion

The results of the different oxygen transfer tests are presented in the three tables below that summarize the following information:

- Frequency of the blower [Hz];
- Power of the blower [kW] and air flowrate [Nm^3/m^2h];
- Volumetric transfer coefficient of the entire HRAP $(k_l a)_R$;
- Volumetric transfer coefficient of the channel $(k_l a)_{channel}$;
- Volumetric transfer coefficient of the airlift $(k_l a)_A$;
- Aeration time, t_a, that is defined as the time needed to obtain 90% of the initial DO starting from the moment where the DO starts to rise.

The aeration time is a simple way to compare the oxygenation capacity of the pond at different conditions. Nevertheless, this time is also influenced by the variations of temperature occurring during the experiments. Indeed, if the temperature increases during a test, the t_a calculated will be higher than the t_a that would have been obtained at constant temperature because the concentration of oxygen at saturation decreases. On the contrary, if the temperature decreases, the t_a calculated is lower than the actual t_a. The conclusions made from the comparison of this parameter have to be considered cautiously.

a. Results

Table 17 – Results of the oxygen transfer tests at a depth of 40cm

Test	Frequency [Hz] – *Power* [kW]	Air flowrate [Nm³/m²h]	$(k_l a)_R$ $[s^{-1}]$	$(k_l a)_{channel}$ $[s^{-1}]$	$(k_l a)_A$ $[s^{-1}]$	Aeration time [min]
O4041	17.8 - *0.6*	<5	$4.17 * 10^{-4}$	$4.66 * 10^{-4}$	$0.29 * 10^{-3}$	40.3
O4061*	30.65 - *1.2*	10	$7.74 * 10^{-4}$	/	/	17.8
O4062*	30.65 - *1.2*	10	$7.36 * 10^{-4}$	/	/	17.2
O4061b	30.65 - *1.2*	10	$11.78 * 10^{-4}$	$10.15 * 10^{-4}$	$1.61 * 10^{-3}$	14.8
O4062b	30.65 - *1.2*	10	$15.17 * 10^{-4}$	$12.62 * 10^{-4}$	$2.18 * 10^{-3}$	15.3
O4081	47.85 - *1.8*	16.67	$16.99 * 10^{-4}$	$11.28 * 10^{-4}$	$3.22 * 10^{-3}$	11.3
O4082	47.85 - *1.8*	16.67	$19.35 * 10^{-4}$	$12.19 * 10^{-4}$	$3.84 * 10^{-3}$	11.3
O40101	49.7 – *2.4*	21.67	$23.53 * 10^{-4}$	$10.98 * 10^{-4}$	$5.70 * 10^{-3}$	9.9

*tests realized with the YSI Multiprobe only

The results of the oxygen transfer tests realized at 40 cm (**Table 17**) seem coherent. The volumetric transfer coefficients of both the entire pond and the airlift increase with increasing air flowrates. The air flowrate being higher, the number of bubbles rising in the airlift is higher which leads to a higher oxygen transfer. The majority of the transfer occurring in the airlift, the $(k_l a)_R$ follow the same evolution as the $(k_l a)_A$. Regarding the volumetric transfer coefficient of the channel, they are in the same range ($\approx 10 * 10^{-4} - 12 * 10^{-4} s^{-1}$) except for O4041. The $(k_l a)_{channel}$ is highly affected by the wind. The experiment O4041 was realized early in the morning when the wind is usually absent which can explain why the value is significantly lower. Moreover, the low water velocity implies smaller turbulences that lead to a smalle $(k_l a)_{channel}$. Theoretically, the $(k_l a)_{channel}$ should be close for each experiment, but the meteorological conditions and the water velocity being different from test to test, the $(k_l a)_{channel}$ also varies.

The aeration time of the pond is more than two times higher for O4041 than for all the other tests. This is the reflect of a very low $(k_l a)_R$ for an air flowrate lower than 5 Nm³/m²h ($0.29 * 10^{-3} s^{-1}$). The other aeration times stand in the same range, between 9.9 and 17.8 min.

It is interesting to notice the difference between the tests O4061/O4062 and O4061b/O4062b. The conditions being the same, the $(k_l a)_R$ should be similar. Nevertheless, the first two experiments resulted in a lower $(k_l a)_R$ than for the last two. A possible cause of these differences could be the "quality" of the water. In general, the water is refreshed every 4 tests because the increasing sodium concentrations from test to test may affect the gas transfer. It was not the case for O4061b and O4062b, the water was kept for 6 experiments (due to the lack of cobalt catalyst) and these two tests were respectively 5th and 6th. The higher $(k_l a)_R$ calculated can be due to the high sodium concentration in the pond. Ideally, the water should be refreshed between each experiment to be sure that the salt concentration does not affect the results. Unfortunately, refreshing the water between each test would have been too long and too expensive (the cobalt being relatively costly).

Finally, one should have a look at the data recorded by the Multiprobe at 40cm with different air flowrates (**Figure 58**). The first important thing to notice is the height of the first stage which increases for higher powers. The main cause of this step being the transfer within the airlift, it explains why the DO increase occurs in a short time (the time corresponding to the residence time in the airlift). For these experiments, only one step is observable. The amplitude of each step being proportional to $C_s - C(t)$, it tends to decrease when the DO increases. The fact that the jumps cannot be seen for the following loops could mean that the transfer in the airlift aeration system is in the same order of magnitude as the transfer occurring in the channel.

The aeration times can be observed approximately, one can see that the saturation value is reached almost three times faster is the case of O40101 compared to O4041. Finally, the injection times can also be seen in **Figure 58**, they correspond to the time during which the DO is ≈0mg/L. As it was the case for the small-scale pilot in Arlon, these injection times are calculated to be slightly lower than the circulation time to avoid any overlapping.

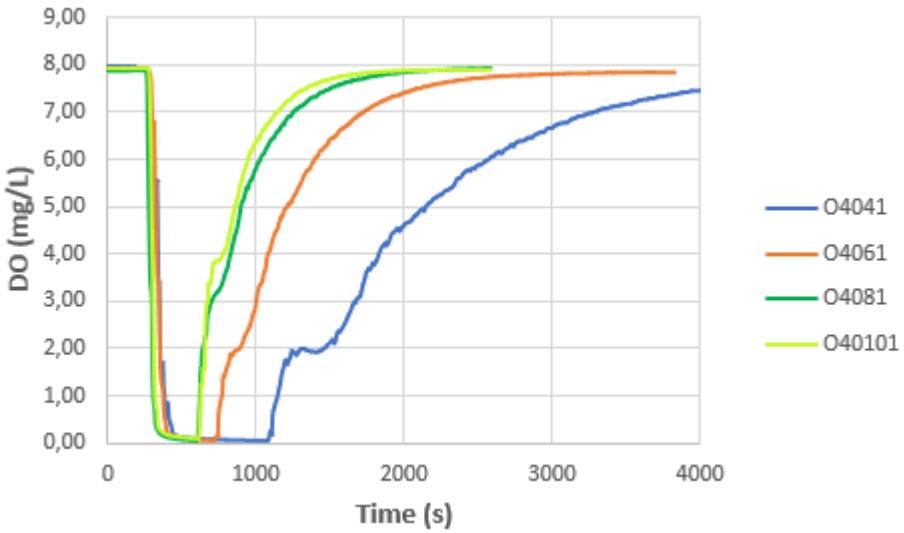

Figure 58 – Comparison of the oxygen transfer tests realized at a depth of 40cm

Table 18 – Results of the oxygen transfer tests at a depth of 25cm

Test	Frequency [Hz] – *Power* [kW]	Air flowrate [Nm³/m²h]	$(k_l a)_R$ $[s^{-1}]$	$(k_l a)_{channel}$ $[s^{-1}]$	$(k_l a)_A$ $[s^{-1}]$	Aeration time [min]
O2541	17.8 - *0.6*	<5	$6.33 * 10^{-4}$	$7.39 * 10^{-4}$	$0.41 * 10^{-3}$	34.4
O2561	30.65 - *1.2*	10	$16.85 * 10^{-4}$	$8.67 * 10^{-4}$	$3.08 * 10^{-3}$	12.7
O2562	30.65 - *1.2*	10	$16.29 * 10^{-4}$	$10.66 * 10^{-4}$	$2.15 * 10^{-3}$	14.8
O2581	47.85 - *1.8*	16.67	$17.42 * 10^{-4}$	$10.88 * 10^{-4}$	$3.12 * 10^{-3}$	10
O2582	47.85 - *1.8*	16.67	$20.68 * 10^{-4}$	$11.37 * 10^{-4}$	$4.03 * 10^{-3}$	11.1
O25101	49.7 – *2.4*	21.67	$28.76 * 10^{-4}$	$10.04 * 10^{-4}$	$6.82 * 10^{-3}$	9.6

Table 18 summarizes the results of the experiments realized at a depth of 25cm. As it was the case for a water level of 40cm, the oxygen transfer is very low at a power of 0.6kW. Besides being less efficient for the mixing, an air flowrate lower than 5Nm³/m²h leads to a poor gas transfer. Again, the $(k_l a)_R$ and $(k_l a)_A$ follow the same pattern, they increase with increasing air flowrates. In this case, the difference between the results for 2.4 kW and 1.8 kW is marked with a $(k_l a)_R$ of $28.76 * 10^{-4} s^{-1}$ for O25101 and a mean $(k_l a)_R$ of $19.05 * 10^{-4} s^{-1}$ for O2581 and O2582. This suggests that increasing the power of the airlift from 1.8 kW to 2.4 kW can be beneficial in case high amounts of oxygen are needed. The volumetric transfer coefficients of the channel vary from $7.39 * 10^{-4}$ to $11.37 * 10^{-4} s^{-1}$. They are similar for each experiment which means that the conditions at the surface of the water were almost identical (same wind conditions).

The transfer being less efficient at 0.6 kW, the aeration time is significantly higher than in the other cases. There is no marked difference between powers 1.2, 1.8 and 2.4kW. The t_a decreases slowly when the air flowrate increases.

Table 19 – Results of the oxygen transfer tests at a depth of 60 cm

Test	Frequency [Hz] – *Power* [kW]	Air flowrate [Nm³/m²h]	$(k_l a)_R$ $[s^{-1}]$	$(k_l a)_{channel}$ $[s^{-1}]$	$(k_l a)_A$ $[s^{-1}]$	Aeration time [min]
O6041	17.8 - *0.6*	<5	$10.25 * 10^{-4}$	$8.77 * 10^{-4}$	$1.63 * 10^{-3}$	45.9
O6061	30.65 - *1.2*	10	$11.16 * 10^{-4}$	$8.70 * 10^{-4}$	$2.13 * 10^{-3}$	24.8
O6062	30.65 - *1.2*	10	$12.16 * 10^{-4}$	$9.91 * 10^{-4}$	$2.14 * 10^{-3}$	16.4
O6081	47.85 - *1.8*	16.67	$18.62 * 10^{-4}$	$10.63 * 10^{-4}$	$5.15 * 10^{-3}$	12.5
O6082	47.85 - *1.8*	16.67	$19.23 * 10^{-4}$	$10.78 * 10^{-4}$	$5.40 * 10^{-3}$	12.4
O60101	49.7 - *2.4*	21.67	$22.24 * 10^{-4}$	$11.05 * 10^{-4}$	$6.83 * 10^{-3}$	12.2

The results for the oxygen transfer tests are presented in **Table 19** above. As it was the case previously, the gas transfers in the airlift and, consequently, in the entire pond increase with increasing air flowrates. The $(k_l a)_{channel}$ stand in the range $8.70 * 10^{-4}$ to $11.05 * 10^{-4} s^{-1}$ and are similar to the ones calculated at a depth of 25 and 40 cm. Once again, the aeration time is much longer for the lowest power then for the three others.

Finally, the graphs presented in "**Appendix F** – Graphs of the oxygen transfer tests (Vietnam)" should be commented. First of all, one can see the presence of "waves" consisting of a small decrease after the first jump (e.g. **Figure 93**, **Figure 96**, **Figure 97**, **Figure 104**). It is likely that the injection time is too short so that the DO is not reduced to 0mg/L in every "slice" of the dispersed plug-flow. Consequently, the first increase is higher than if one really started from 0mg/L because the initial DO is significantly higher than 0mg/L. Then, after the first increase, the values of DO decrease because at this time, the initial DO is close to 0mg/L before the first passing through the airlift. Then, one can observe that the tests O4062b, O4082, O2561 and O2582 present some peaks when the oxygen is supposed to be totally removed from the water. It is explained by the injection that was temporarily stopped because the pump used for the injection has been turned off during a few seconds due to technical difficulties. The consequences of these interruptions can be seen in the data recorded by Probe B but not Probe A. The dispersion within the pond may have dispersed the sulfite in the zones where the peaks first occurred so that the peaks disappear after a certain time. Finally, the test O60101 presents two important peaks when the saturation oxygen concentration is reached. These peaks are probably due to the presence of air bubbles on the probe. The air flowrate being maximal in this case, it is possible that some bubbles persist until they meet the probes.

b. Comparison

As it has been done for the tracer tests, it is also important to compare all the results to identify the impact that different conditions (depth, air flowrate) have on the oxygen transfers into the pond. First, the $(k_l a)_R$ and $(k_l a)_A$ are compared together because they are highly related. Then, the evolution of the $(k_l a)_{channel}$ and, finally, the aeration time t_a are discussed. All the following graphs are realized as a function of the air flowrate (left) and the power of the blower (right). Knowing that powers 0.6kW, 1.2kW, 1.8kW and 2.4kW correspond to air flowrates of <5Nm³/m²h, 10 Nm³/m²h, 16.67 Nm³/m²h and 21.67 Nm³/m²h respectively, the parallel between the power and the air flowrate can be done easily. For the purpose of the representation, it was decided to set the air flowrate corresponding to a power 0.6kW to 3 Nm³/m²h even though the exact value is not known. Moreover, one will notice that the graphs are almost identical and only the x-axis scale changes.

- $(k_l a)_R$ and $(k_l a)_A$

As mentioned, the evolution of the volumetric transfer coefficient of the airlift follows the same trend as the one of the entire pond because the majority of the oxygenation occurs within the airlift aeration system. Nevertheless, the transfer in the channel is not negligible contrary to the pilot in Arlon. It explains why the $(k_l a)_R$ and $(k_l a)_A$ are not exactly the same. From **Figure 59** and **Figure 60**, it is difficult to make clear conclusions. The volumetric transfer coefficients are similar at the three depths but tend to be slightly lower at 40 cm. At 25cm, the water volume to be oxygenated is smaller which means that, with a same air flowrate, the aeration is faster. The transfer within the airlift depends on the time during which the bubbles are in contact with the wastewater. This contact time depends on the water level and is thus higher at 60cm. This would explain why the transfer is higher at 60cm than at 40cm. Once again, these preliminary conclusions have to be taken cautiously because the number of experiments is very low and the accuracy of the data is not optimal.

The $(k_l a)$ calculated at 40cm may suggest the linear relationship between the volumetric transfer coefficient and the power of the blower. But this trend is not exactly repeated at 25cm and 60cm so that it could also just be a coincidence. To conclude properly, a larger number of experiments should be conducted and more powers should be evaluated.

Finally, it has to be mentioned that the different $(k_l a)_i$ cannot be directly compared. The volumetric transfer coefficients is an interesting parameter that provides the necessary information about the oxygen transfer, but the overall gas transfer is given by $(k_l a)_i V_i (C_s - C(t)_i)$, meaning that it depends on the volume considered as well as on the concentration gradient. Thus, one needs to keep in mind that the volume of the airlift corresponds to more or less one fifth of the total volume when interpreting the results.

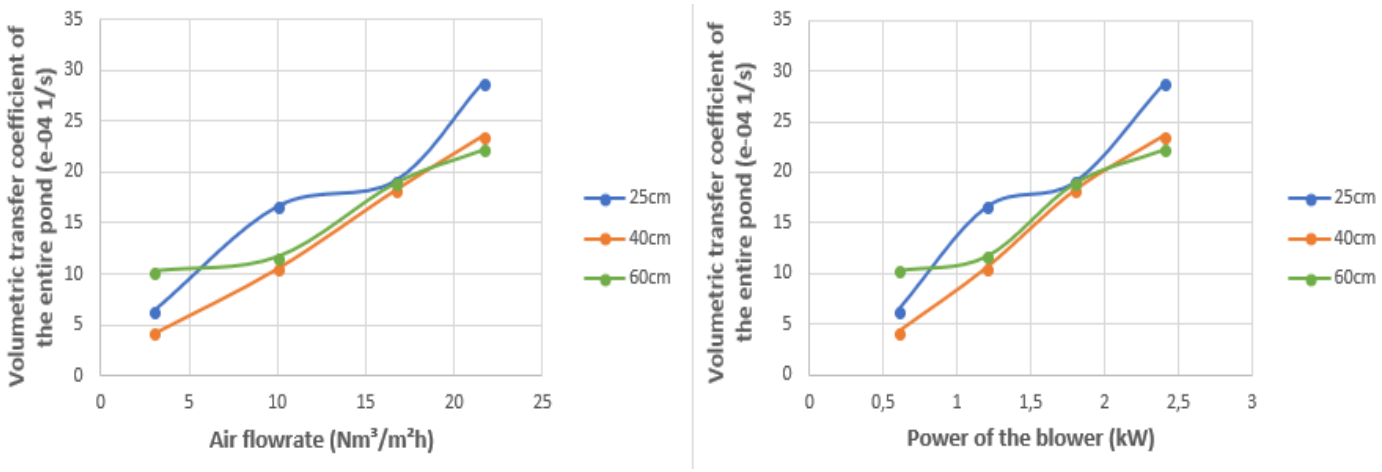

Figure 59 – Comparison of the volumetric transfer coefficients of the entire pond for all tests

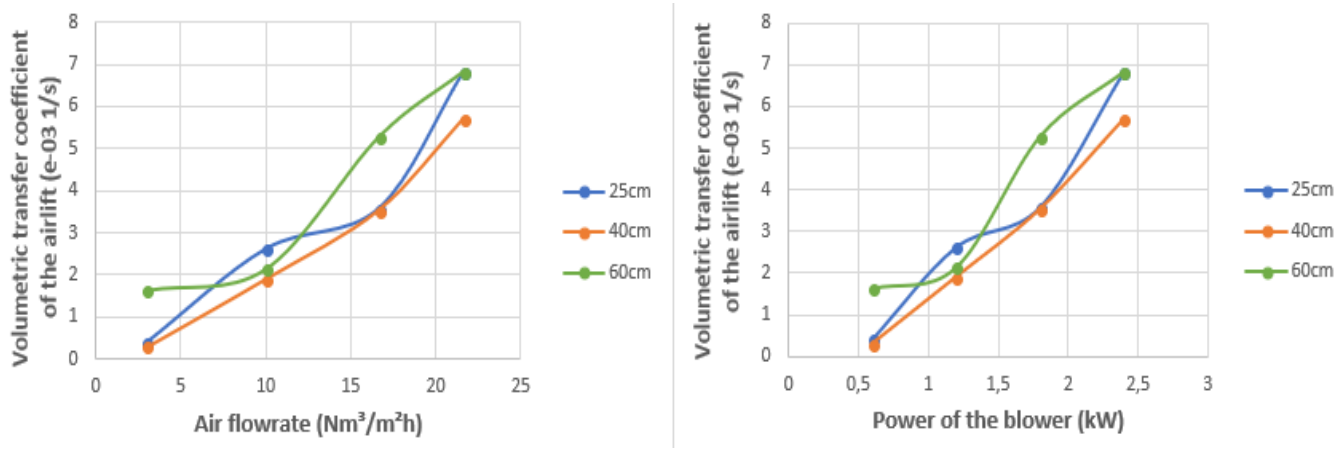

Figure 60 – Comparison of the volumetric transfer coefficients of the airlift for all tests

- $(k_l a)_{channel}$

If the water was perfectly flat or if the turbulences were exactly the same from test to test, at an identical temperature, the $(k_l a)_{channel}$ would be very close. It is not the case in practice, the wind creating irregularities at the water surface and the flow itself inducing turbulences, especially in the curves of the pond, the $(k_l a)_{channel}$ is affected by these changes of conditions. Indeed, the tests reveal that, in reality, the $(k_l a)_{channel}$

varies from $4.66 * 10^{-4}s^{-1}$ at the lowest (O4041) up to $12.19 * 10^{-4}s^{-1}$ (O4082). Given the channel and its volumetric transfer coefficient that is non-negligible, one should take it into account for the design and operations of the HRAP.

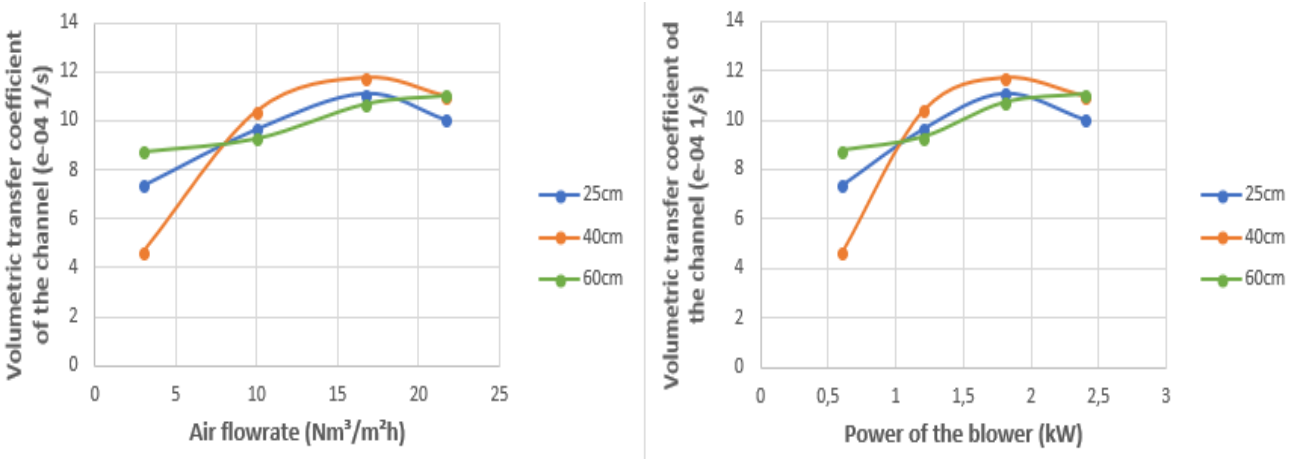

Figure 61 – Comparison of the volumetric transfer coefficients of the channel for all tests

- **Aeration time, t_a**

The aeration time t_a is the last parameter that has been calculated from the oxygen transfer tests. As it has been said, it may be affected by the temperature changes that affect the DO values at saturation. But it gives a general idea of the efficiency of the HRAP aeration system. From 0.6kW to 1.2kW, one can notice a 60.03%, 59.61% and 55.12% reduction of t_a at 25cm, 40cm and 60cm respectively. Then the decreases of the aeration time are lower. The evolutions of t_a at the three different depths are similar (**Figure 62**). The lowest values correspond to a depth of 25cm while the highest values are for the maximal water level. This is clearly related to the water volume of the pond which is lower at 25cm than 60cm. Given the fact that the aeration efficiency of the pond is similar for each depth, the results presented in the following figure were thus expected.

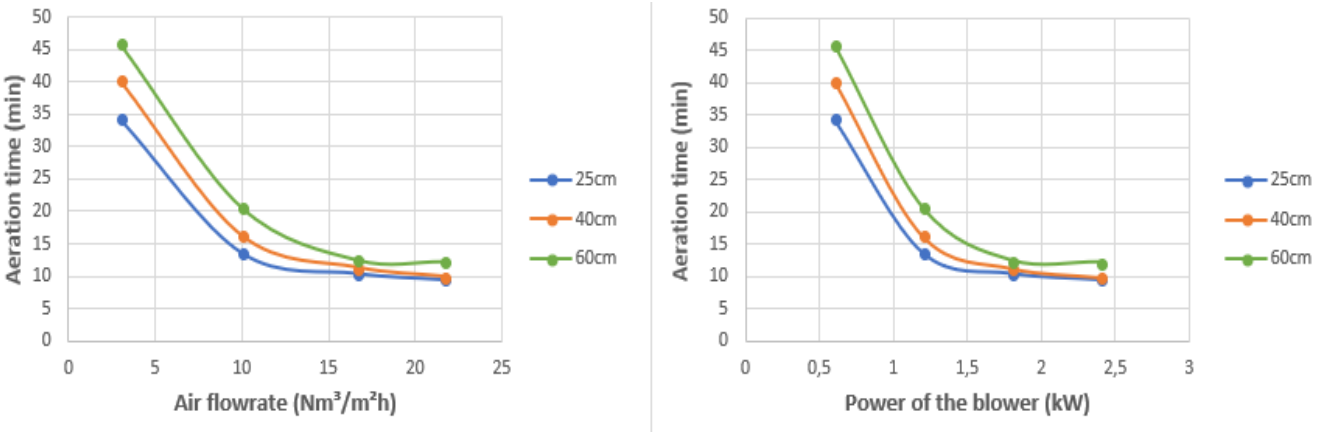

Figure 62 – Comparison of the aeration times for all tests

c. Discussion

The results of the oxygen transfer tests quantify what was expected to obtain, namely the fact that the aeration efficiency of the HRAP increases with increasing air flowrates. The two principal elements that were unknown are the relative importance of the transfer between the atmosphere and the water circulating in the pond and, also, the fact that the water level has no marked influence on the different volumetric transfer coefficients. The water level affects only the time it takes to re-oxygenate the pond because it is directly related to the water volume to be aerated.

An increase of the power leads to an increase of the oxygen transfer within the pond. There is no difference if the increase occurs at high or low power (contrary to the case of the tracer tests). It means that 1kW invested at high power is worth the same – in terms of efficiency improvement – as 1kW invested at low power. This results directly from the linear tendency that was highlighted previously.

The transfers occurring between the atmosphere and the wastewater circulating into the pond are relatively similar for each experiment and stand in the range $4.66 * 10^{-4} s^{-1}$ at the lowest and up to $12.19 * 10^{-4} s^{-1}$. These transfers occurring at the water surface, they are highly related to the flow velocity and the strength of the wind. It could be beneficial to exploit the gas transfers occurring along the channel. For example, one can adjust the height of the pond walls compared to the water level to increase the effect of the wind on the water surface. If the water level is low compared to the walls height, the water surface is "protected" and the effects of the wind are lower.

On the one hand, the temperature has an influence on the oxygen transfers. High temperatures lead to higher overall oxygen transfer coefficient which may mean that the transfer is higher at high temperature. But one should also take into account that the oxygen saturation concentration is lower at high temperatures which counters – partially – the increase of the transfer coefficient. Incidentally, it has been shown that the oxygen transfer rate is constant between 20 to 55°C for tap water [62]. On the other hand, it has been noticed that the air flowrate has an influence on the water temperature. The temperature is lower at higher air flowrates which is notably due to the turbulences and the increased evaporation rate. It could be interesting to evaluate these effects in more details knowing that the temperature affects greatly the microalgae productivity.

Even though the carbon dioxide transfers have not been evaluated in this work, one could have a global idea of the CO_2 transfer efficiencies using the results of the oxygen transfer tests. Indeed, the evolution of the volumetric transfer coefficients for the carbon dioxide is expected to follow the same trend as for the oxygen transfers. Nevertheless, it could be interesting to perform some carbon dioxide transfer tests to get an accurate knowledge of the different parameters because the CO_2 is often considered as a limiting factor for microalgae growth. A suitable management of the dissolved CO_2, which is the main carbon source, is required to obtain a high productivity. It has been proven that managing the C:N ratio or, more generally, the C:N:P ratio can lead to a significant productivity increase. For example, the highest productivity for the benthic microalgae is obtained for a C:N:P ratio of 119:17:1 [63]. This ratio is specific for each microalgae strain.

5. General conclusion and perspectives

The RENEWABLE project aims at developing a sustainable and efficient aquaculture wastewater treatment technology using microalgae in order to offer to Vietnamese local companies the possibility to treat the wastewaters at low cost. The first step of the project is to find a suitable microalgae strain or mix of strains capable of removing the pollution load contained in the wastewater. The selected species should also be suitable for the valorization afterwards (e.g. a high lipid content is advantageous for the biofuel production). The second step, which is directly linked to the present work, is to install and characterize a HRAP pilot in the Ninh Thuan province in order to find the optimal operational conditions and to develop a model designed for the representation of both the hydrodynamics of the HRAP and the biological phenomena occurring into the pond. After that, a third step is to grow and harvest the selected microalgae into the pilot knowing the hydrodynamic of the HRAP and the biological characteristics of the biomass. Finally, an economical assessment of the wastewater treatment technology developed will be realized to evaluate its economic feasibility. If the results obtained are conclusive, the treatment technique can be installed in several different aquaculture companies that currently discharge their wastewaters directly into the sea and the environment.

The results of the tracer and oxygen transfer tests conducted on the HRAP pilot are a wealthy source of information to evaluate the appropriate way to operate the pond. They give the conditions of mixing encountered into the pond, the water velocity as well as the oxygenation capacity of the raceway pond. The optimal operating conditions depend on the strain(s) of microalgae that will be grown into the HRAP. Indeed, each strain is different and the suitable medium parameters to cultivate them can vary dramatically. Knowing that, the researchers in charge of the following steps of the RENEWABLE project should use the results presented in this work and should adapt the growth conditions to the selected microalgae.

From the results collected, one can conclude that it is not worth considering to run the blower at an air flowrate smaller than $5Nm^3/m^2h$ (0.6kW). Indeed, this would lead to a poor mixing, the maximal dispersion coefficient E_z being $0.2228m^2/s$ in the case of the test T2541. The resulting water velocity corresponding to 0.6kW is lower than 9cm/s at each of the three depths. As it has been mentioned in **Section 3.1.2**, the quality of the mixing into the pond is one of the most important factors. A low degree of mixing could notably lead to photolimitation, photoinhibition or microalgae sedimentation, all of them causing a dramatic decline in productivity. On top of that, operating the airlift system

at a power of 0.6kW results in poor oxygenation capacity which leads to an aeration time at least 122% higher than the t_a obtained at 1.2kW and to a $(k_l a)_A$ at least 23.6% lower than at 1.2kW. It is thus interesting and necessary to invest a higher amount of energy to run the pilot in order to improve the growing medium.

If only the dispersion and water velocity are considered, it is conceivable to grow the microalgae at an air flowrate of 10Nm^3/m^{2}h. At this power, the minimal dispersion coefficient is 0.2687m^2/s at a water level of 60cm and the water velocity is more or less equal to 15cm/s at each depth. The degree of mixing is sufficient even for high water levels, and the velocity ranges in the suitable range of 10 to 30cm/s. Increasing the power would lead to higher operational costs and, maybe, to a higher productivity. But future tests should evaluate if the cost increase is counterbalanced by the productivity rise. It goes without saying that if the additional quantity of microalgae resulting from a power augmentation is worth double the additional operational costs induced by a higher air flowrate, one has to run the blower at a higher power. But, as it has been discussed, the benefits of an air flowrate augmentation decrease at high powers. Finally, it has to be said that the higher the water level, the lower the dispersion. The decrease in the mixing capacity of the airlift may be offset by an air flowrate increase and thus, a higher cost.

In the case where only the oxygenation capacity of the reactor is considered, the conclusions are highly related to the microalgae needs. Once the amounts of oxygen and carbon dioxide required by the biomass are determined, one can use the data of this work to identify the suitable air flowrate. The quantities of gas (O_2, CO_2) that must be supplied to the culture medium should be equal to the consumption of the biomass. The future work will be to identify both mixing and gas transfer requirements considering the resulting productivity and the operational costs. The carbon dioxide transfers should also be evaluated because the amount of CO_2 is often a limiting factor to microalgae growth.

The present work reveals that the HRAP pilot is efficient but can be improved. First the position of the airlift should be reconsidered. The current position is in the middle of the width and it results that the output of the airlift ends directly in a curve. Positioning the aeration system in the length rather than in the width may improve the hydrodynamic. Second, the shape of the curves can also be slightly redesigned. Indeed, it appears that the actual design leads to some recirculation zones at the exit of each bend and, consequently, to an energy loss. After that, the shape of the aluminum sheet used to build the airlift system is not optimal according to Prof. Vasel who studied the ideal design. It could be interesting to evaluate the impact of an improvement of the airlift design on both the flow and the gas transfer. Finally, as it has been said, the relative height of the walls of the pond in comparison to the water level should be considered.

Another future challenge that the researchers working on the RENEWABLE project will have to take up is the formation of foam at the water surface. The bubbles rising in the ascending part of the airlift induce the formation of a considerable amount of foam. This foam follows the flow and accumulates at the input of the airlift. The accumulation is non-negligible and can cover up to one and a half length of the HRAP. The presence of froth at the water surface will decrease the amount of light received by the microalgae due to photolimitation which may result in a significant decrease in productivity. There are several possible causes of the foam formation: presence of organic materials, pollution, wind or other sources of turbulences [64]. The researchers will have to consider this aspect when operating the HRAP and manage to control the foam formation.

The RENEWABLE project is part of a positive perspective of collaboration between developed and emerging countries to develop innovative and sustainable technologies in various fields such as energy production, wastewater treatment, pollution management, recycling, etc. This work paves the way for the next steps of the project during which numerous challenges will have to be taken up. If satisfying final results are obtained, the outcome of this project will enable the installation of wastewater treatment facilities in several aquaculture companies by providing a technology combining efficient nutrients removal and potential valorization pathways of harvested microalgae leading to reduced total operating costs. The completion of this interdisciplinary project can lead to a dramatic decrease in seawater and groundwater consumption as well as a major improvement of the seawater quality by avoiding the discharge of the untreated wastewaters.

From a personal point of view, this master thesis was a great challenge in terms of organization, learning, adaptation to a foreign culture and surpassing oneself. Applying some theoretical background that has been seen partially during my studies to a practical project realized in a foreign country was very interesting and rewarding. This work really mattered to me due to its possible openings and the possible benefits that could be provided to developing countries companies in terms of environmental protection and economic development. This project also allowed me to develop and improve several skills such as the capacity to react and adapt to unexpected situations, the communication – in English – to foreign workers and, finally, an extensive knowledge about microalgae technologies and wastewater treatment in general.

References

[1] D. L. Sutherland, M. H. Turnbull, P. A. Broady, and R. J. Craggs, "Wastewater microalgal production , nutrient removal and physiological adaptation in response to changes in mixing frequency," *Water Res.*, vol. 61, pp. 130–140, 2014.

[2] S. Reen, H. Chyuan, K. Wayne, P. Loke, S. Phang, D. Nagarajan and D. Lee, "Sustainable approaches for algae utilisation in bioenergy production," *Renew. Energy*, pp. 1–15, 2017.

[3] P. Venckus, J. Kostkevičienė, and V. Bendikienė, "Green algae Chlorella vulgaris cultivation in municipal wastewater and biomass composition," *J. Environ. Eng. Landsc. Manag.*, vol. 25, pp. 56–63, 2017.

[4] J. Alberto, V. Costa, and M. G. De Morais, "The role of biochemical engineering in the production of biofuels from microalgae," *Bioresour. Technol.*, vol. 102, pp. 2–9, 2011.

[5] B. Zhang and K. Ogden, "Recycled wastewater from anaerobic digestion of lipid extracted algae as a source of nutrients," *Fuel*, vol. 210, pp. 705–712, 2017.

[6] E. Sforza, A. Bertucco, T. Morosinotto, and G. M. Giacometti, "Chemical Engineering Research and Design Photobioreactors for microalgal growth and oil production with Nannochloropsis salina : From lab-scale experiments to large-scale design," *Chem. Eng. Res. Des.*, vol. 90, pp. 1151–1158, 2012.

[7] N. Uduman, Y. Qi, M. Danquah, G. Forde and A. Hoadley, "Dewatering of microalgal cultures : A major bottleneck to algae-based fuels," *J. Renew. Sustain. ENERGY*, vol. 2, 2010.

[8] B. S. M. Sturm and S. L. Lamer, "An energy evaluation of coupling nutrient removal from wastewater with algal biomass production," *Appl. Energy*, vol. 88, no. 10, pp. 3499–3506, 2011.

[9] B. D. Fernandes, A. Mota, A. Ferreira, G. Dragone, J. A. Teixeira, and A. A. Vicente, "Characterization of split cylinder airlift photobioreactors for efficient microalgae cultivation," *Chem. Eng. Sci.*, vol. 117, pp. 445–454, 2014.

[10] E. Lee, M. Jalalizadeh, and Q. Zhang, "Growth kinetic models for microalgae cultivation : A review," *ALGAL*, vol. 12, pp. 497–512, 2015.

[11] R. Pierong, "Modelling of algae based wastewater treatment," *UPPSALA Univ.*, 2014.

[12] D. L. Sutherland, V. Montemezzani, C. Howard-williams, M. H. Turnbull, P. A. Broady, and R. J. Craggs, "Modifying the high rate algal pond light environment and its effects on light absorption and photosynthesis," *Water Res.*, vol. 70, pp. 86–96, 2014.

[13] E. M. Grima and J. M. Femtidez, "A study on simultaneous photolimitation and photoinhibition in dense microalgal taking into account incident and averaged irradiances," *J. Biotechnol.*, vol. 45, pp. 59–69, 1996.

[14] F. Mespl, C. Casellas, M. Troussellier, and J. Bontoux, "Some difficulties in modelling chlorophyll a evolution in a high rate algal pond ecosystem," *Ecol. Modell.*, vol. 78, pp. 25–36, 1995.

[15] J. H. Steele, "Report : Environmental control of photosynthesis in the sea", Marine Laboratory of Aberdeen, 1962.

[16] D. L. Sutherland, M. H. Turnbull, and R. J. Craggs, "Increased pond depth improves algal productivity and nutrient removal in wastewater treatment high rate algal ponds," *Water Res.*, vol. 53, pp. 271–281, 2014.

[17] D. Chiaramonti, M. Prusi, D. Casini, M. R. Tredici, L. Rodolfi, N. Bassi, G. Chini and P. Bondioli, "Review of energy balance in raceway ponds for microalgae cultivation : Re-thinking a traditional system is possible," *Appl. Energy*, vol. 102, pp. 101–111, 2013.

[18] G. Padovani, L. Rodolfi, G. C. Zittelli, N. Biondi, G. Bonini and M. R. Tredici, "Microalgae for Oil : Strain Selection , Induction of Lipid Synthesis and Outdoor Mass Cultivation in a Photobioreactor," *Biotechnol. Bioeng.*, vol. 102, pp. 100–112, 2008.

[19] A. Martins, N. S. Caetano, and T. M. Mata, "Microalgae for biodiesel production and other applications : A review," *Renew. Sustain. Energy Rev.*, vol. 14, pp. 217–232, 2010.

[20] A. Solimeno, R. Samso, E. Uggetti, B. Sialve, J.-P. Steyer, A. Gabarro and J. Garcia, "New mechanistic model to simulate microalgae growth," *ALGAL*, vol. 12, pp. 350–358, 2015.

[21] H. Pei and L. Jiang, "Mixing Seawater with a Little Wastewater to Produce Bioenergy from Limnetic Algae," *Trends in Biotechnology*, Cell Press Reviews, 2017.

[22] D. L. Sutherland, C. Howard-williams, M. H. Turnbull, P. A. Broady, and R. J. Craggs, "The effects of CO2 addition along a pH gradient on wastewater microalgal photo-physiology , biomass production and nutrient removal," *Water Res.*, vol. 70, pp. 9–26, 2014.

[23] I. Teles, D. Cabanelas, J. Ruiz, Z. Arbib, F. Alexandre, C. Garrido-Pérez, F. Rogalla, I. Andrade and J. A. Perales, "Comparing the use of different domestic wastewaters for coupling microalgal production and nutrient removal," *Bioresour. Technol.*, vol. 131, pp. 429–436, 2013.

[24] R. Craggs, J. Park, S. Heubeck, and D. Sutherland, "High rate algal pond systems for low-energy wastewater treatment , nutrient recovery and energy production," vol. 52:1, pp. 60–73, 2014.

[25] H. Hadiyanto, S. Elmore, T. Van Gerven, and A. Stankiewicz, "Hydrodynamic evaluations in high rate algae pond (HRAP) design," *Chem. Eng. J.*, vol. 217, pp. 231–239, 2013.

[26] S. Nacir, N. Ouazzani, J. Vasel, H. Jupsin and L. Mandi, "TRAITEMENT DES EAUX USÉES DOMESTIQUES PAR UN CHENAL ALGAL À HAUT RENDEMENT (CAHR) AGITÉ PAR AIR LIFT SOUS CLIMAT SEMI-ARIDE," *J. Water Sci.*, vol. 23, no. 1, pp. 57–72, 2010.

[27] B. Cancino, "Design of high efficiency surface aerators Part 2 . Rating of surface aerator rotors," *Aquac. Eng.*, vol. 31, pp. 99–115, 2004.

[28] C. E. Boyd, "Pond water aeration systems," *Aquac. Eng.*, vol. 18, pp. 9–40, 1998.

[29] C. Ruper, P. Jason, S. Donna, and H. Stephan, "Economic construction and operation of hectare-scale wastewater treatment enhanced pond systems," *J. Appl. Phycol.*, vol. 27, no. 5, pp. 1913–1922, 2015.

[30] E. L. Peterson and M. B. Walker, "Effect of speed on Taiwanese paddlewheel aeration," *Aquac. Eng.*, vol. 26, pp. 129–147, 2002.

[31] S. M. J. Jones and S. T. L. Harrison, "Aeration energy requirements for lipid production by Scenedesmus sp . in airlift bioreactors," *ALGAL*, vol. 5, pp. 249–257, 2014.

[32] A. Massart, A. Mirisola, D. Lupant, D. Thomas, and A. Hantson, "Experimental characterization and numerical simulation of the hydrodynamics in an airlift photobioreactor for microalgae cultures," *ALGAL*, vol. 6, pp. 210–217, 2014.

[33] A. Pirouzi, M. Nosrati, S. Abbas, and S. Shakhesi, "Improvement of mixing time , mass transfer , and power consumption in an external loop airlift photobioreactor for microalgae cultures," *Biochem. Eng. J.*, vol. 87, pp. 25–32, 2014.

[34] E. Mihalyfalvy, H. T. Johnston, M. K. Garrett, H. J. Fallowfield, and N. J. Cromar, "Research note improved mixing of high rate algal ponds," vol. 4, no. 97, pp. 1334–1337, 1998.

[35] I. Fernández, F. G. Acién, J. L. Guzmán, M. Berenguel, and J. L. Mendoza, "Dynamic model of an industrial raceway reactor for microalgae production," *ALGAL*, vol. 17, pp. 67–78, 2016.

[36] K. Liffman, D. A. Paterson, P. Liovic, and P. Bandopadhayay, "Chemical Engineering Research and Design Comparing the energy efficiency of different high rate algal raceway pond designs using computational fluid dynamics," *Chem. Eng. Res. Des.*, vol. 91, no. 2, pp. 221–226, 2012.

[37] C. Chen, K. Yeh, R. Aisyah, D. Lee, and J. Chang, "Bioresource Technology Cultivation , photobioreactor design and harvesting of microalgae for biodiesel production : A critical review," *Bioresour. Technol.*, vol. 102, no. 1, pp. 71–81, 2011.

[38] Q. Huang, F. Jiang, L. Wang, and C. Yang, "Design of Photobioreactors for Mass Cultivation of Photosynthetic Organisms," *Engineering*, vol. 3, no. 3, pp. 318–329, 2017.

[39] E. Lee, J. Pruvost, X. He, R. Munipalli, and L. Pilon, "Design tool and guidelines for outdoor photobioreactors," *Chem. Eng. Sci.*, vol. 106, pp. 18–29, 2014.

[40] R. Gutiérrez, F. Passos, I. Ferrer, E. Uggetti, and J. García, "Harvesting microalgae from wastewater treatment systems with natural flocculants : Effect on biomass settling and biogas production," *ALGAL*, vol. 9, pp. 204–211, 2015.

[41] W. Mo, L. Soh, J. R. Werber, M. Elimelech, and J. B. Zimmerman, "Application of membrane dewatering for algal biofuel," *ALGAL*, vol. 11, pp. 1–12, 2015.

[42] L. Xu, C. Guo, F. Wang, S. Zheng, and C. Liu, "A simple and rapid harvesting method for microalgae by in situ magnetic separation," *Bioresour. Technol.*, vol. 102, no. 21, pp. 10047–10051, 2011.

[43] M. Cerff, M. Morweiser, R. Dillschneider, A. Michel, K. Menzel, and C. Posten, "Harvesting fresh water and marine algae by magnetic separation : Screening of separation parameters and high gradient magnetic filtration," *Bioresour. Technol.*, vol. 118, pp. 289–295, 2012.

[44] S. Salim, M. H. Vermuë, and R. H. Wijffels, "Ratio between autoflocculating and target microalgae affects the energy-efficient harvesting by bio-flocculation," *Bioresour. Technol.*, vol. 118, pp. 49–55, 2012.

[45] E. M. Grima, F. G. Acie, A. R. Medina, and Y. Chisti, "Recovery of microalgal biomass and metabolites : process options and economics," *Biotechnol. Adv.*, vol. 20, pp. 491–515, 2003.

[46] "M.W.WATERMARK." [Online]. Available: http://www.mwwatermark.com/en_US/what-is-a-filter-press/. [Accessed: 26-Feb-2018].

[47] "Filtration separation." [Online]. Available: http://www.filtsep.com/chemicals/features/solid-liquid-filtration-understanding-filter/. [Accessed: 26-Feb-2018].

[48] J. W. Richardson, M. D. Johnson, R. Lacey, J. Oyler, and S. Capareda, "Harvesting and extraction technology contributions to algae biofuels economic viability," *ALGAL*, vol. 5, pp. 70–78, 2014.

[49] Y. Li, H. Gao, W. Li, J. Xing, and H. Liu, "Bioresource Technology In situ magnetic separation and immobilization of dibenzothiophene-desulfurizing bacteria," *Bioresour. Technol.*, vol. 100, no. 21, pp. 5092–5096, 2009.

[50] I. Safarik and M. Safarikova, "REVIEW : Magnetic nano- and microparticles in biotechnology," *Chem. Pap.*, vol. 63, no. 5, pp. 497–505, 2009.

[51] T. Wang, W. Yang, Y. Hong, and Y. Hou, "Magnetic nanoparticles grafted with amino-riched dendrimer as magnetic flocculant for efficient harvesting of oleaginous microalgae," *Chem. Eng. J.*, vol. 297, pp. 304–314, 2016.

[52] Z. N. Norvill, A. Shilton, and B. Guieysse, "Emerging contaminant degradation and removal in algal wastewater treatment ponds : Identifying the research gaps," *J. Hazard. Mater.*, vol. 313, pp. 291–309, 2016.

[53] S. Rasoul-amini, N. Montazeri-najafabady, S. Shaker, and A. Safari, "Removal of nitrogen and phosphorus from wastewater using microalgae free cells in bath culture system," *Biocatal. Agric. Biotechnol.*, vol. 3, no. 2, pp. 126–131, 2014.

[54] J. Wolf, I. L. Ross, K. Adzfa, G. Jakob, E. Stephens, and B. Hankamer, "High-throughput screen for high performance microalgae strain selection and integrated media design," *ALGAL*, vol. 11, pp. 313–325, 2015.

[55] R. Guo and J. Chen, "Application of alga-activated sludge combined system (AASCS) as a novel treatment to remove cephalosporins," *Chem. Eng. J.*, vol. 260, pp. 550–556, 2015.

[56] University of Michigan, *Elements of Chemical Reaction Engineering*. 2008.

[57] L. Houille, B. August, and A. Line, "Numerical simulation of gas-liquid reactors used in water treatment," *La Houille Blanche*, no. August, 1998.

[58] H. El Ouarghi, B. E. Boumansour, O. Dufayt, B. El Hamouri, and J. L. Vasel, "Hydrodynamics and oxygen balance in a high-rate algal pond," *Water Sci. Technol.*, vol. 42, pp. 349–356, 1996.

[59] O. Levenspiel, J. Wiley and Sons, *Chemical Reaction Engineering, 3rd edition*. 1999.

[60] Maine volunteer lake monitoring program, "Report : Maximum Dissolved Oxygen Concentration Saturation Table," Available: https://www.mainevlmp.org/wp-content/uploads/2014/01/Maximum-Dissolved-Oxygen-Concentration-Saturation-Table.pdf

[61] F. Zouhir, H. Jupsin, L. Mandi and J.-L. Vasel, "COMPARISON OF TWO AGITATION SYSTEMS IN," *Univ. Liège*, pp. 1–8, 2003.

[62] J. C. T. Vogelaar, A. M. Klapwijk and W. H. Rulkens, "Temperature effects on the oxygen transfer rate between 20 and 55°C," *Water Res.*, vol. 34, no. 3, pp. 1037–1041, 2000.

[63] "The nutrient stoichiometry of benthic microalgal growth : Redfield proportions are optimal," *American Society of Limnology and Oceanography*, 1999. [Online]. Available: https://aslopubs.onlinelibrary.wiley.com/doi/pdf/10.4319/lo.1999.44.2.0440. [Accessed: 04-Jun-2018].

[64] State of Michigan's environmental department, "Foam: a naturally-occurring phenomenon," 2016. [Online]. Available: https://www.michigan.gov/documents/deq/deq-oea-nop-foam_378415_7.pdf. [Accessed: 29-May-2018].

Appendices

Appendix A – Technical characteristics and instructions for the Vietnamese HRAP pilot

In this appendix are summarized the principal characteristics and the instructions for the operations of the HRAP pilot installed in the Ninh Thuan province in Vietnam.

- **Plan of the HRAP pilot**

In the following figures are presented a drawing of the HRAP pilot and a more detailed plan of the airlift aeration system. In **Figure 63**, the dimensions are noted down in blue, the airlift in red and the concrete structure in **black**.

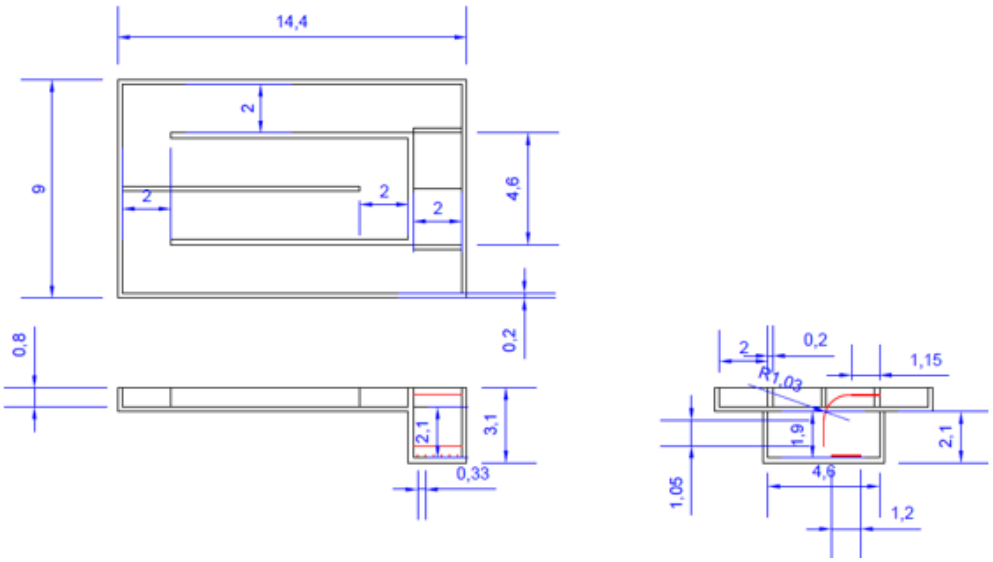

Figure 63 – Drawing of the HRAP pilot (measures in meter)

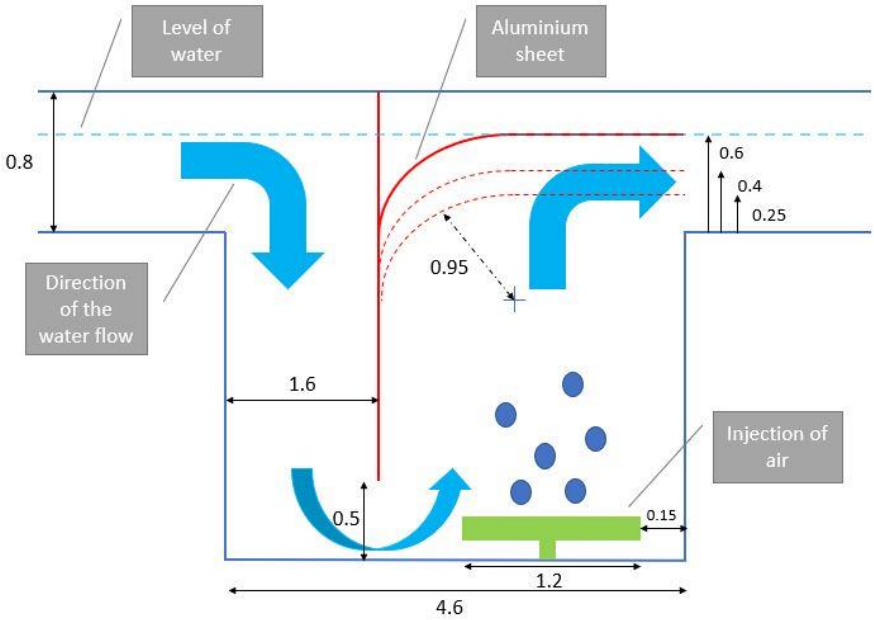

Figure 64 – Drawing of the airlift aeration system (measures in meter)

- **Plan of the ROBUSCHI® Robox evolution installation**

The airlift system is supplied in air with the help of the ROBUSCHI® Robox evolution which is a small size blower. The following figures represent the basic plan of the blower as well as the electric installation. After that, the instructions for the operations of the pilot are summarized.

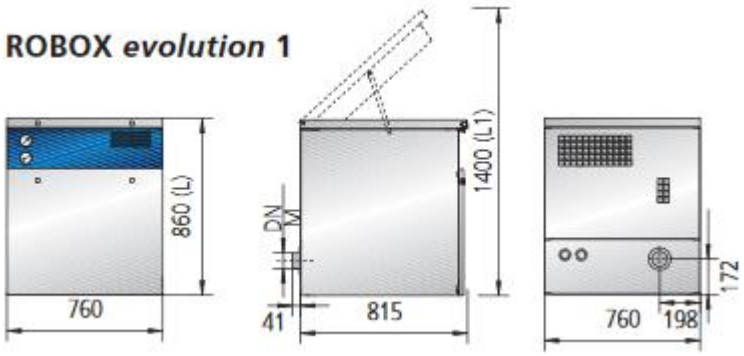

Figure 65 – Robox evolution[12]

[12]Reference: http://www.robuschi.com.au/wp-content/uploads/2013/11/Robuschi-Lobe-Blowers.pdf

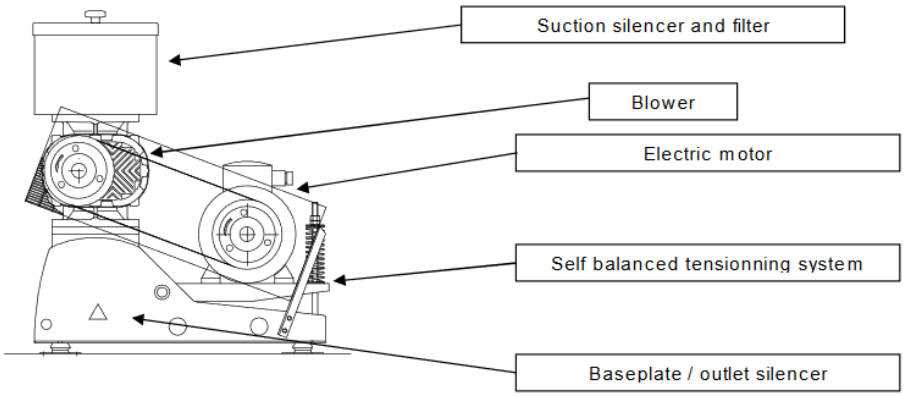

Figure 66 – Basic features of the Robox evolution[13]

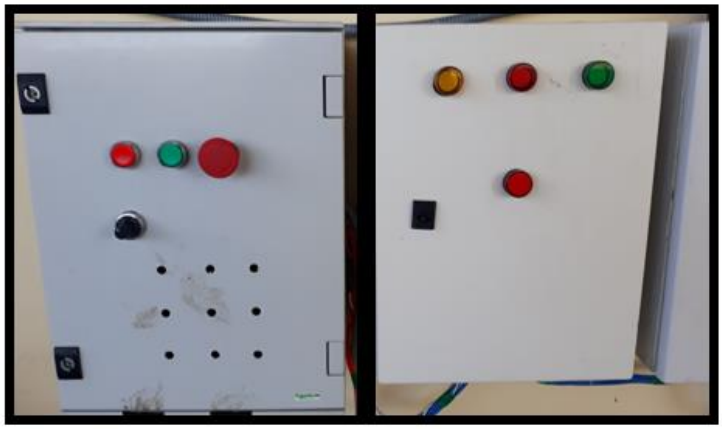

Figure 67 – Control (left) and alimentation (right) cases for the Robox evolution

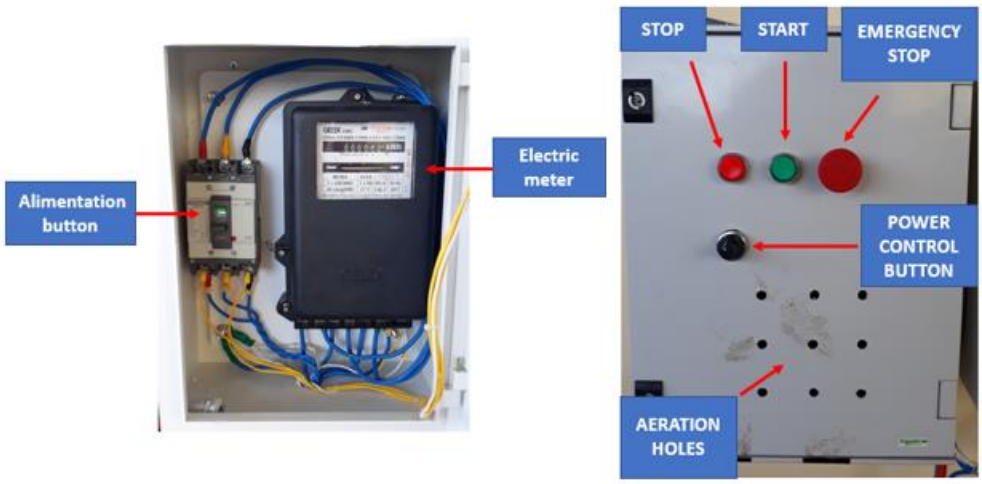

Figure 68 – Alimentation case (left) and control case (right)

[13]Reference: https://asiavacuumpumps.com/download/catalog/blower/ROBOX-evolution-DATA-SHEET-ROBOX-ing1.pdf

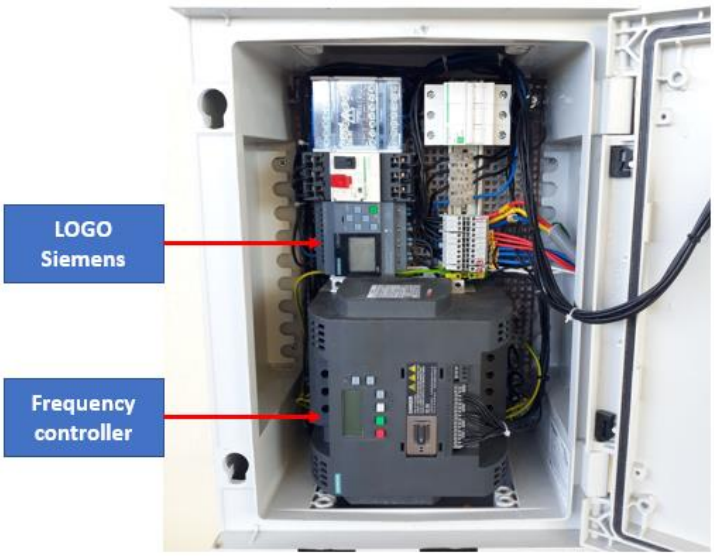

Figure 69 – Inside of the control case

The control case contains a LOGO Siemens that can be used in the future for the programming of the operations of the pond. It is also equipped with a frequency controller that regulates the frequency of the blower which is linked to the air flowrate.

How to start the airlift system?

1. Turn ON the alimentation using the alimentation button. The fan of the Robox automatically starts.
2. Press the **START** button of the controlling case during 5 seconds. The Robox starts.
3. Change the air flowrate using the **POWER CONTROL** button

How to stop the airlift system?

1. Press the **STOP** button one time. The Robox stops running but the fan is still working.
2. Turn OFF the alimentation using the alimentation button.
   REMARK: in case of emergency, press the **EMERGENCY** button one time.

Appendix B – Calibration curves of three different potential salts

The three figures below represent the calibration curves of three different types of salt that have been tested for the tracer tests. These curves are done using the water that will be used later for the experiments. The choice of the salt has been influenced by the crystal size which is bigger for the salt n°1 – and, thus, more difficult to solubilize – than for the others (**Figure 73**) and the price which is higher for the first two salts than for the last one. The linear interpolation is satisfying and shows a correlation coefficient of $R^2 = 0.9995$. Also, the linear response of the conductivity with the increase of salt concentration is tested for concentrations up to 20 g/L of added salt. The curve keeps an almost perfect linear trends ($R^2 = 0.9997$) as can be seen in **Figure 74**.

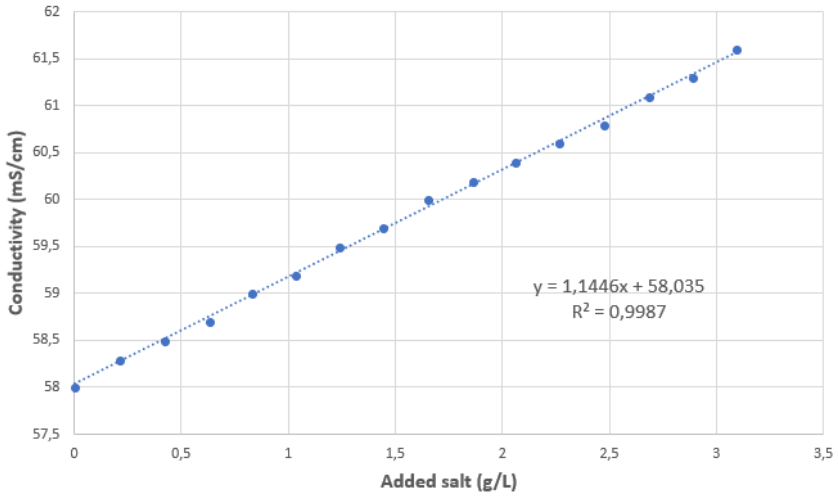

Figure 70 – Calibration curve for salt n°1 (HandyLab 680)

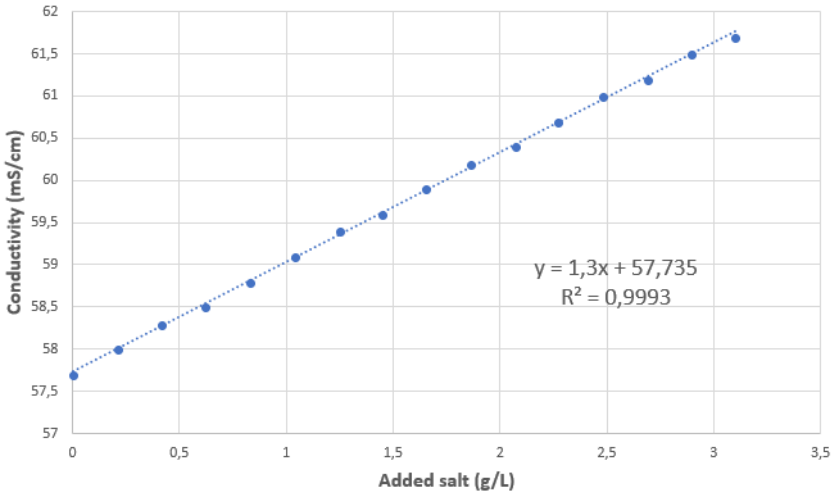

Figure 71 – Calibration curve for salt n°2 (HandyLab 680)

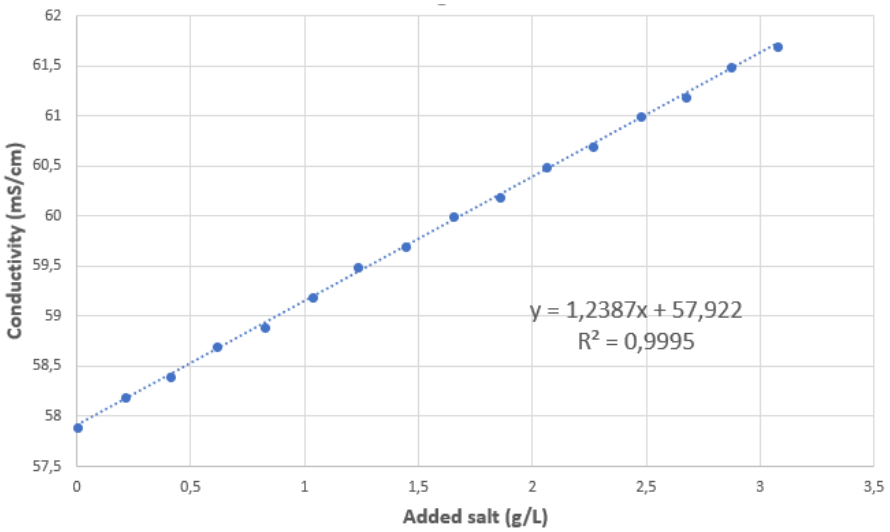

Figure 72 – Calibration curve for salt n°3 (HandyLab 680)

Figure 73 – From left to right, salts n°1 to 3

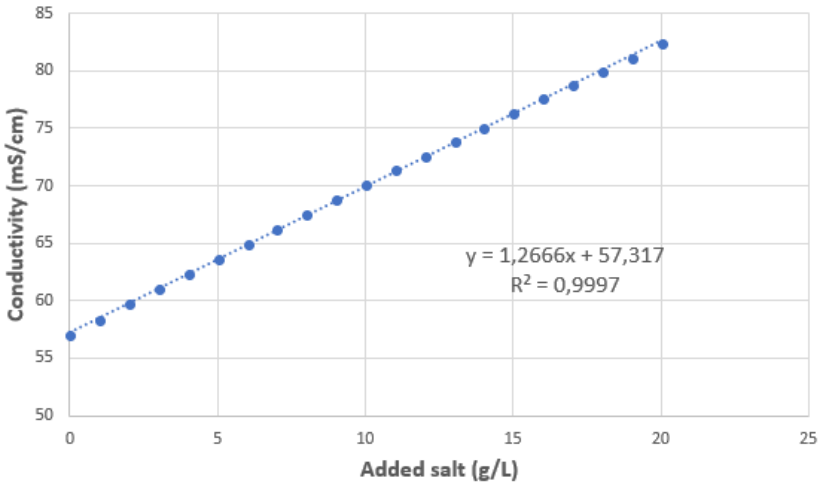

Figure 74 – Calibration curve of the salt n°3 up to 20 g/L of added salt (HandyLab 680)

Appendix C – Calibration curves for the tracer tests (Vietnam)

In the following appendix are presented the linear interpolations that have been made each time the water in the HRAP was refreshed.

Table 20 – Recapitulative table of the linear interpolations linking the conductivity to the concentration of added salt

Date	HandyLab 680	Multiprobe
13-05-2018	$Cond\left(\frac{mS}{cm}\right) = 1.2393 * Conc.\left(\frac{g}{L}\right) + 61.4$	$Cond.\left(\frac{\mu S}{cm}\right) = 1207.3 * Conc.\left(\frac{g}{L}\right) + 59299$
15-05-2018 (1)	$Cond\left(\frac{mS}{cm}\right) = 1.281 * Conc.\left(\frac{g}{L}\right) + 60.008$	$Cond.\left(\frac{\mu S}{cm}\right) = 1239.9 * Conc.\left(\frac{g}{L}\right) + 57893$
15-05-2018 (2)	$Cond\left(\frac{mS}{cm}\right) = 1.281 * Conc.\left(\frac{g}{L}\right) + 60.433$	$Cond.\left(\frac{\mu S}{cm}\right) = 1244.8 * Conc.\left(\frac{g}{L}\right) + 58305$
16-05-2018	$Cond\left(\frac{mS}{cm}\right) = 1.2845 * Conc.\left(\frac{g}{L}\right) + 61.733$	$Cond.\left(\frac{\mu S}{cm}\right) = 1240 * Conc.\left(\frac{g}{L}\right) + 59626$

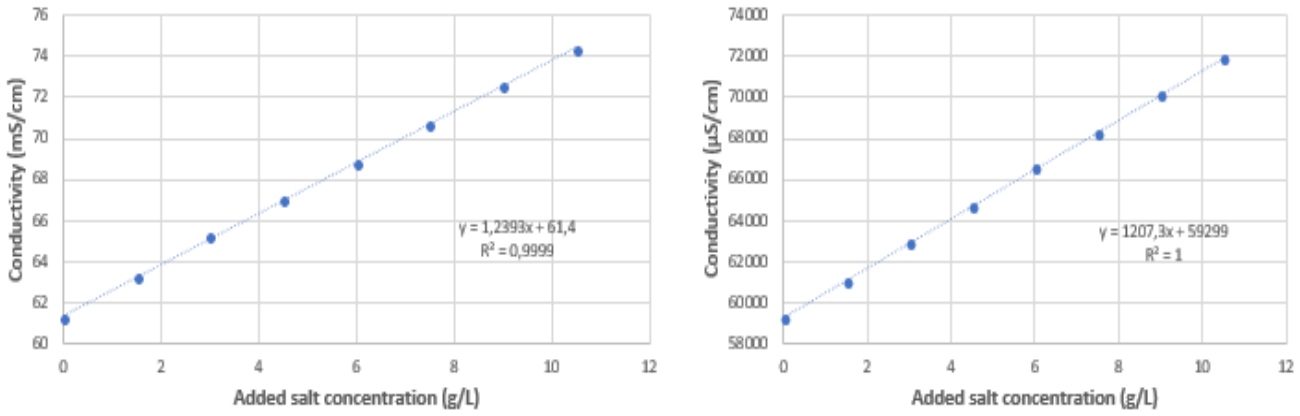

Figure 75 – Calibration curves 13-05-2018 for HandyLab 680 (left) and the Multiprobe (right)

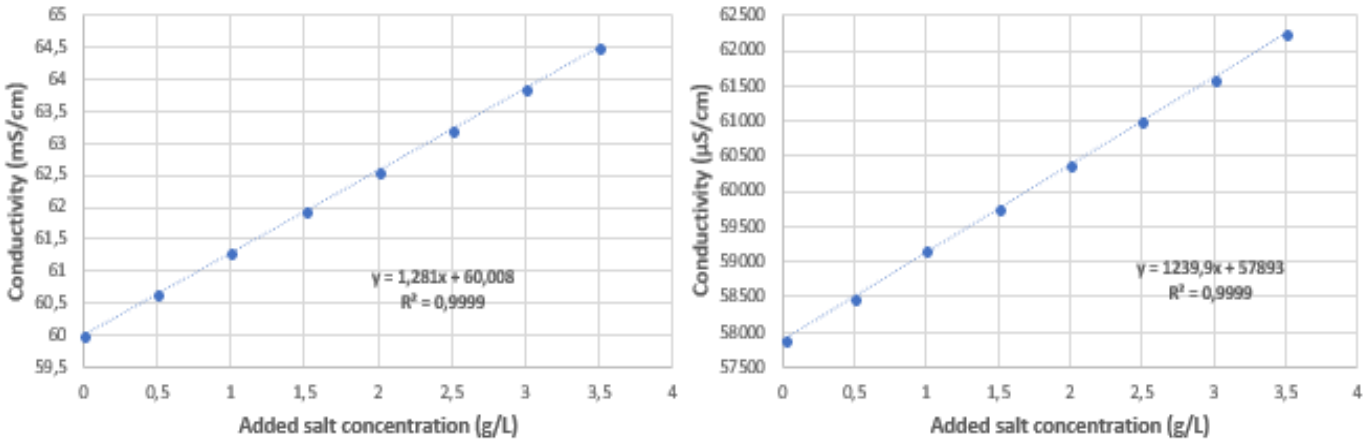

Figure 76 – Calibration curves 15-05-2018 (salt 1) for HandyLab 680 (left) and the Multiprobe (right)

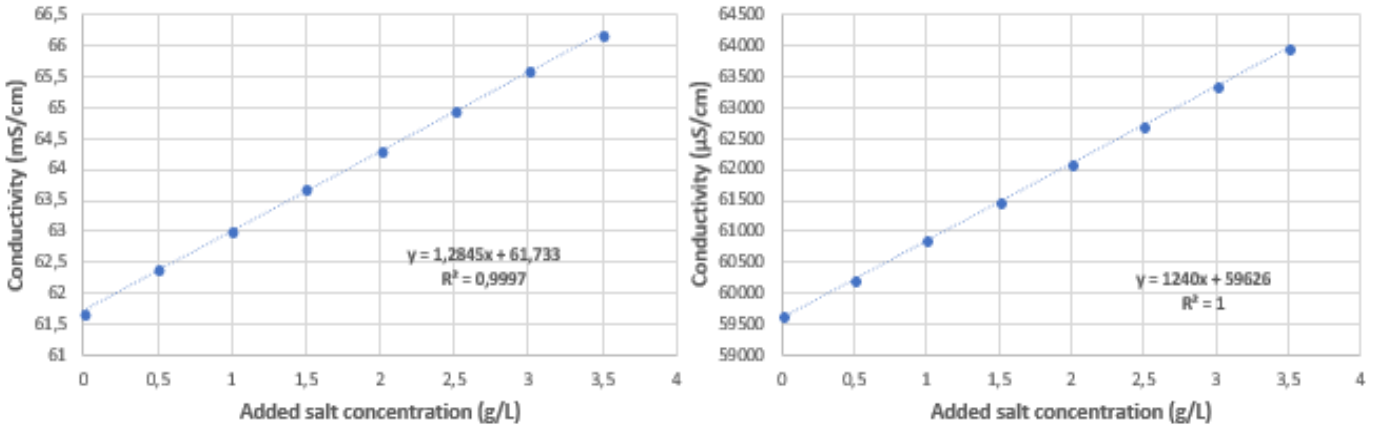

Figure 77 – Calibration curves 15-05-2018 (salt 2) for HandyLab 680 (left) and the Multiprobe (right)

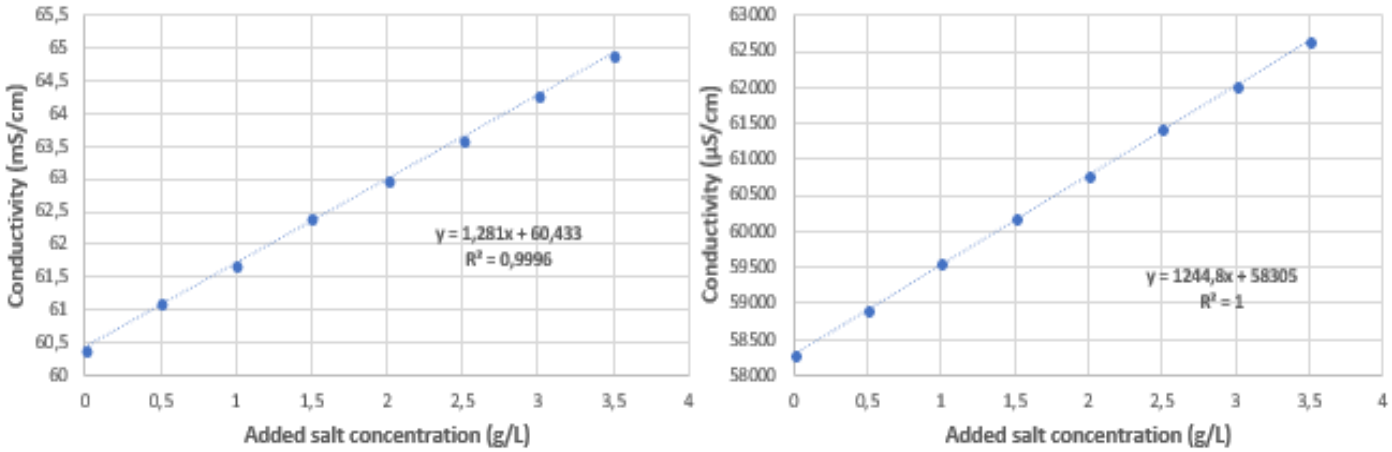

Figure 78 – Calibration curves 16-05-2018 for HandyLab 680 (left) and the Multiprobe (right)

Appendix D – Graphs of the tracer tests (Vietnam)

This appendix summarizes all the graphs of the different tracer tests. Each of the following figures is labelled with the following code: TXXYZ where:

- T stands for tracer test;
- XX is the depth (cm);
- Y is the speed of the blower;
- Z is the number of the test.

The scales of both abscissa and ordinate may vary from one test to another, one may pay attention to this when analyzing the graphs.

a. Graphs for a depth of 40 cm

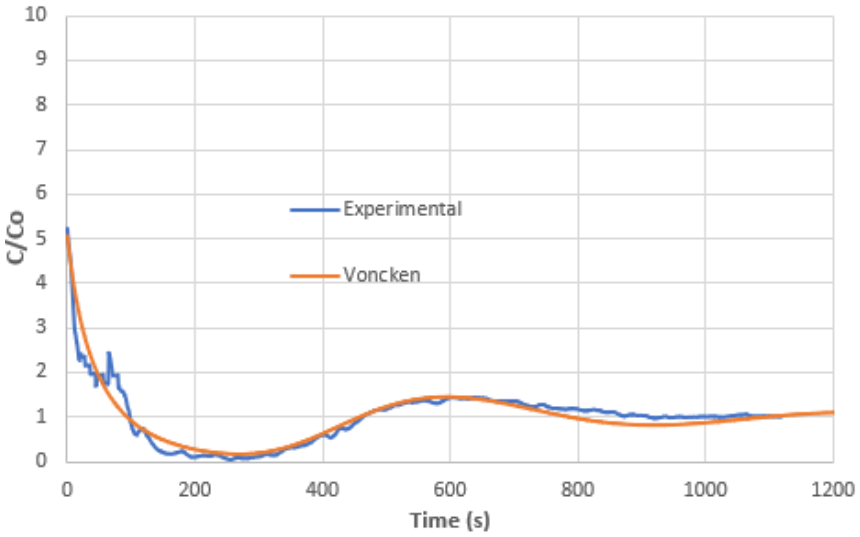

Figure 79 – T4041

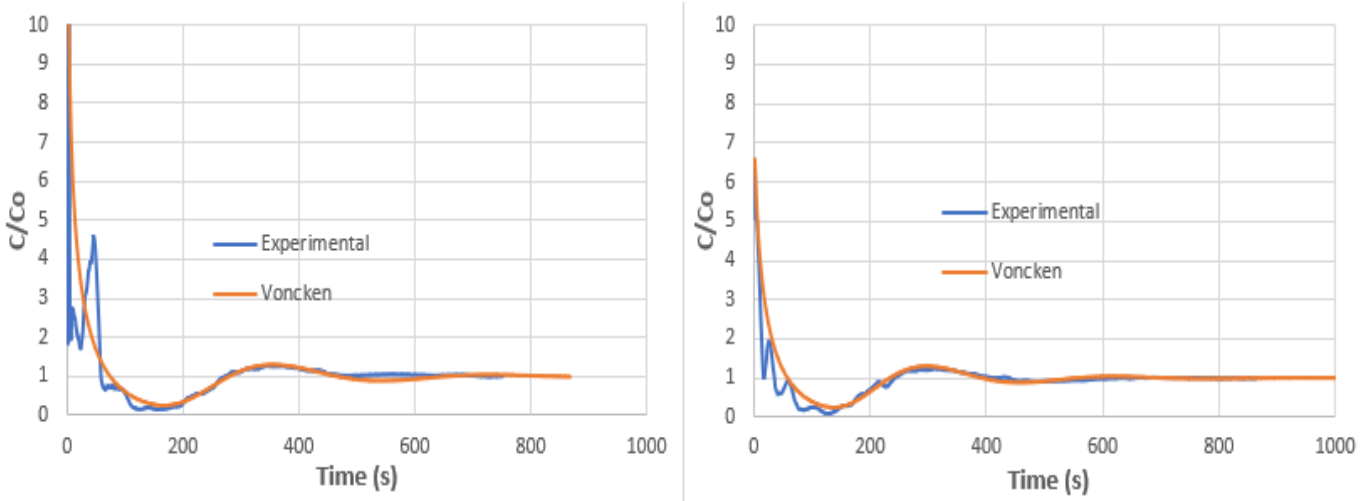

Figure 80 – T4061 (left) and T4062 (right)

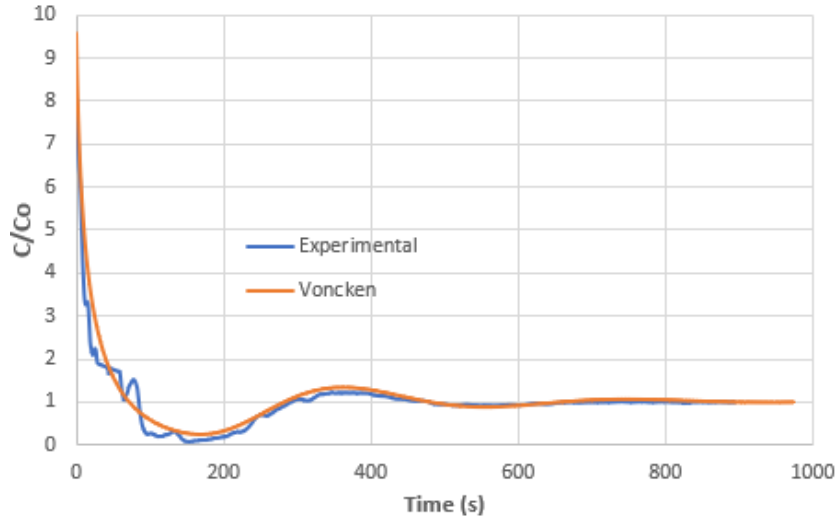

Figure 81 – T4063

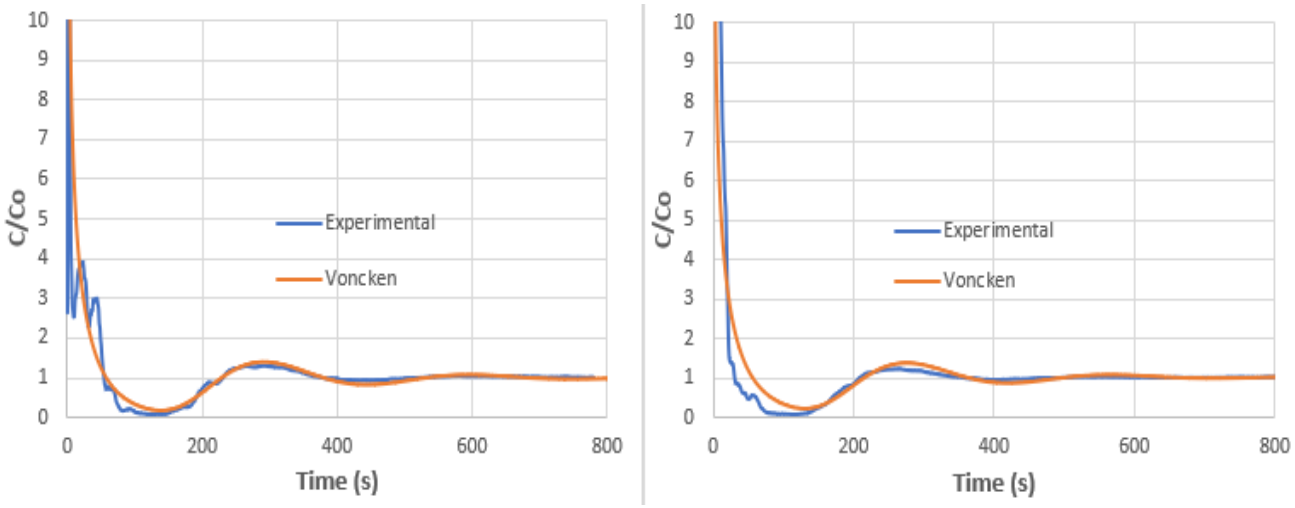

Figure 82 – T4081 (left) and T4082 (right)

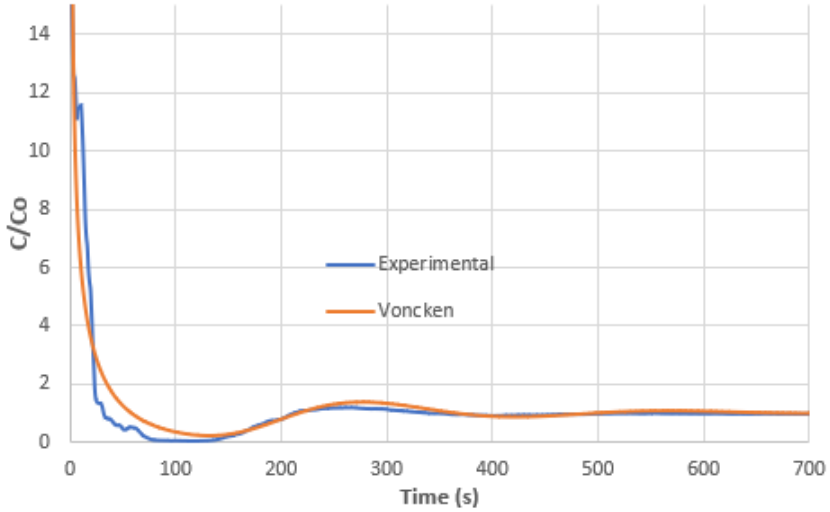

Figure 83 – T40101

b. Graphs for a depth of 25 cm

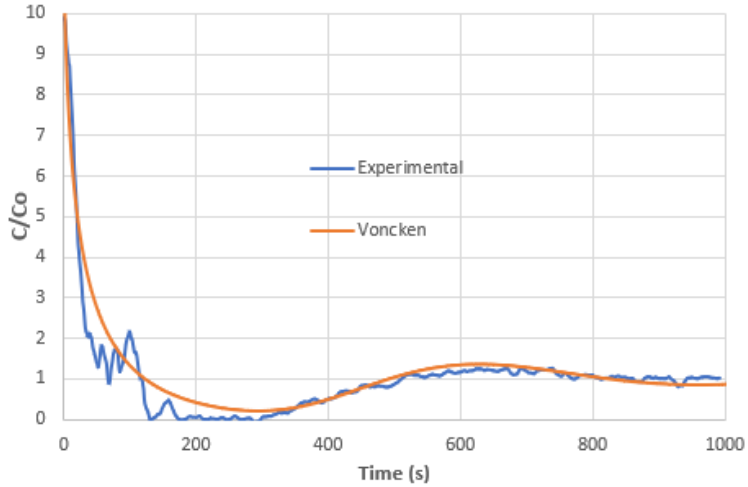

Figure 84 – T2541

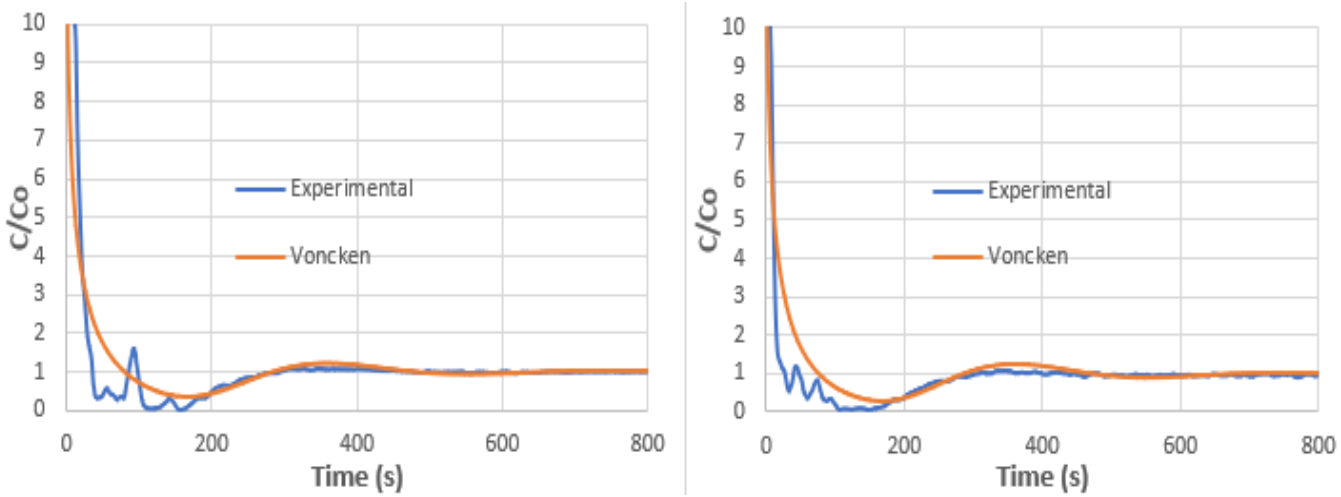

Figure 85 – T2561 (left) and T2562 (right)

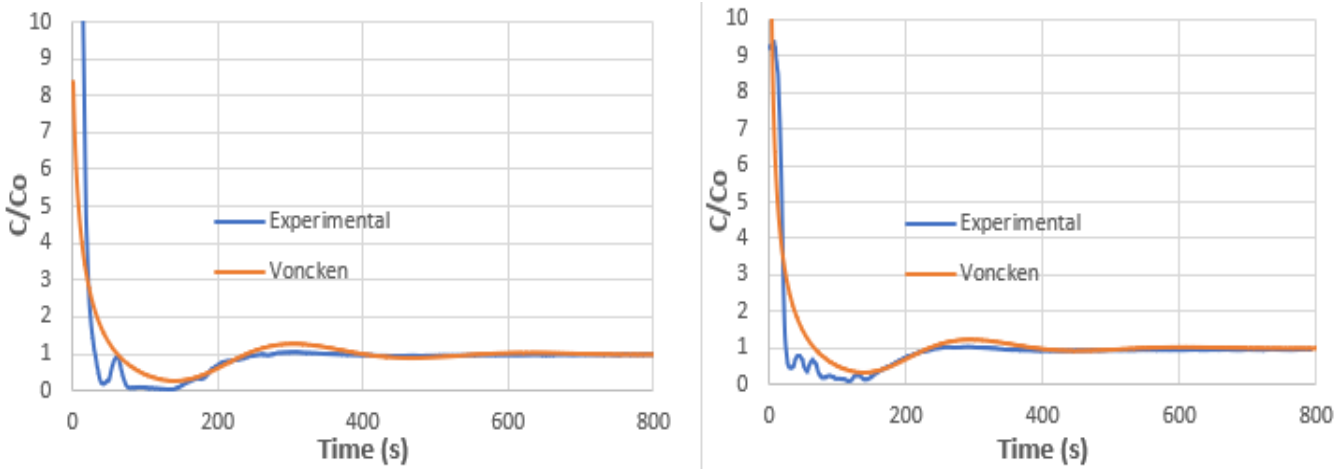

Figure 86 – T2581 (left) and T2582 (right)

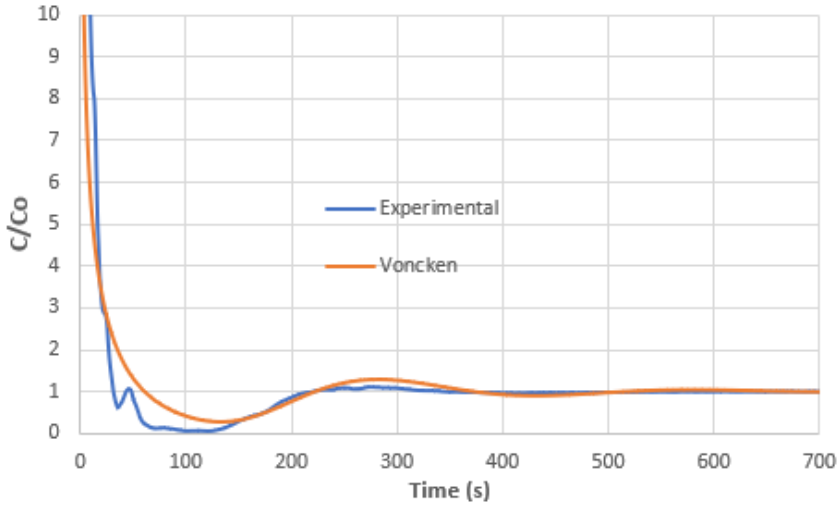

Figure 87 – T25101

c. Graphs for a depth of 60 cm

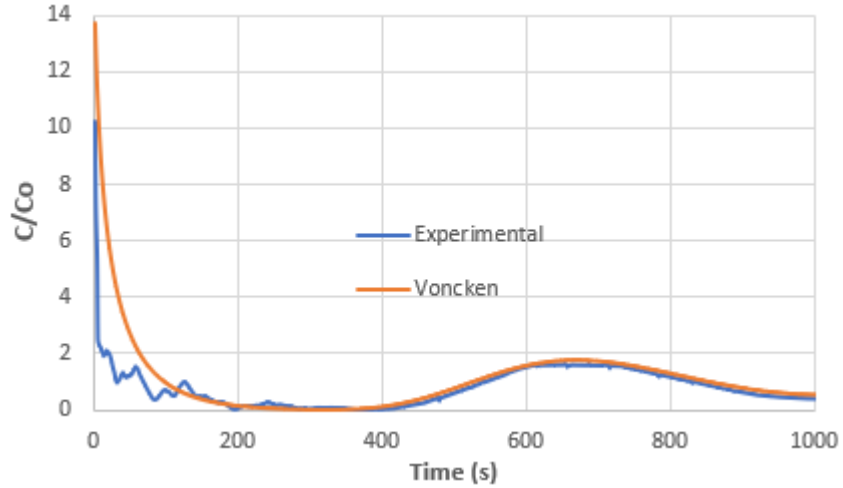

Figure 88 – T6041

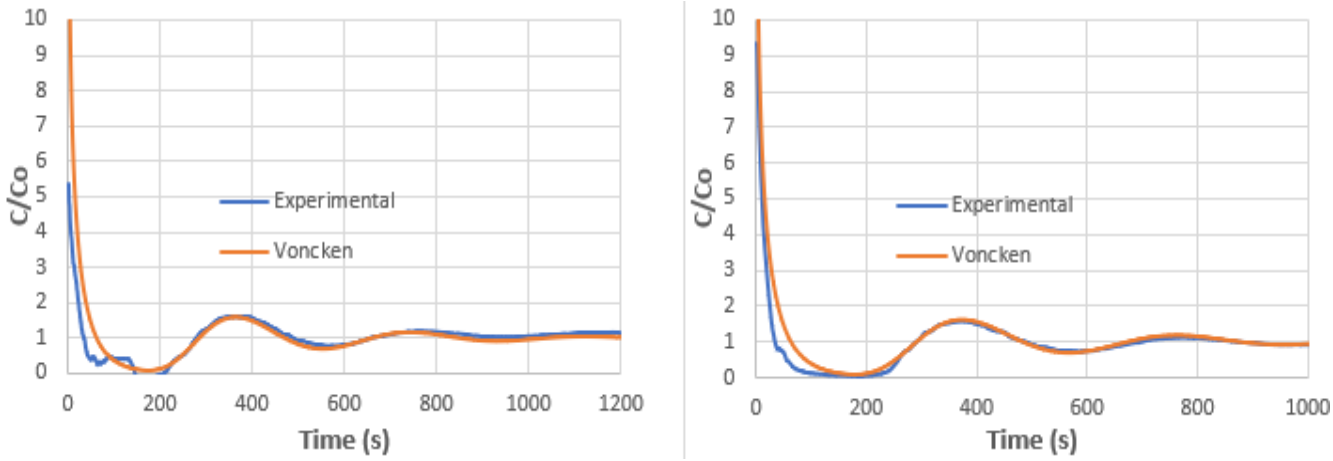

Figure 89 – T6061 (left) and T6062 (right)

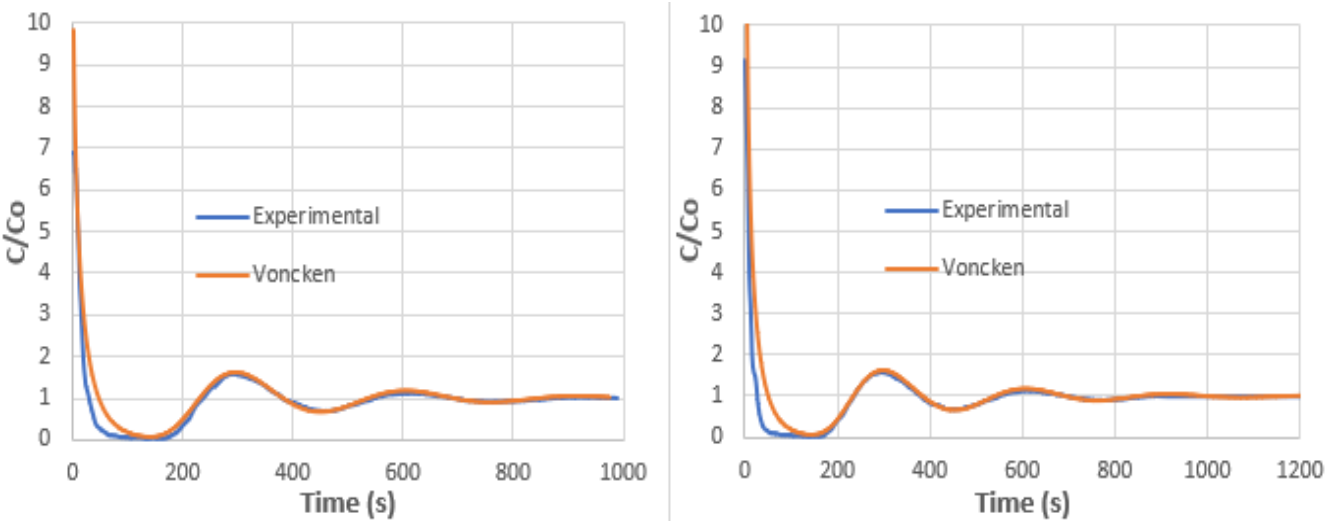

Figure 90 – T6081 (left) and T6082 (right)

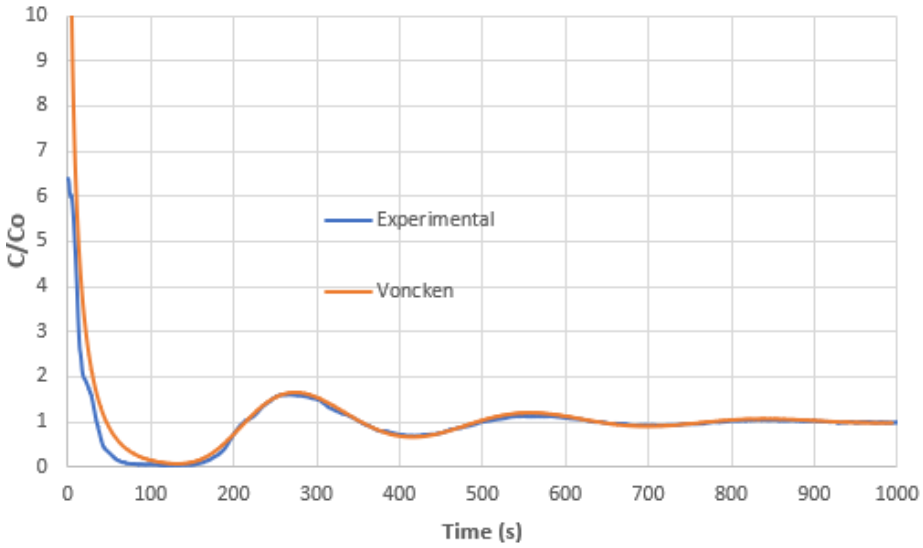

Figure 91 – T60101

Appendix E – Comparison between the theoretical data and the results of the tracer tests

Different data (air flowrate, water velocity) measured on the Vietnamese HRAP pilot can be compared to the theoretical values that are provided first by the ROBUSCHI® company, and second, by a model developed by Sustainwater. The air flowrates are given by the performance test curves provided by ROBUSCHI® (**Figure 92**). The differential pressure is estimated 350 mbar and is mainly due to the level of water (250 mbar) and the diffusive pipes (100 mbar). Using the approximated powers, one can obtain the theoretical air flowrates that are summarized in the following **Table 21**.

Table 21 – Comparison between the theoretical and the measured air flowrates

Power (kW) & rpm	Theoretical air flowrate (Nm^3/h)	Measured air flowrate (Nm^3/h)
0.6 - /	/	<30
1.2 – 1500 rpm	48	60
1.8 – 2100 rpm	87	100
2.4 – 3000 rpm	142.8	130

Then, a model has been developed by Sustainwater in order to predict water velocity in the HRAP. This model takes into account the material constituting the pond, the design as well as the characteristics of the airlift. The differences between the theoretical values and the reality could be caused by the modified shape of the curves and the coat of paint added that smooths the walls surface. The assumptions of the model are:

- Air flowrate: 114 Nm^3/h;
- Differential pressure: 350 mbar;
- Water level in the airlift: 2.5m (0.6m in the channel)

The tests that correspond the most to these conditions are T6081 and T6082. The data are presented in **Table 22**.

Table 22 – Comparison between the theoretical and the calculated water velocities

Theoretical velocity (cm/s)	Measured velocity (cm/s)
11	T6081: 18.64 T6082: 18.70

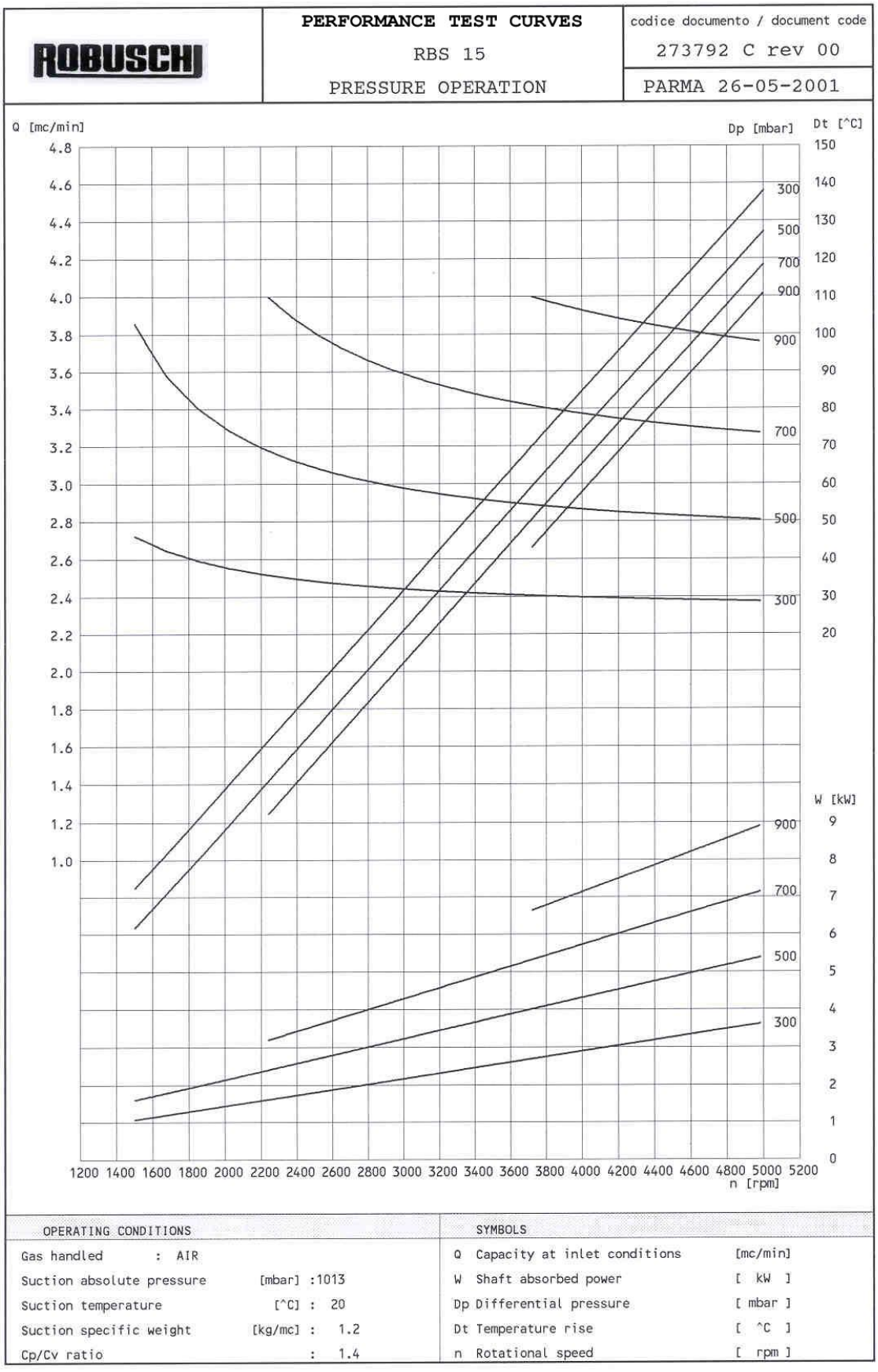

Figure 92 – Performance test curves

Appendix F – Graphs of the oxygen transfer tests (Vietnam)

This appendix summarizes all the graphs of the different oxygen transfer tests. Each of the following figures is labelled with the following code: OXXYZ where:

- O stands for oxygen transfer test;
- XX is the depth (cm);
- Y is the speed of the blower;
- Z is the number of the test.

The scales of both abscissa and ordinate may vary from one test to another, one may pay attention to this when analyzing the graphs.

a. Graphs for a depth of 40cm

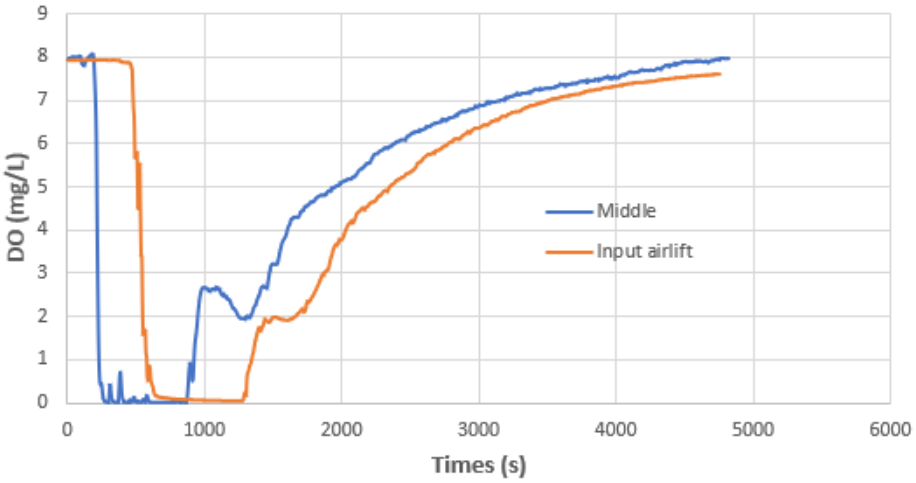

Figure 93 – O4041

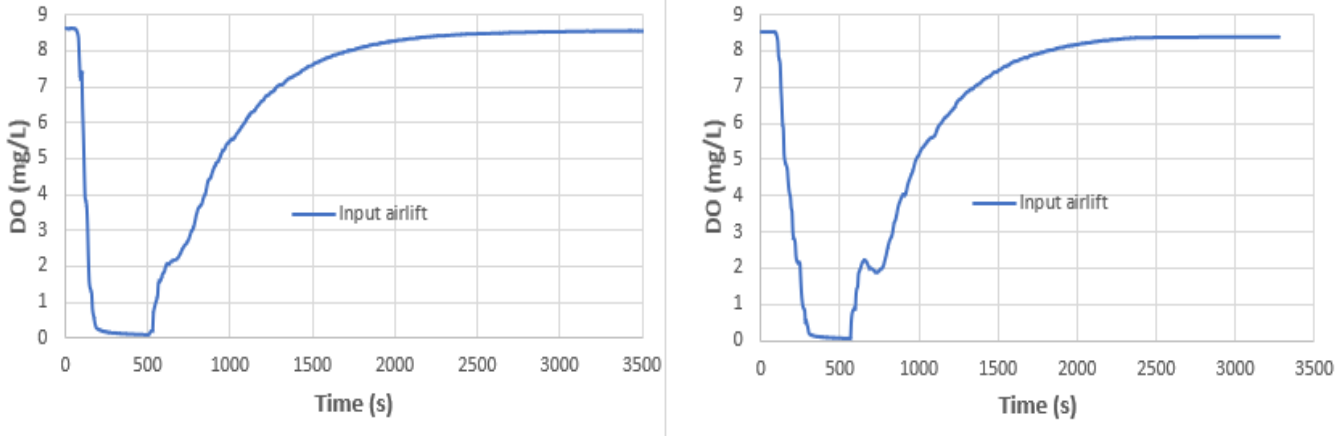

Figure 94 – O4061 (left) and O4062 (right)

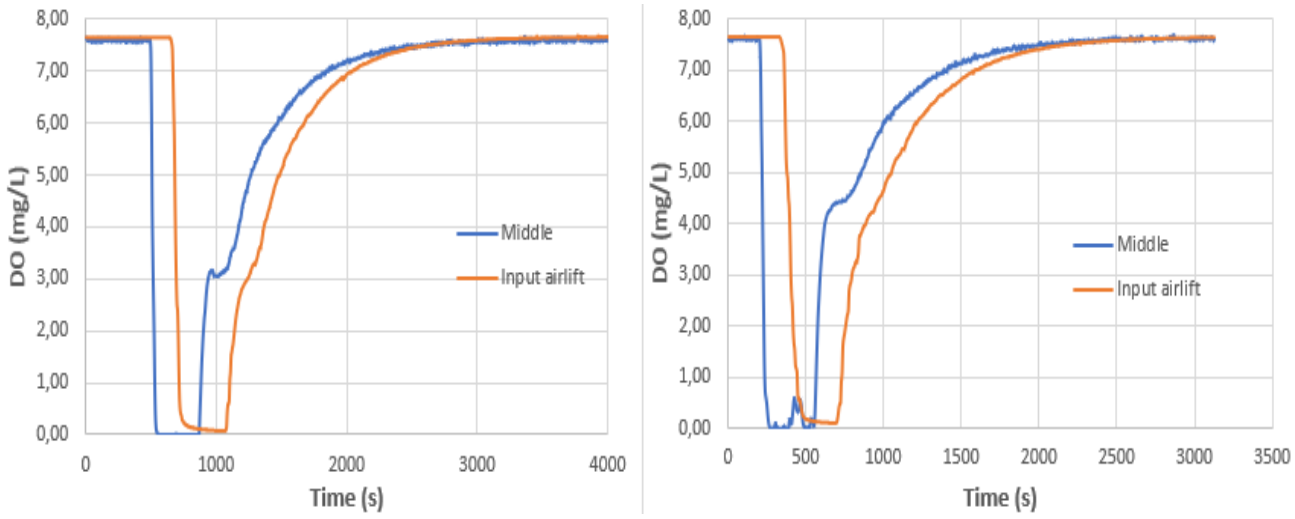

Figure 95 – O4061b (left) and O4062b (right)

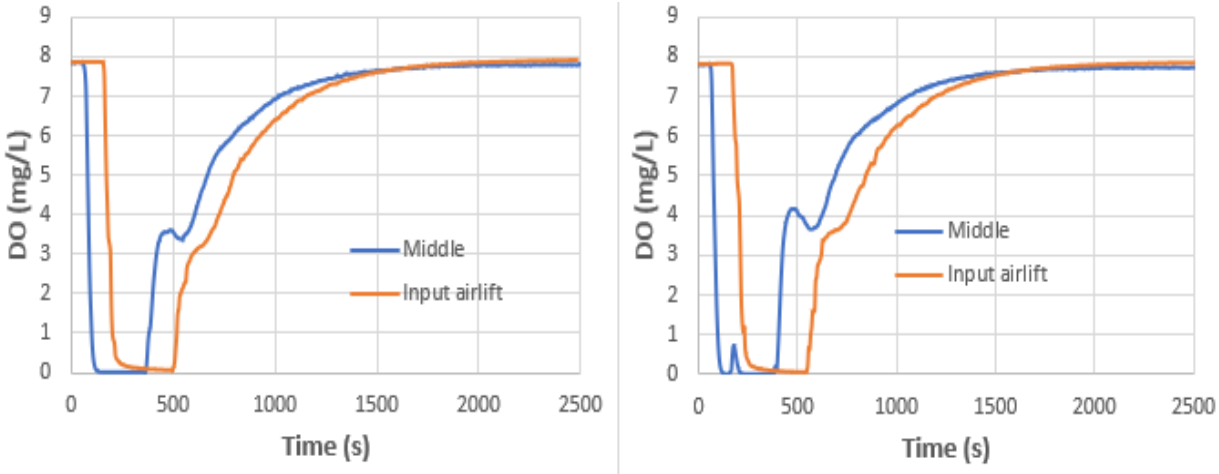

Figure 96 – O4081 and O4082

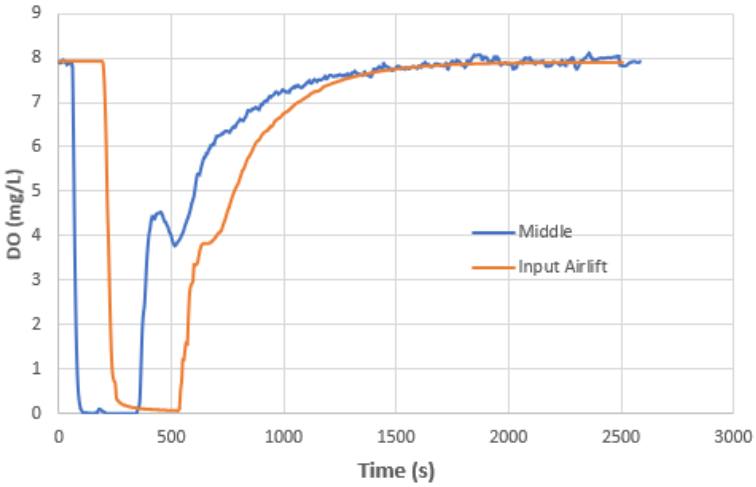

Figure 97 – O40101

b. Graphs for a depth of 25cm

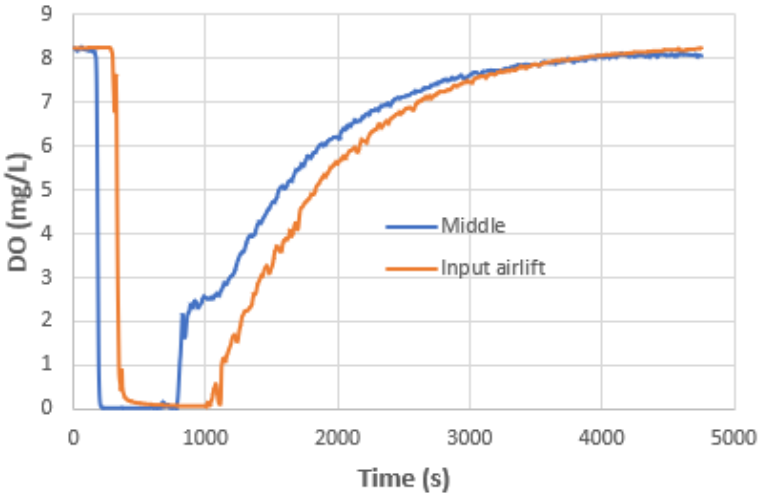

Figure 98 – O2541

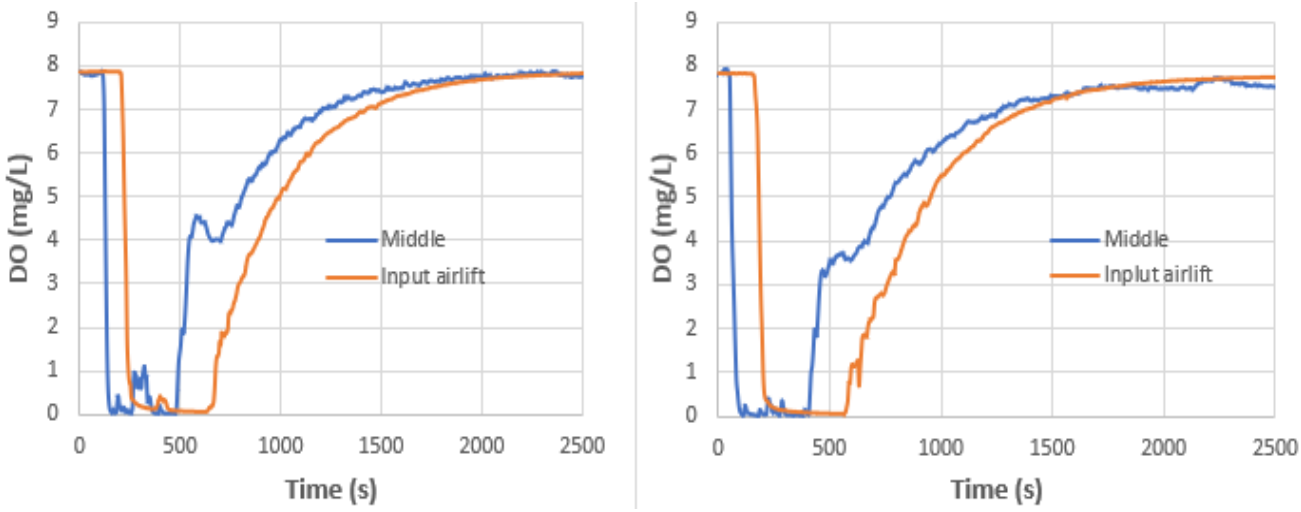

Figure 99 – O2561 (left) and O2562 (right)

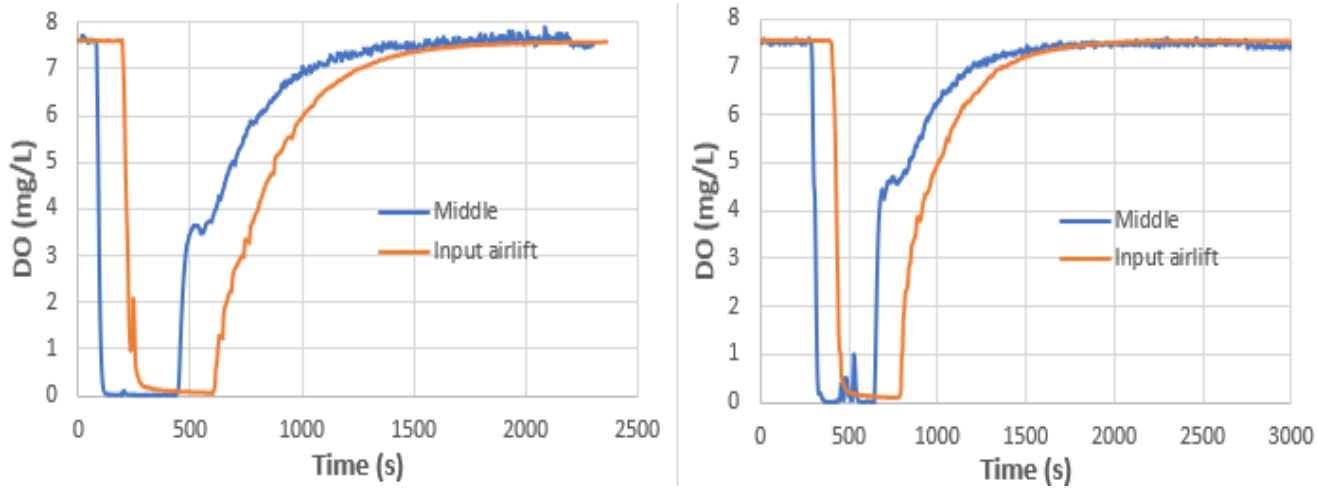

Figure 100 – O2581 (left) and O2582 (right)

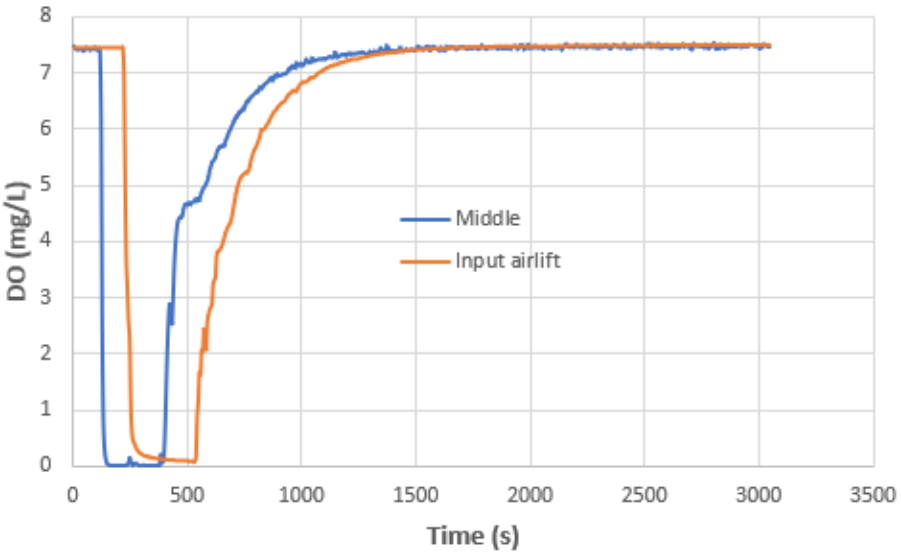

Figure 101 – O25101

c. Graphs for a depth of 60cm

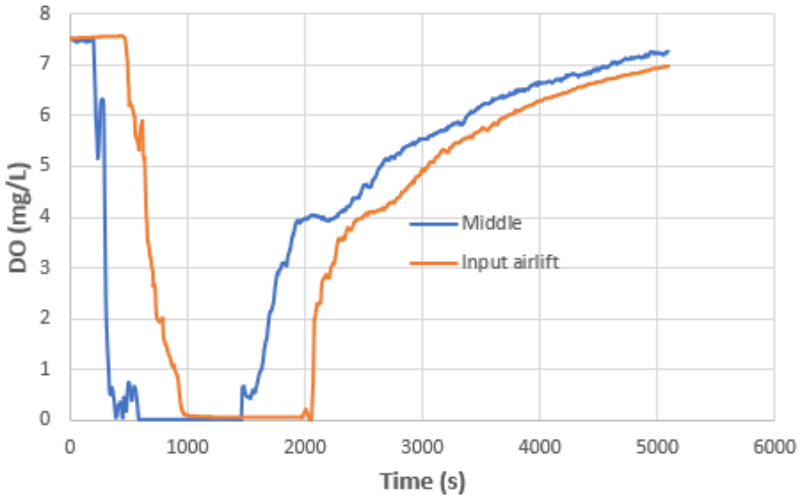

Figure 102 – O6041

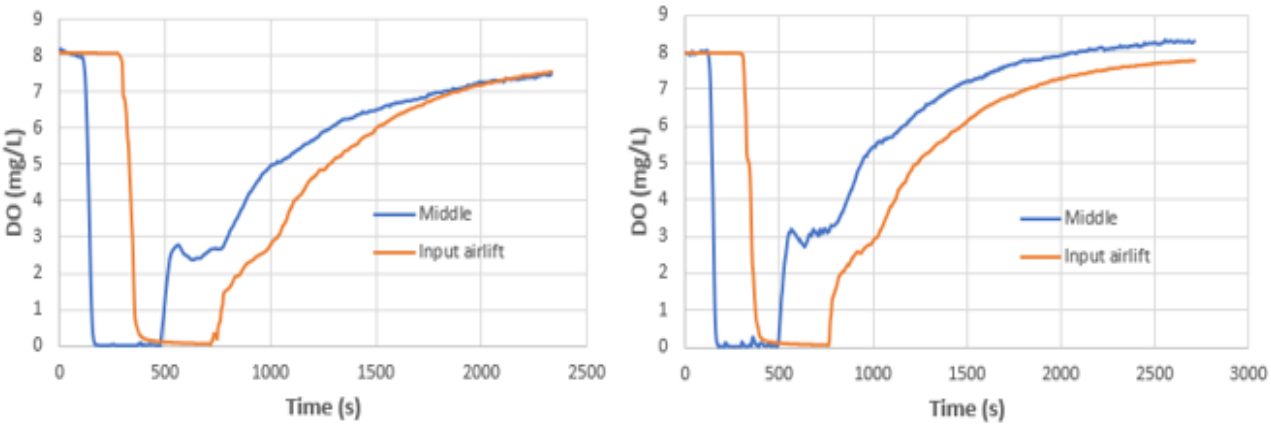

Figure 103 – O6061 (left) and O6062 (right)

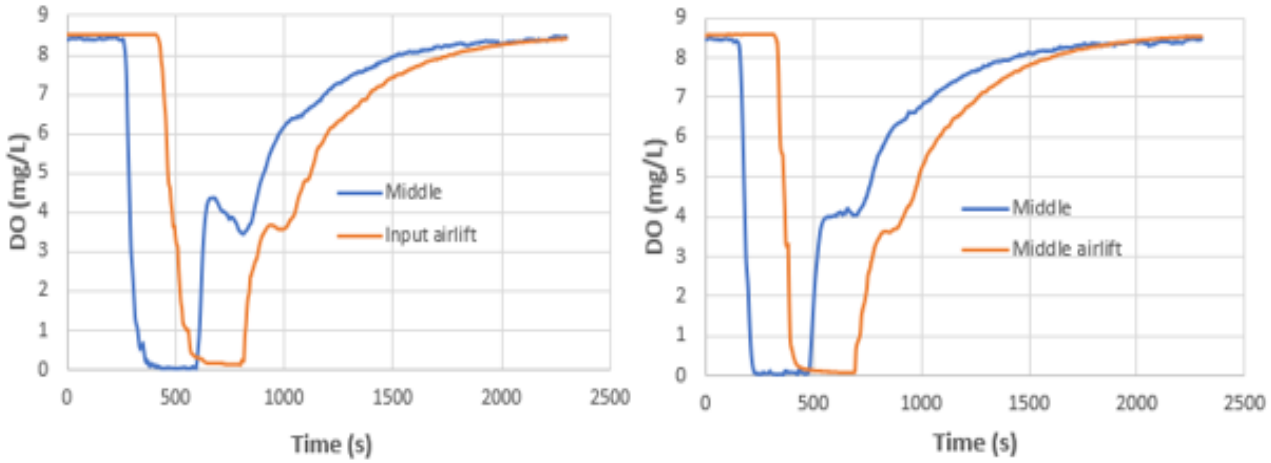

Figure 104 – O6081 (left) and O6082 (right)

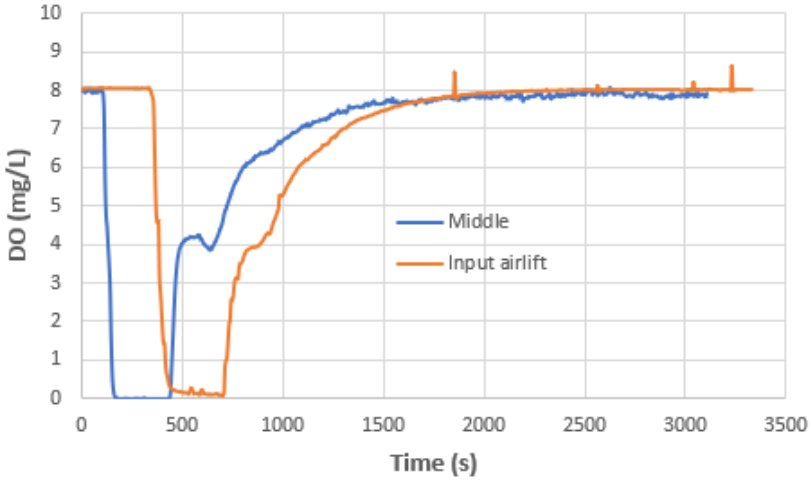

Figure 105 – O60101